

AIRWORTHINESS ANALYSIS OF A MODIFIED KR-2 EXPERIMENTAL
AIRCRAFT

A Project

Presented to

The Faculty of the Department of Mechanical and Aerospace Engineering
San Jose State University

In Partial Fulfillment

of the Requirements for the Degree

Master of Science in Aerospace Engineering

by

Boris Bravo

December 2011

© 2011

Boris M. Bravo

ALL RIGHTS RESERVED

The Designated Project Committee Approves the Project Titled

AIRWORTHINESS ANALYSIS OF A MODIFIED KR-2 EXPERIMENTAL
AIRCRAFT

By

Boris Bravo

APPROVED FOR THE DEPARTMENT OF MECHANICAL AND AEROSPACE
ENGINEERING

SAN JOSE STATE UNIVERSITY

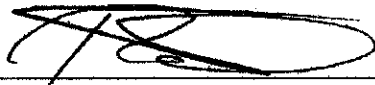
December 2011



Dr. Nikos J. Mourtos, Committee Chair
Department of Mechanical and Aerospace Engineering

12-12-2011

Date



Dr. Periklis Papadopoulos, Committee Member
Department of Mechanical and Aerospace Engineering

12-12-11

Date



Mr. Michael J. Nordin, Committee Member
Novellus Systems, Inc.

12-13-2011

Date

ABSTRACT

Airworthiness Analysis of a Modified KR-2 Experimental Aircraft

By Boris Bravo

The original KR-2 is a side to side, low wing, monoplane experimental airplane. This airplane originally comes with a 65 HP Volkswagen engine, and it is capable of developing up to 200 mph cruise speed. While capable of developing such a speed with such a small engine, this airplane is also known for having a pitch sensitivity problem and poor performance at high altitudes. Particularly affected at high altitudes are its climb rate and its stall speed. In order to improve performance at high altitude, the original KR2 was modified by increasing the wing span 3 feet and by changing the engine to an 85 HP continental engine. The goal of this Master's project is to make sure that after these modifications the airplane airworthiness has not being affected. Preliminary calculation of lift and drag were done in the first part of the project to generate the airplane's lift and drag polar and performance curves. The airworthiness analysis was done by building and studying the airplane's trim diagrams, and controllability and stability derivatives for all the airplane's configurations and flight conditions. After checking these parameters for airworthiness compliance against the regulations, it was found that while the airplane complies with the regulations regarding longitudinal controllability and longitudinal static stability. It does not comply with the regulations regarding dynamic longitudinal stability. Based on a derivative sensitivity study, the analysis was concluded with some recommendations to address the dynamic longitudinal stability compliance.

Table of Contents	page
List of Figures	ix
List of Tables	xi
List of Symbols	xiii
1. Introduction	15
1.1. <i>The Original KR-2</i>	16
1.2. <i>Problem Statement</i>	17
1.3. <i>The Modified KR-2</i>	18
1.4. <i>Project Goal</i>	19
1.5. <i>Airworthiness Analysis Approach</i>	20
2. Literature Review	21
2.1. <i>Wing Contribution to stability and control</i>	23
2.2. <i>Tail Contribution to stability and control</i>	25
2.3. <i>The Fuselage Contribution to stability and control</i>	28
2.4. <i>Neutral Point</i>	30
2.5. <i>Power Effect</i>	32
2.5.1. <i>Power effect due to forces within the propeller itself</i>	32
2.5.2. <i>Power effect due to the propeller slip stream</i>	34
2.5.3. <i>Elevator angle versus equilibrium lift coefficient</i>	36
2.6. <i>Literature Review Summary</i>	37
3. Preliminary Calculations	38
3.1. <i>Airfoil Lift and Drag</i>	38

3.2.	<i>Wing Lift and Drag</i>	40
3.3.	<i>Airplane Lift and Drag</i>	44
3.3.1.	Airplane Lift.....	44
3.3.1.1.	Airplane zero-angle-of-attack lift coefficient, C_{L_0}	45
3.3.1.2.	Airplane lift curve slope, C_{L_α}	47
3.3.2.	Airplane Drag.....	49
3.3.2.1.	Wing Drag Coefficient Prediction, $C_{D_{WING}}$:	50
3.3.2.2.	Fuselage Drag Coefficient Prediction, $C_{D_{FUSELAGE}}$:	52
3.3.2.3.	Empennage Drag Coefficient Prediction, $C_{D_{EMPENNAGE}}$:	55
3.3.2.4.	Landing Gear Lift Coefficient, C_{DGear}	56
3.3.2.5.	Airplane Drag Polar	57
3.4.	<i>Airplane Performance</i>	59
3.4.1.	Stall Speed.....	59
3.4.2.	Take off.....	60
3.4.3.	Climb.....	60
4.	Airworthiness Analysis	62
4.1.	<i>Regulations Requirements</i>	62
4.2.	<i>Configurations & Flight conditions</i>	64
4.3.	<i>Airplane Weight and Balance</i>	65
4.4.	<i>Airplane Trim diagrams</i>	69
4.4.1.	Construction of airfoil lift and pitching moment curves.....	69

4.4.2.	Construction of wing lift and pitching moment curves.....	70
4.4.2.1.	Wing pitching moment coefficient at zero-lift, $C_{m_{0w}}$	70
4.4.2.2.	Wing pitching moment curve slope, $(dc_m/dc_L)_w$	70
4.4.3.	Construction of Airplane lift and pitching moment curves.....	71
4.4.3.1.	Airplane pitching moment coefficient at zero-lift, C_{m_0}	72
4.4.3.2.	Airplane pitching moment curve slope, (dc_m/dc_L)	73
4.4.3.3.	Aerodynamic center shift due to fuselage, Δx_{acf}	74
4.4.4.	Ground effect on airplane lift.....	76
4.4.5.	Ground effect on airplane pitching moment.....	79
4.4.5.1.	Decrease in tail downwash due to ground effect, $(\Delta \epsilon)_g$	80
4.4.6.	Power effect on airplane lift.....	82
4.4.7.	Power effect on airplane pitching moment.....	84
4.4.7.1.	Power effect on pitching moment at zero lift coefficient, ΔC_{m_0T}	85
4.4.7.2.	Power effect on longitudinal stability, $\Delta(dc_m/dc_L)_T$	86
4.4.8.	Prediction of trimmed lift and trimmed maximum lift coefficient.....	91
4.5.	<i>Longitudinal Controllability and Trim</i>	94
4.6.	<i>Static Longitudinal Stability</i>	96
4.7.	<i>Dynamic Longitudinal Stability</i>	97
4.7.1.	Class II method for analysis of phugoid characteristics.....	97
4.7.2.	Class II method for analysis of short period characteristics.....	98
5.	Conclusions	99
6.	Appendix	102

<i>A. Airplane dimensions</i>	102
7. Acknowledgements	109
References	110

List of Figures	page
Figure 1: Modified KR-2 CAD Model	15
Figure 2: Sea Level and Altitude Performance Curve - IO-540-K, -L, -M, -S	17
Figure 3: Reinforced Truss Joints	19
Figure 4: Airworthiness analysis approach	20
Figure 5: Airfoil Nomenclature and Geometry	21
Figure 6: Forces and moments in plane of symmetry	22
Figure 7: Typical pitching moment curves	23
Figure 8: Downwash distribution in front and behind a finite wing	27
Figure 9: Normal values for upwash ahead of the wing	29
Figure 10: Typical longitudinal stability breakdown	31
Figure 11: Direct forces cause by propeller	32
Figure 12: $CL-\alpha$ Curve Comparison – plotted with <i>Xfoil</i>	39
Figure 13: Drag Polar Comparison – plotted with <i>Xfoil</i>	39
Figure 14: Lift Coefficient Distribution for Level Flight	42
Figure 15: Local wing lift coefficient distribution for varying angle of attack	43
Figure 16: Wing lift vs. angle of attack	44
Figure 17: Airplane and wing lift vs. alpha curves	49
Figure 18: Turbulent Flat Plate Friction Coefficient as Function of Velocity	51
Figure 19: Fuselage Turbulent Flat Plate Friction Coefficient as Function of Velocity	54
Figure 20: Drag Polar for Modified KR-2 at Gross Weight	58
Figure 21: Rate of Climb vs. Velocity, 6000 Ft. Density Altitude (Nordin, 2006)	61
Figure 22: Flight phases	63

Figure 23: Locations of Major Components for Weight and Balance	65
Figure 24: Airplane center of gravity (cg) diagram	66
Figure 25: Airplane lift curves for all flight phases	76
Figure 26: Ground effect on lift at take off	78
Figure 27: Ground effect on landing	78
Figure 28: Ground effect on pitching moment for take off	81
Figure 29: Ground effect on pitching moment for landing	82
Figure 30: Power and Ground effect on lift for take off	84
Figure 31: Power and Ground effect on pitching moment curve for take off	88
Figure 32: Power and Ground effect on pitching moment curve for climb	89
Figure 33: Power and Ground effect on pitching moment curve for level cruise	89
Figure 34: Power and Ground effect on pitching moment curve for descend	90
Figure 35: Power and Ground effect on pitching moment curve for landing	90
Figure 36: Trim diagram for cruise	94
Figure 37: Airplane Top View	102
Figure 38: Airplane Back View	102
Figure 39: Airplane wing planform	103
Figure 40: Equivalent wing planform	103
Figure 41: Wing dihedral and incident angle	105
Figure 42: Canopy and wheel	106
Figure 43: Empennage	107

List of Tables	page
Table 1: KR Series Aircraft Specifications.....	16
Table 2: Airfoil lift and drag parameters.....	40
Table 3: Tabulation of Lift Coefficient Distribution for Level Flight)	41
Table 4: Local $C_{L,MAX}$ for wing sections	42
Table 5: Wing lift and drag parameters.....	43
Table 6: Airplane lift parameters.....	48
Table 7: Tabulation of Class II Drag Polar for Modified KR-2.....	57
Table 8: Airplane Types.....	62
Table 9: Relation between airplane type and applicable regulations.....	63
Table 10: Regulation Requirements.....	64
Table 11: Flight conditions	64
Table 12: Flight Configurations	65
Table 13: Weight and Balance Calculations and Summary	67
Table 14: Other flight conditions and configurations.....	68
Table 15: Other flight conditions and configurations continuation.....	68
Table 16: Airfoil lift and pitching moment curve parameters	69
Table 17: Wing lift and pitching moment curve parameters	71
Table 18: Airplane lift and pitching moment parameters.....	75
Table 19: Airplane lift and pitching moment parameters continuation 1	75
Table 20: Airplane lift and pitching moment parameters continuation 2.....	75
Table 21: Ground effect on lift parameters.....	77
Table 22: Ground effect on pitching moment.....	81

Table 23: Power effect on lift.....	83
Table 24: Power effect on pitching moment.....	87
Table 25: Power effect on pitching moment continuation	88
Table 26: Effect of control surface deflection on lift	92
Table 27: Effect of control surface deflection on pitching moment.....	93
Table 28: Longitudinal controllability parameters.....	95
Table 29: Wing parameters	104
Table 30: Empennage parameters.....	107

List of Symbols

- a = lift curve slope
 b = wingspan
 bhp = engine shaft brake horsepower
 c = chord length
 \bar{c} = mean geometric chord
 C_f = turbulent flat plate friction coefficient
 C_L = coefficient of lift
 C_D = coefficient of drag
 CG = center of gravity
 D = drag
 d_f = maximum fuselage diameter
 EW = empty weight
 h = CG location, fraction of \bar{c}
 h_{ac} = aerodynamic center location, fraction of \bar{c}
 h_n = neutral point location, fraction of \bar{c}
 L = lift
 LE = leading edge
 m = lift curve slope
 OEW = operating empty weight
 P = air pressure
 P_A = power available
 P_R = power required
 \bar{q} = dynamic viscosity
 R = leading edge suction parameter
 R_{wf} = wing - fuselage interference factor

Re = Reynolds number
 R/C = rate of climb
 s = 1/2 wingspan
 s_{LO} = lift off distance
 S = wing area
 S_{wet} = wetted area
 t/c = thickness ratio
 T = thrust
 TVT = trailing vortices theory
 TOW = take off weight
 V_{∞} = free stream velocity
 α = geometric angle of attack
 α_0 = effective angle of attack
 $\alpha_{C_L=0}$ = zero lift angle of attack
 ε = span efficiency factor
 ε_t = wing twist angle
 η = propeller efficiency
 η = drag of finite cylinder / drag of infinite cylinder
 κ = vortex strength
 κ_0 = local vortex strength
 λ = taper ratio
 Λ = sweep angle
 μ = dynamic viscosity for air
 v = induced drag factor due to linear twist
 ρ_{∞} = air density

1. Introduction

Since I started college, my education focus has been on airplane design. One afternoon after sharing with a classmate, my good friend Michael Nordin, my desire to do a project that encompasses in-depth airplane engineering design, he mentioned his father had a half-built airplane in his garage. This was an experimental airplane, the KR-2, which original design had been modified following trial and error recommendations. So inspired by the audacity of these individuals and recognizing the need of an engineering analysis, I chose to do an airworthiness analysis of this airplane for my master's project. Michael Nordin and I worked together during the first part of this project where we developed the aircraft drag polar. A challenging stage of this analysis was to find the lift distribution of a non-constant taper wing with twist. For this we used xfoil to construct the local airfoil lift curve. The wing lift distribution was found by solving the trailing vortices equations with MATLAB using the local airfoil lift curves as input.

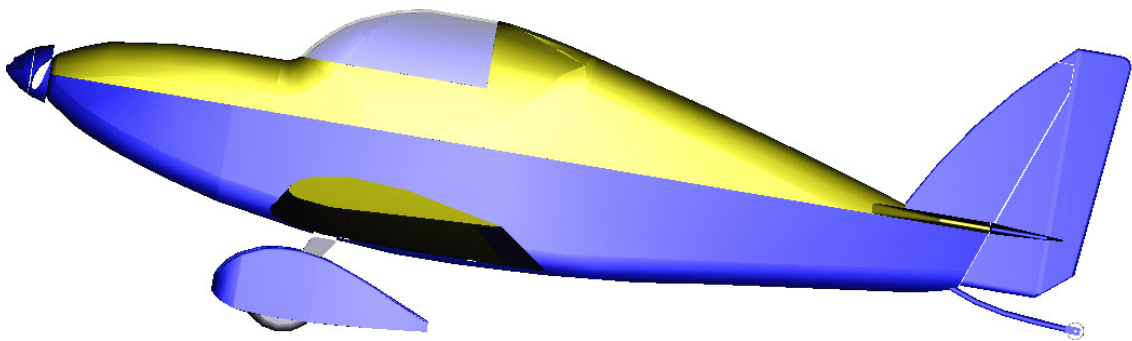


Figure 1: Modified KR-2 CAD Model (Nordin, 2006)

1.1. *The Original KR-2*

Original design by Ken Rand and Stuart Robinson, the KR2 is a side to side, low wing, monoplane experimental aircraft. Its wood-composite materials construction method put it between the fastest, more affordable and easier to build homebuilt airplanes. Performance published for the original KR-2 shows that the airplane is capable of developing 200 mph cruise speed with a 65 HP Volkswagen engine.

Table 1: KR Series Aircraft Specifications (Glove)

KR Series Aircraft Specifications			
	KR-1	KR2	KR2-S
Length	12' 9"	14' 6"	16'
Wing Span	17' 0"	20' 8"	23'
Total Wing Area	62 sq. ft.	80 sq. ft.	82 sq. ft.
Empty weight	375 lbs.	480 lbs.	---
Gross weight	750 lbs.	900 lbs.	980 lbs.
Useful load	375 lbs.	420 lbs.	460 lbs.
Baggage capacity	20 lbs. max	35 lbs. max	35 lbs.
Take off distance	350 ft.	350 ft.	350 ft.
Landing distance	900 ft.	900 ft.	600 ft.
Stall Speed	52 mph	52 mph	52 mph
Maximum Speed	200 mph	200 mph	200 mph
Cruise Speed	180 mph	180 mph	180 mph
Range	1400 miles	1600 miles (35 gal. fuel)	1080 miles
Rate of Climb (light)	1200 fpm	1200 fpm	1200 fpm
Rate of Climb (gross)	800 fpm	800 fpm	800 fpm
Service ceiling	15,000 ft.	15,000 ft.	15,000 ft.
Engine	VW 1834	VW 2100	VW 2180, Subaru EA-81, Continental O-200
Fuel	8-30 gal.	12-35 gal.	---
Fuel consumption	3.8 gph	3.8 gph	3.8-5.5 gph (depending on engine)
Seating	1	2 across	2 across
Landing Gear	Fixed conventional or trigear, or retractable conventional	Fixed conventional or trigear, or retractable conventional	Fixed conventional

1.2. Problem Statement

While this airplane is able to cruise at 200 miles per hour, experience has shown a poor performance at high altitudes, i.e., 6200 ft at Lake Tahoe. Particularly affected at this altitude is the climb rate and stall speed. This airplane is also well-known for having pitch sensitivity issues.

The climb rate is affected because of the reduction of available power with altitude as we can observe in **Figure 2**.

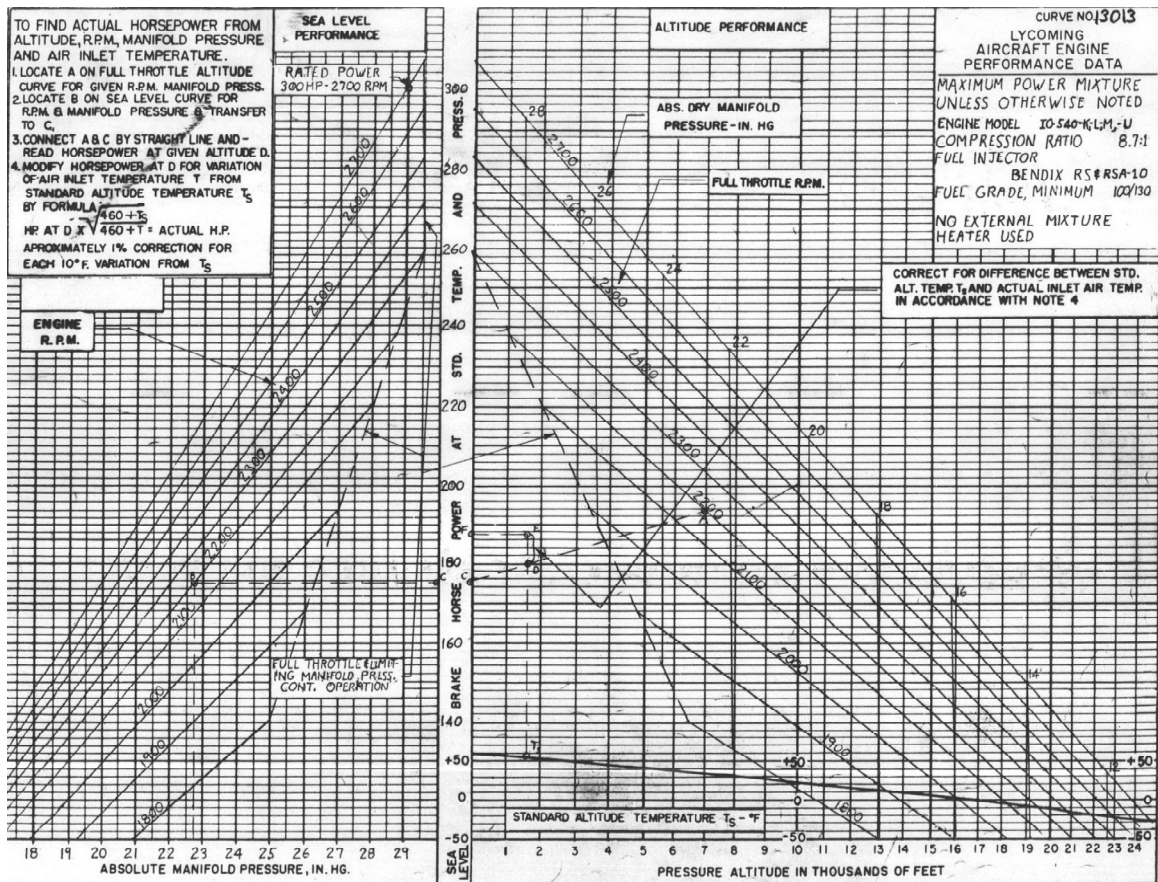


Figure 2: Sea Level and Altitude Performance Curve - IO-540-K, -L, -M, -S (Lycoming)

From the stall speed equation we can also see how this speed is affected with the change of density at high altitude.

$$V_{STALL} = \sqrt{\frac{2W}{\rho_w SC_{L,MAX,W}}} \quad 1.1$$

1.3. The Modified KR-2

In order to improve performance at high altitude, KR-2 builders approach has been to decrease power loading and wind loading. To achieved this, the KR-2 airplane under consideration was equipped with an 85 HP Continental engine, and three feet were added two the wing span. These modifications resulted in approximately an 8% and 20% decrease in wing loading and power loading respectively, as shown by equation 1.2

$$\begin{aligned} \text{Wing loading} &= \frac{\text{Gross Weigth}}{\text{Wing Area}} \\ \text{Wing Loading}_{KR2} &= \frac{900 \text{ lb}}{80 \text{ ft}^2} = 11.25 \text{ psi} \\ \text{Wing Loading}_{MODKR2} &= \frac{950 \text{ lb}}{86.4 \text{ ft}^2} = 12.25 \text{ psi} \\ \text{Wing Loading decrease} &= 1 - \frac{11.25}{12.25} = 8 \% \end{aligned}$$

$$\begin{aligned} \text{Power loading} &= \frac{\text{Gross Weigth}}{\text{Engine HP}} \\ \text{Power Loading}_{KR2} &= \frac{900 \text{ lb}}{65 \text{ HP}} = 13.9 \text{ lb/HP} \\ \text{Power Loading}_{MODKR2} &= \frac{950 \text{ lb}}{85 \text{ HP}} = 11.2 \text{ lb/HP} \\ \text{Power Loading decrease} &= 1 - \frac{11.2}{13.9} = 19 \% \end{aligned}$$

1.2

It is worth mentioning that reinforcement at all stress joints has been placed in order to account for the stress increased caused by the mentioned modifications, but the structural integrity of the airplane is out of the scope of this project.

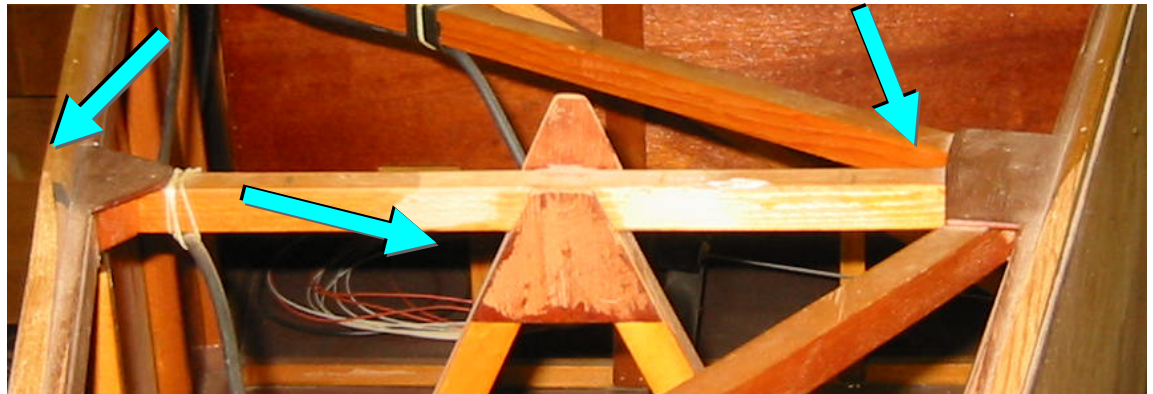


Figure 3: Reinforced Truss Joints (Nordin, 2006)

1.4. Project Goal

The goal of this project is to determine if these modifications will have the expected performance enhancement results, while making sure they won't affect the airworthiness of the airplane. Because no modifications have been done that could significantly affect the airplane's lateral stability and control, and acknowledging the airplane's pitch sensitivity issue, the focus of this study would be on the longitudinal stability of the airplane.

1.5. *Airworthiness Analysis Approach*

The airworthiness analysis will be carried-out following a Class II preliminary design method as described by Roskam Part VII page 1; this method describes all the procedures for determining the stability and control characteristics of an airplane, and consists of making sure the aircraft satisfy all its mission requirements, while complying with all the applicable airworthiness regulations (Roskam, Airplane Design, Part I - VIII, 1990). The following diagram illustrates this approach:

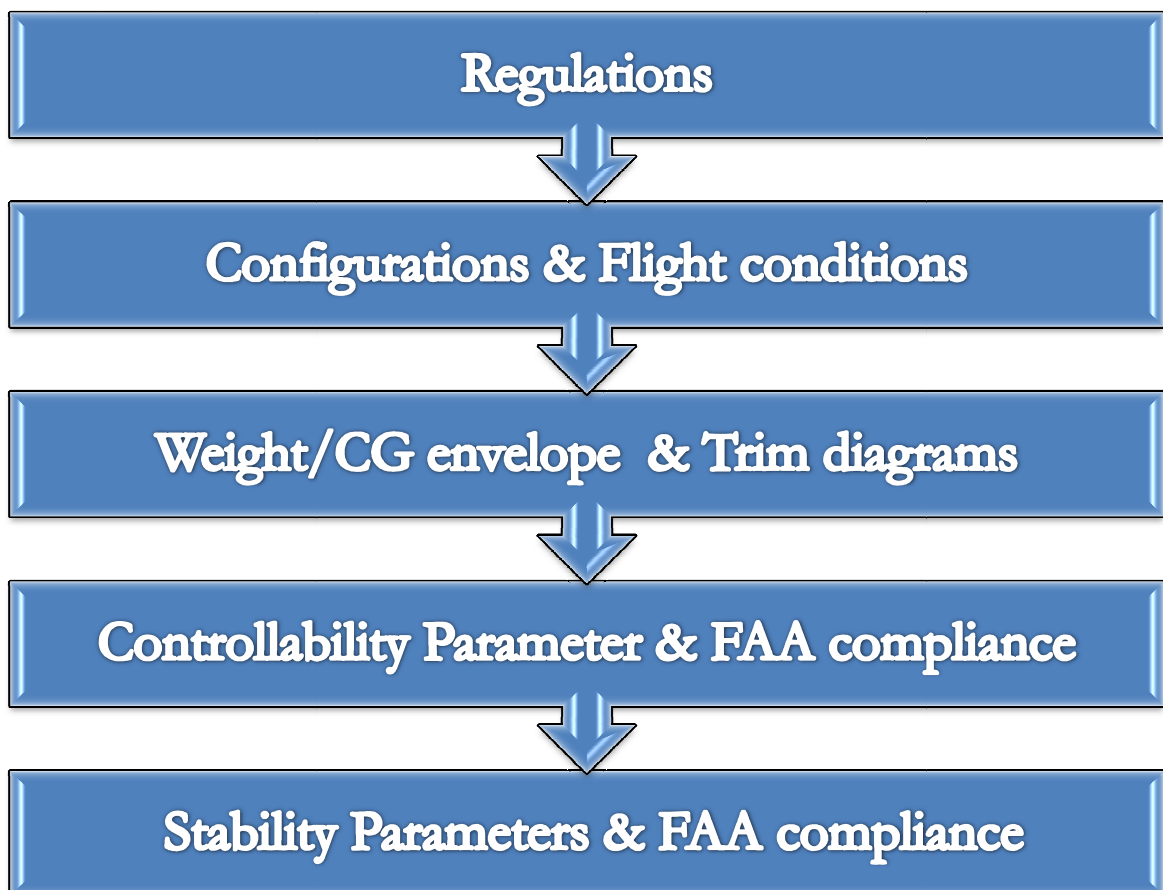


Figure 4: Airworthiness analysis approach

2. Literature Review

The equilibrium and static longitudinal stability of an airplane is assessed by studying the moments of the airplane about its center of gravity (c.g.). For the airplane to be in equilibrium the summation of these moments is required to be zero, and for the airplane to be considered statically stable, an increase of lift from equilibrium should result in a diving moment and a decrease of lift should result in a stalling moment.

By definition, the aerodynamic center (a.c.) of a lifting device is a point where the variation of moments is independent of lift. All forces and moments of an airplane wing and tail could be considered acting at this point as illustrated in **Figure 5**.

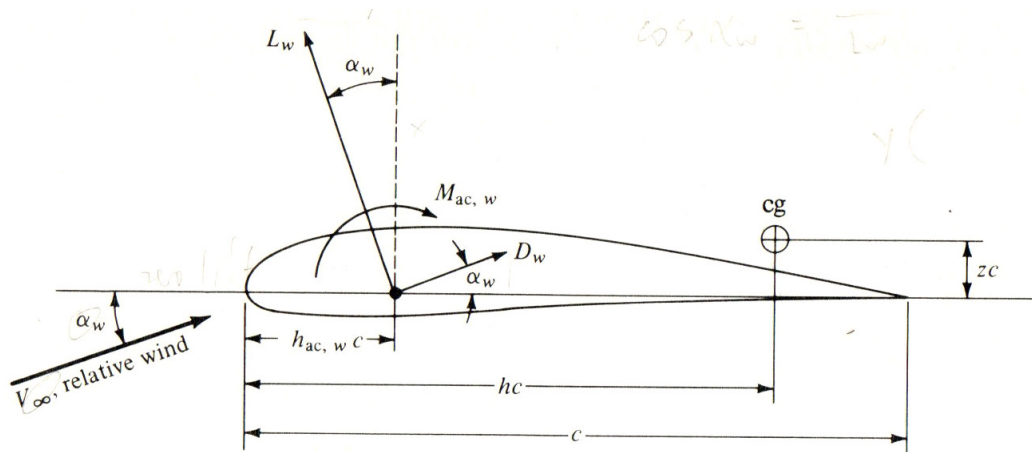


Figure 5: Airfoil Nomenclature and Geometry (Anderson, 1978)

Resolving all forces and moments about the c.g., as shown in **Figure 6**, for unaccelerated, propeller off flight, and dividing this by $qS_w c$, the coefficient form equilibrium equation of the airplane is:

$$C_{m_{cg}} = C_N \frac{x_a}{c} + C_c \frac{z_a}{c} + C_{m_{ac}} + C_{m_{FUS_{Nac}}} - C_{m_{act}} \frac{S_t}{S_w} \frac{c_t}{c} \eta_t + C_{c_t} \frac{S_t}{S_w} \frac{h_t}{c} \eta_t - C_{N_t} \frac{S_t}{S_w} \frac{l_t}{c} \eta_t$$

2.1 (Perkins & Hage, 1949)

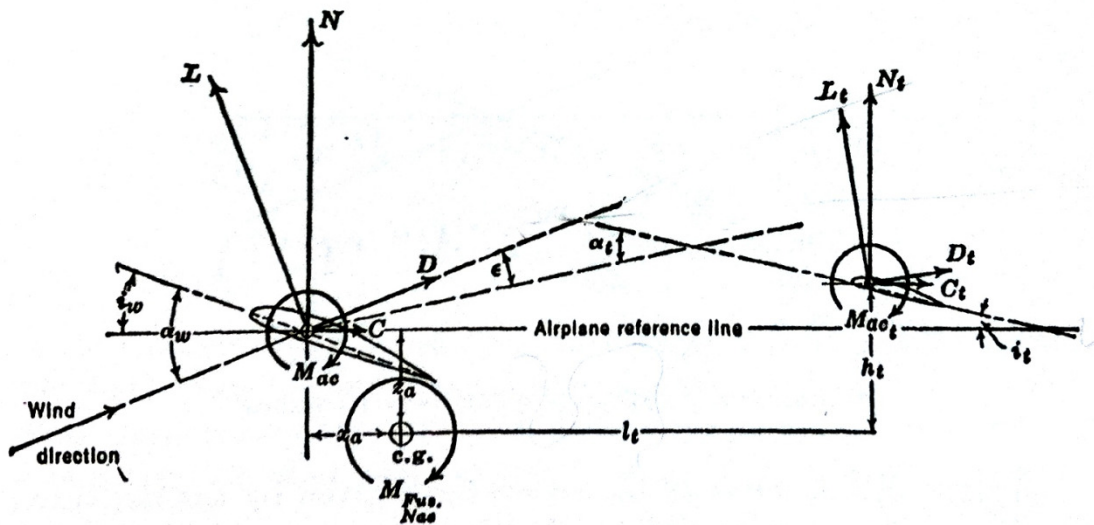


Figure 6: Forces and moments in plane of symmetry (Perkins & Hage, 1949)

where q is the dynamic pressure, S_w is the wing area, and c is the wing's mean geometric chord.

Neglecting the moment contribution from the stabilizer drag and the tail moment about its $a.c$, terms fifth and sixth, the resulting airplane equilibrium equation is:

$$C_{m_{cg}} = C_N \frac{x_a}{c} + C_c \frac{z_a}{c} + C_{m_{ac}} + C_{m_{Fus, Nas}} - C_{N_t} \frac{S_t}{S_w} \frac{l_t}{c} \eta_t$$

2.2 (Perkins & Hage, 1949)

As shown in **Figure 7**, equation two is plotted as a function of the lift coefficient to study the stability of the airplane. It can be seen here how a negative slope curve produces the stable condition previously mentioned, a diving moment when the coefficient of lift (CL) increases from equilibrium; and a positive slope curve is accompanied by a stalling moment.

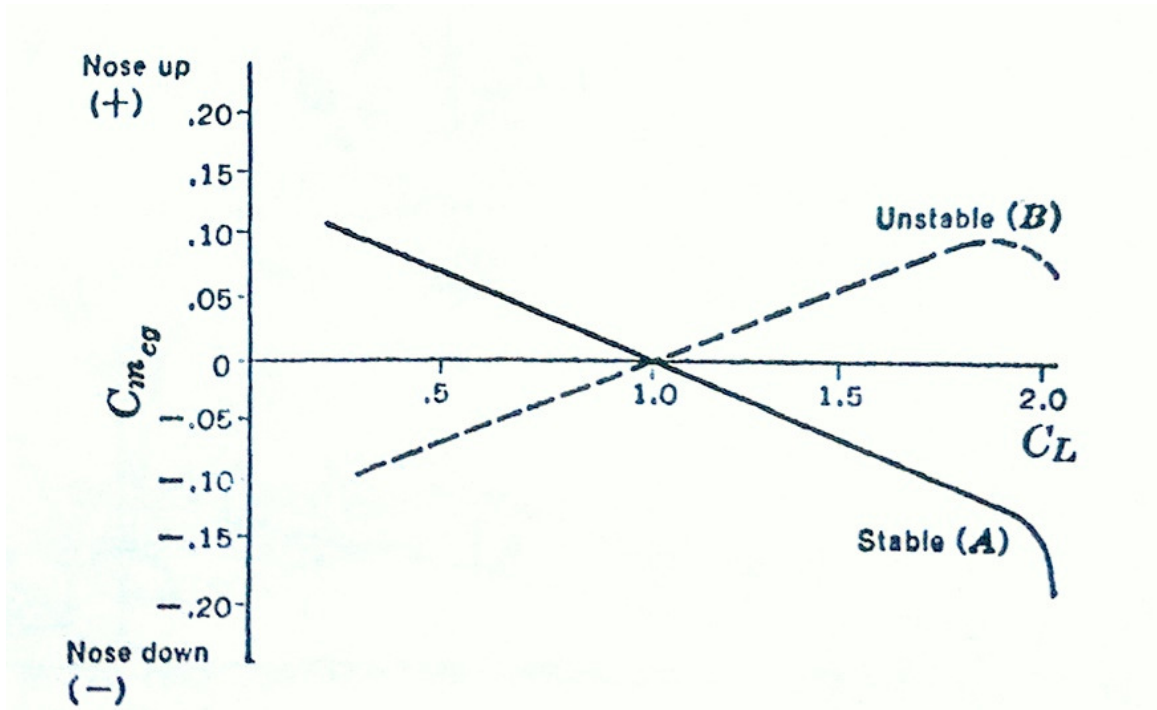


Figure 7: Typical pitching moment curves (Perkins & Hage, 1949)

The slope of these curves represents the stability contribution of various parts of the airplane and it is found by taking the derivative of equation 2.2 with respect to lift:

$$\frac{dC_m}{dC_L} = \left(\frac{dC_N}{dC_L} \frac{x_a}{c} + \frac{dC_c}{dC_L} \frac{z_a}{c} + \frac{dC_{m_{ac}}}{dC_L} \right)_{Wing} + \left(\frac{dC_m}{dC_L} \right)_{Fus_{Nac}} - \left(\frac{dC_{N_t}}{dC_L} \frac{S_t}{S_w} \frac{l_t}{c} n_t \right)_{Tail} \quad 2.3$$

2.1. Wing Contribution to stability and control

The first three terms of 2.3 are the wing's contribution to the airplane's stability. By definition of aerodynamic center, the third term, $\frac{dC_{m_{ac}}}{dC_L}$, is equal to zero, and the other two terms can be studied by writing C_N and C_c as a function of lift, and by taking their

derivatives with respect to lift. The wing forces perpendicular and parallel to the airplane, written in coefficient form are:

$$C_N = C_L \cos(\alpha - i_w) + C_D \sin(\alpha - i_w)$$

$$C_C = C_D \cos(\alpha - i_w) - C_L \sin(\alpha - i_w)$$

2.4 (Perkins & Hage, 1949)

where α and i_w are the airplane's angle of attack and the wing implant angle respectively. The derivatives of 2.4 with respect to lift are:

$$\frac{dC_N}{dC_L} = \cos(\alpha - i_w) - C_L \sin(\alpha - i_w) \frac{d\alpha}{dC_L} + \frac{dC_D}{dC_L} \sin(\alpha - i_w) + C_D \cos(\alpha - i_w) \frac{d\alpha}{dC_L}$$

$$\frac{dC_C}{dC_L} = \frac{dC_D}{dC_L} \cos(\alpha - i_w) - C_D \sin(\alpha - i_w) \frac{d\alpha}{dC_L} - C_L \cos(\alpha - i_w) \frac{d\alpha}{dC_L} + \sin(\alpha - i_w)$$

2.5 (Perkins & Hage, 1949)

Using the parabolic polar approximation, as explained by Perkins & Hage, the drag as a function of lift can be expressed as:

$$C_D = C_{Df} + \frac{C_L^2}{\pi A e} \quad 2.6$$

therefore its derivative with respect to the lift coefficient is:

$$\frac{dC_D}{dC_L} = \frac{2C_L}{\pi A e} \quad 2.7$$

For small angles of attack, and considering that C_D is considerably less than one, equation 2.5 can be simplified. Combining 2.5, 7 & 3 the wing's contribution to the airplane's stability can be written as:

$$\left(\frac{dC_m}{dC_L}\right)_{wing} = \frac{x_a}{c} + C_L \left(\frac{2}{\pi A e} - \frac{.035}{dC_L/d\alpha} \right) \frac{z_a}{c}$$

2.8 (Perkins & Hage, 1949)

As seen in equation 2.8 and **Figure 6**, the stability of the airplane is mainly influenced by the position of the wing's (z_a) and the airplane's a.c., with respect to the airplane's c.g. For the first term to have a stabilizing effect, negative value, the airplane's c.g. is required to be ahead of the airplane's a.c. For an average airplane, the constant between parentheses, in the second term is usually negative. This means that a wing above the airplanes c.g. has a stabilizing effect while a wing below the airplanes c.g. has a destabilizing effect.

2.2. Tail Contribution to stability and control

To study the contribution of the tail, the wing downwash needs to be taken into consideration. Because of this downwash, the angle of attack the tail experiences is not the same as the angle of attack of the wing. As **Figure 6** shows, this angle of attack is:

$$\alpha_t = \alpha_w - \epsilon + i_t - i_w$$

2.9 (Perkins & Hage, 1949)

The coefficient of the vertical force of the tail can be expressed as a function of the tail's angle of attack multiplied by the derivative of this force with respect to the angle of attack:

$$C_{N_t} = \left(\frac{dC_N}{d\alpha} \right)_t (\alpha_w - \epsilon + i_t - i_w) \quad 2.10$$

And taking the derivative with respect to lift coefficient, the tail contribution to stability becomes:

$$\left(\frac{dC_m}{dC_L} \right)_{Tail} = -\frac{a_t}{a_w} \bar{V} n_t \left(1 - \frac{d\epsilon}{d\alpha} \right) \quad 2.11 \text{ (Perkins \& Hage, 1949)}$$

where: $\left(\frac{dC_N}{d\alpha} \right)_w = a_w$, $\left(\frac{dC_N}{d\alpha} \right)_t = a_t$ and $\frac{S_t l_t}{S c} = \bar{V}$

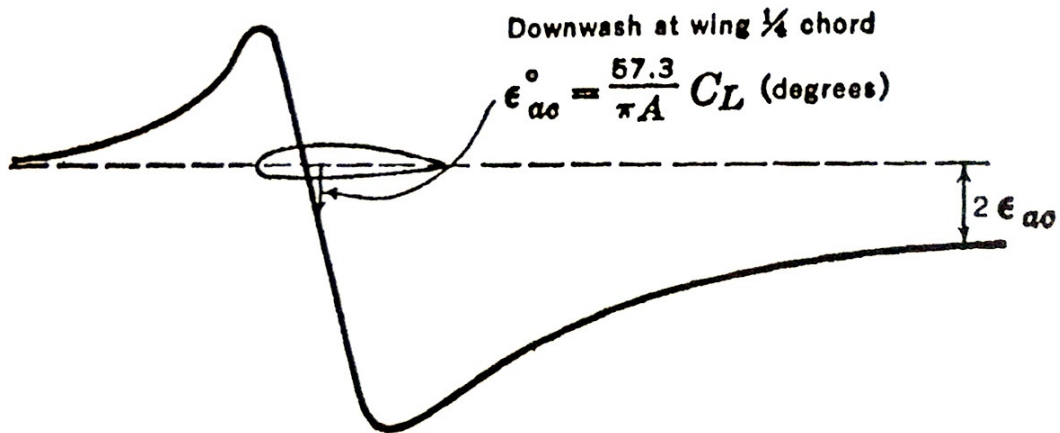


Figure 8: Downwash distribution in front and behind a finite wing. (Perkins & Hage, 1949)

As illustrated in **Figure 8**, the downwash varies significantly along the airplane. At the tail, it is safe to assume the downwash value is equal to the theoretical downwash at infinity, which is twice as big as the theoretical value at quarter chord:

$$\epsilon^o = \frac{114.6C_L}{\pi A} \tag{2.12}$$

therefore its derivative with respect to alpha is:

$$\frac{d\epsilon}{d\alpha} = \frac{114.6}{\pi A} a_w \tag{2.13}$$

This downwash value is a good initial approximation. In reality the downwash at the tail varies significantly upon the vertical position of the tail relative to the wing. As we can see in equation 2.11, the stability contribution of the tail is greatly affected by the downwash; therefore, for a more accurate prediction of this contribution, the NACA TR 628 methodology should be used for the calculation of the downwash.

2.3. *The Fuselage Contribution to stability and control*

In order to understand how the fuselage or nacelle contributes to the airplane's stability, we need to analyze the flow around these objects. For ideal potential flow, a slender cylindrical body, like a fuselage, generates a destabilizing free moment due to negative pressure in the upper side of the bow and on the lower side of the stern, and positive pressure in the lower side of the bow and in the upper side of the stern (**Figure**).



Figure 9: Fuselage in Ideal Flow (Multhopp, 1942)

Due to the wing's induced downwash after the wing, and upwash ahead of the wing, this hull-like free moment is significantly altered for the real case. Based on frictional lift theory for small aspect ratios, the fuselage's lift is proportional to the square of the fuselage width (w_f^2). In 1942 Multhopp developed a method in which he accounted for the wing's influence. The method estimates the fuselage's frictional lift using the angle (β) the fuselage would form with the flow after considering the downwash and upwash; and consists of integrating the fuselage's lift multiplied by a reference arm, along the entire length of the fuselage. As expressed by this method, the pitching moment - airplane's angle of attack gradient is:

$$\frac{dM}{d\alpha} = \frac{q}{36.5} \int_0^l w_f^2 \frac{d\beta}{d\alpha} dx$$

2.14 (Perkins & Hage, 1949)

Behind the wing, the variation of the fuselage angle of attack with respect to the airplane's angle of attack, $\frac{d\beta}{d\alpha}$, is proportional to the familiar term for calculating the downwash at the tail, $(1 - \frac{d\epsilon}{d\alpha})$, and is less than the unity since the downwash subtracts from the airplane's angle of attack. Ahead of the wing, this gradient is more than one, since the upwash adds to the airplane's angle of attack, as can be seen in **Figure 9**. This analysis affords great importance to the position of the wing along the fuselage when considering stability.

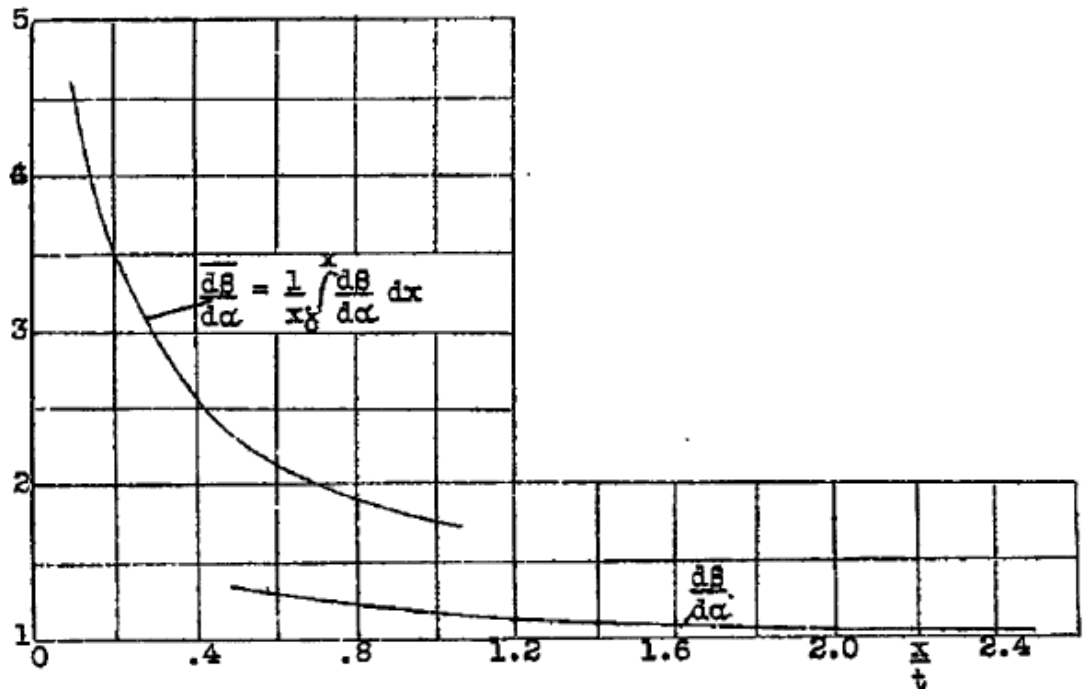


Figure 9: Normal values for upwash ahead of the wing (Multhopp, 1942)

Finally the contribution of the fuselage to the airplane's stability can be found by dividing equation 2.14 by qS_wca_w ,

$$\left(\frac{dC_m}{dC_L}\right)_{Fus, Nac} = \frac{(dM/d\alpha)_{Fus, Nac}}{qS_wca_w} \quad 2.15 \text{ (Perkins \& Hage, 1949)}$$

2.4. Neutral Point

The second term of the wing contribution to stability, drag term, is very small in comparison to the first term. Neglecting this drag term, the stability equation of the airplane can be written as:

$$\frac{dC_m}{dC_L} = \frac{x_a}{c} + \frac{(dM/d\alpha)_{Fus, Nac}}{qS_wca_w} - \frac{a_t}{a_w} \bar{V}_H \left(1 - \frac{d\epsilon}{d\alpha}\right) \quad 2.16$$

It can be appreciated from this equation how the wing and fuselage has a destabilizing effect while the tail has a stabilizing one. To illustrate this better, **Figure 10** shows separately the contribution of the discussed parts of the airplane.

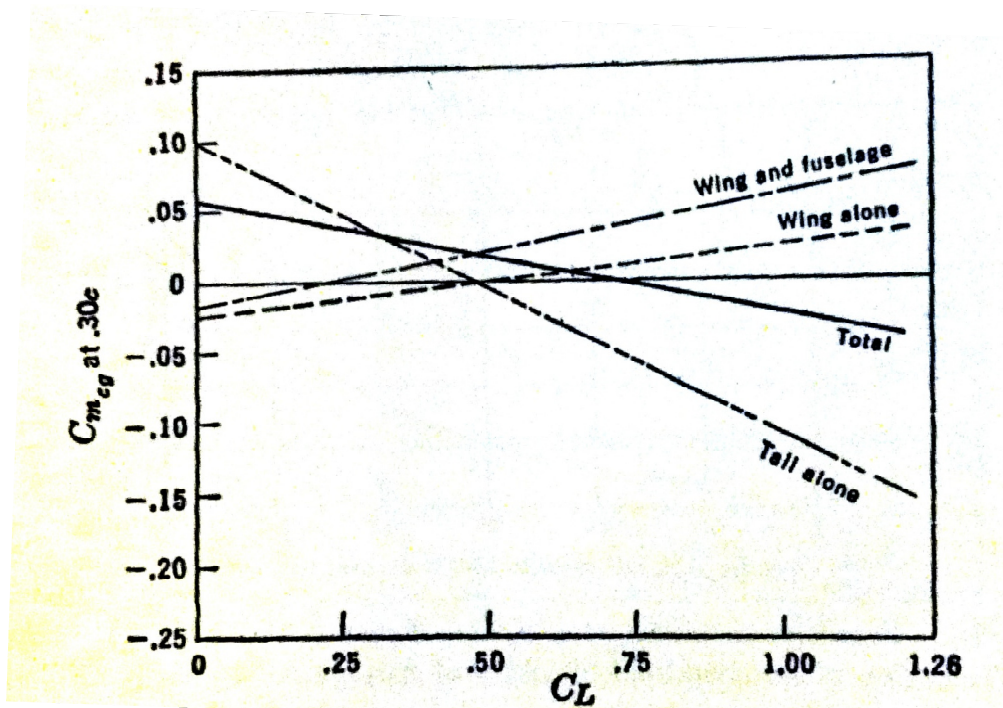


Figure 10: Typical longitudinal stability breakdown (Perkins & Hage, 1949)

After a close examination of the stability equation, it is evident that for a completed airplane the stability contribution of the tail and fuselage is fixed, but the contribution of the wing varies as the airplane's $c.g.$ varies. This variation causes the slope of the pitching moment curve $\left(\frac{dC_m}{dC_L}\right)$ to become more positive as the airplane's $c.g.$ moves aft. When this slope is zero, the airplane is said to be neutrally stable, and this state dictates the most aft position, or neutral point, which the airplane $c.g.$ could afford before becoming unstable.

Remembering that $x_a = x_{cg} - x_{ac}$ (Figure 6), the calculation of the neutral point is performed by equating equation 2.16 to zero and solving for \bar{x}_{cg} in percentage of mean aerodynamic chord.

$$N_0 = \bar{x}_{ac} - \frac{(dM/d\alpha)_{Fus.Nac}}{qS_w c a_w} + \frac{a_t}{a_w} \bar{V} \eta_t \left(1 - \frac{d\epsilon}{d\alpha}\right) \quad 2.17$$

2.5. Power Effect

The power effect on the airplane's stability comes from two sources: the effect due to forces within the propeller itself, and the effect due to the interaction of the propeller slip stream with the airplane.

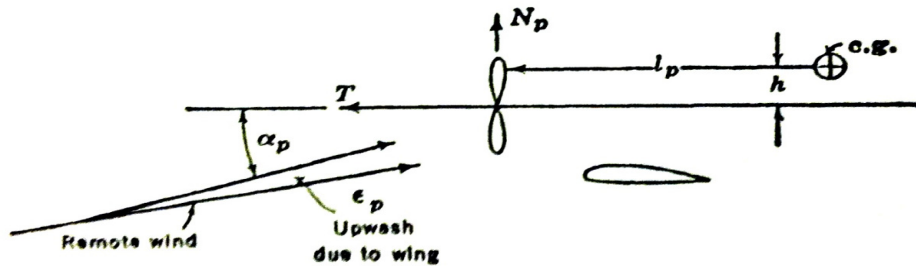


Figure 11: Direct forces cause by propeller (Perkins & Hage, 1949)

2.5.1. Power effect due to forces within the propeller itself

As illustrated in **Figure 11**, the forces responsible for the direct effect from the propeller on the airplane's stability are the thrust force T , with a thrust line at a distance h from the airplane's $c.g.$, and a normal force N_p acting in the plane of the propeller, with a line of action at a distance l_p from the airplane's $c.g.$

$$M_{cgp} = T * h + N_p * l_p \quad 2.18$$

Taking the derivative of equation 2.18 with respect to lift and expressing the result in coefficient form:

$$\frac{dC_{mp}}{dC_L} = \frac{dT_c}{dC_L} \frac{2D^2 h}{S_w c} + \frac{dC_{Np}}{dC_L} \frac{l_p S_p}{S_w c} \quad 2.19 \text{ (Perkins \& Hage, 1949)}$$

To find the thrust coefficient derivative with respect to lift, we need to express the thrust coefficient as a function of lift. From the vertical forces' equilibrium equation for unaccelerated level flight, the speed of the airplane can be written as a function of lift. Doing this and writing the thrust T in a break horse power form, $550Bhp\eta_p$, the coefficient of trust can be written as:

$$T_c = \frac{550Bhp\eta_p C_L^{\frac{3}{2}} \rho^{\frac{1}{2}}}{(2W/S)^{\frac{3}{2}} D^2} \quad 2.20$$

therefore its derivative with respect of lift coefficient is:

$$\frac{dT_c}{dC_L} = \frac{3}{2} \frac{550Bhp\eta_p C_L^{\frac{1}{2}} \rho^{\frac{1}{2}}}{(2W/S)^{\frac{3}{2}} D^2} \quad 2.21$$

$$dC_{mp}dC_L = dT_c dC_L \frac{2D^2 h}{S_w c} + dC_{Np} dC_L \frac{l_p S_p}{S_w c}$$

2.19, it can be seen how the contribution of thrust to stability mainly depends on the position of the thrust line with respect to the airplanes center of gravity $\left(\frac{h}{c}\right)$. This effect is stabilizing for thrust-lines above c.g. and destabilizing for thrust-lines bellow c.g.

The contribution of the propeller normal force to the airplane stability can be estimated by taking the derivative with respect to lift of the normal force at the propeller. To do this, this derivative is expressed as the variation of propeller normal force with propeller angle $\left(\frac{dC_{Np}}{d\alpha_p}\right)$, multiplied by the variation of propeller angle of attack with lift $\left(\frac{d\alpha_p}{dC_L}\right)$.

Expressing the last term as a function of downwash at the propeller, the resulting equation is:

$$\left(\frac{dC_{Np}}{dC_L}\right)_{Np} = \frac{\left(\frac{dC_{Np}}{d\alpha}\right)_p \left(1 + \frac{d\epsilon}{d\alpha}\right) l_p S_p}{S_w c a_w} \quad 2.22$$

as it is depicted in equation 2.22, the contribution of the propeller normal force depends mainly on the horizontal distance of the propeller to the airplane's c.g. This contribution is stabilizing for pushing propellers, and destabilizing for pulling propellers.

Besides the direct contribution to the airplane stability from forces within the airplane's power plant, the indirect contributions due to the interaction of the propeller slipstream is also important. This contribution will be studied next.

2.5.2. Power effect due to the interaction of the propeller slip stream with the airplane

There are four mayor consequences of the interaction of the propeller slipstream with the airplane, the change in pitching moment contribution from the wing and fuselage, the change of lift coefficient from the wing, the change of downwash at the tail, and the change of the dynamic pressure at the tail. Since the effect of the propeller slipstream on the

wing and fuselage is small in comparison of the effect in the tail, these effects will be neglected.

Writing the tail efficiency as a function of the change in dynamic pressure $\left(\frac{v_s}{v}\right)^2$, and differentiating the generalized tail term from the equilibrium equation (eq 2.2), the contribution of this term to stability can be written as follows:

$$\left(\frac{dC_{m_t}}{dC_L}\right)_t = -\frac{dC_{L_t}}{dC_L} \bar{V} \left(\frac{v_s}{v}\right)^2 - C_{L_t} \bar{V} \frac{d(v_s/v)^2}{dC_L} \quad 2.23$$

Including the downwash caused by the wing and the propeller, equation 2.23 can be rewritten as follows:

$$\left(\frac{dC_{m_t}}{dC_L}\right)_t = -\frac{a_t}{a_w} \bar{V} \left(1 - \frac{d\epsilon}{d\alpha} - \frac{d\epsilon_p}{d\alpha}\right) \left(\frac{v_s}{v}\right)^2 - C_{L_t} \bar{V} \frac{d(v_s/v)^2}{dC_L} \quad 2.24$$

Analyzing the first term of equation 2.24, the contribution to stability of the propeller downwash $\left(\frac{d\epsilon_p}{d\alpha}\right)$ is evident. It can be shown that the variation of the propeller downwash with angle of attack is a function of thrust and the force at the propeller. The value of this variation can be evaluated from charts developed by (Ribner, 1942). Since this value is always positive, its contribution is destabilizing. The contribution to stability due to the variation of the propeller slipstream dynamic pressure is also embedded in this term with $\left(\frac{v_s}{v}\right)^2$.

$$dC_{Np}dC_{LNp} = dC_{Np}d\alpha p_1 + d\epsilon d\alpha p S p S w c a w$$

2.22, the variation of the propeller slipstream dynamic pressure with coefficient of lift also contributes to stability. Since this parameter is always positive, the final contribution of the second term to stability will depend on the load at the tail. If the tail has a positive or upward lift the effect will be stabilizing, whereas if the tail has a negative or downward lift its effect will be destabilizing.

2.5.3. Elevator angle versus equilibrium lift coefficient

A stable airplane will always tend to fly at its equilibrium lift coefficient, or corresponding equilibrium wind speed. This is because in a stable condition, or negative pitching moment curve slope, an increase in angle of attack or lift (reduction of speed), is accompanied by a negative pitching moment that will bring the airplane back to the equilibrium angle of attack, or lift coefficient. This means that in order to change an airplane flight speed its equilibrium lift coefficient needs to be change as well. This is what the elevator control is for. The elevator deflection changes the stabilizer effective angle of attack, therefore changing the pitching moment contribution of the tail. The variation of the airplane pitching moment with elevator deflection (elevator power, or $C_{m\delta}$) can be estimated with the following equation:

$$\frac{dC_m}{d\delta_e} = - \left(\frac{dC_L}{d\alpha} \right)_t \bar{V} \eta_t \frac{d\alpha_t}{d\delta_e} \quad 2.25$$

where $\frac{d\alpha_t}{d\delta_e}$ is the variation of the horizontal stabilizer effective angle with elevator deflection.

This parameter is a function of the ratio of the elevator area to the stabilizer area, and it is

obtained from empirical charts. The equation of the elevator angle required for equilibrium lift coefficient can be written as follows:

$$\delta_e = \delta_{e0} + \frac{d\delta_e}{dC_L} C_L \quad 2.26$$

Adding to the propeller-off equilibrium equation the change in effective angle of attack at the tail due to the elevator deflection, it can be shown that the elevator deflection required to vary the equilibrium lift coefficient is directly proportional to the stick-fix longitudinal stability, and inversely proportional to the elevator power:

$$\delta_e = \delta_{e0} + \frac{dC_m/dC_L}{C_{m\delta}} C_L \quad 2.27$$

Considering that for a finished airplane the elevator power is constant, the slope of the elevator-deflection-required curve only depends on the airplane stick-fix longitudinal stability or cg position of the airplane. This property is used to experimentally determine the neutral point of the airplane by varying the c.g. position of the airplane during flight until the elevator deflection curve slope vanishes.

2.6. *Literature Review Summary*

As this section has explained, the static longitudinal stability of an airplane can be studied analytically and experimentally. Both methods are built from the same theoretical background and complement each other in the sense that a final reliable conclusion can't be achieved without an experimental validation and experiments can't be appropriately carried-out, nor its result interpreted, without analytical knowledge. This section's main purpose was

to describe an alternative approach to determine the stability characteristics of an airplane, and also has served to lay out the theoretical background needed to understand both: the alternative approach and the approach described in the rest of this paper.

3. Preliminary Calculations

Knowledge of lift, drag, pitching moment, and other relevant characteristics of an airplane, is required for an airworthiness analysis. Because data of these characteristics was not available or not thorough for the airplane under consideration, the first part of this project was dedicated entirely to obtaining this information analytically. The analysis started with the airfoil, continued with the wing and finished with the airplane.

3.1. Airfoil Lift and Drag

Two airfoils were studied and compared for the modified KR2 wing: the original airfoil, RAF42, and the AS5046 airfoil. With a maximum t/c ratio of 15%, the original RAF48 airfoil was design and used during WWI (Anderson, 1978). There is not much information about this airfoil except for a sparse collection of C_l/C_d data (Langford, 1997). On the other hand, the AS5046 is a relatively new airfoil and has a maximum t/c ratio of 16%. This airfoil was designed by Dr. Ashok Gopalarathnam in 1998.

Both airfoils' lift vs. angle of attack, and drag curves were built for cruise condition (180 mph at 15000 feet elevation) using Xfoil (Drela & Youngren, 2001) at the following Reynolds and Mach number: $3.24E+06$ Re, 0.188 M.

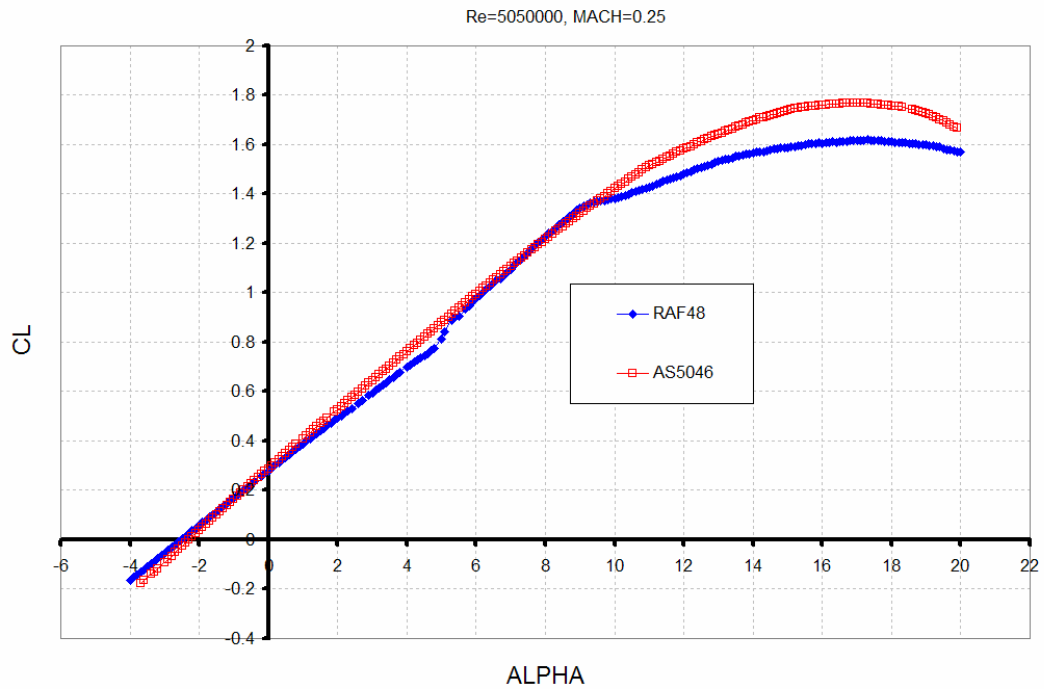


Figure 12: CL- α Curve Comparison – plotted with *Xfoil* (Nordin, 2006)

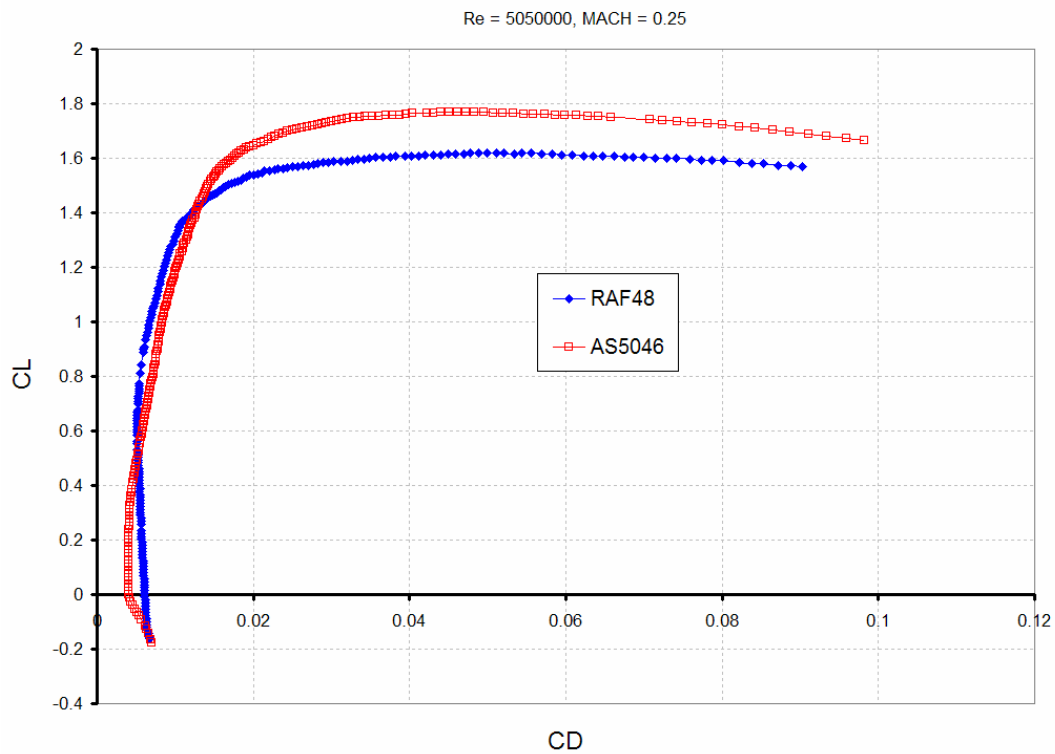


Figure 13: Drag Polar Comparison – plotted with *Xfoil* (Nordin, 2006)

As one can see in Figure 12 & 13 the AS5046 airfoil performs well at low speeds, but its performance at cruise speed is poor in comparison with the performance of the RAF48. Since most of the operating conditions of the modified airplane would be at cruise speed, or low C_l , the RAF48 airfoil is recommended, and the rest of the analysis will be done assuming this will be the airfoil of the airplane studied.

Several parameters were obtained from the Xfoil analysis. These parameters are tabulated next, and will be used in the formulation of the wing's lift distribution in the next section.

Table 2: Airfoil lift and drag parameters

α_{0l}	$C_{l\alpha}$	α^*	C_l^*	α_{clmax}	C_{lmax}	C_{do}	C_{mo}	dc_m/dc_L
-2.5	0.105	9.5	1.487	17	1.561	0.0071	-0.0469	0.007

In this table, α_{0l} is the angle of attack at zero lift coefficient, $C_{l\alpha}$ is the lift curve slope, α^* and C_l^* are the linear limit of the lift vs. angle of attack curve, α_{clmax} is the angle of attack at maximum lift coefficient or stall angle, C_{lmax} is the maximum lift coefficient, C_{do} is the skin and pressure drag coefficient at zero angle of attack, C_{mo} is the pitching moment coefficient at zero angle of attack, and last but not least, dc_m/dc_L is the pitching moment – lift coefficient gradient.

3.2. *Wing Lift and Drag*

Using as input the airfoil lift parameters previously found, the wing lift parameters for cruise condition were found by solving the Trailing Vortices Equations in Matlab. To estimate $C_{L\alpha_w}$, α_{0L_w} , the code was run over the linear range of angle of attacks. The local lift

coefficients, and overall lift coefficient were obtained, and the wing's lift coefficient distribution was tabulated and plotted as follow:

$$C_{L(1,3,5,7)} = \{0.6253, .5369, 0.3812, 0.3240\}$$

$$C_{L,W} = 0.5143$$

$$C_{Di,W} = 0.0138$$

Table 3: Tabulation of Lift Coefficient Distribution for Level Flight (Nordin, 2006)

x/s	i	s (in)	c (in)	$CL\phi$
1.00	8	-142.0	36.00	0
0.96	7	-136.3	36.77	0.324
0.85	5	-120.7	38.64	0.381
0.50	3	-71.0	44.60	0.537
0.00	1	0.0	48.00	0.625
0.50	3	71.0	44.60	0.537
0.85	5	120.7	38.64	0.381
0.96	7	136.3	36.77	0.324
1.00	8	142.0	36.00	0
Wing Lift Coef.			CLw	0.514
Wing Induced Drag Coef.			CDiw	0.014

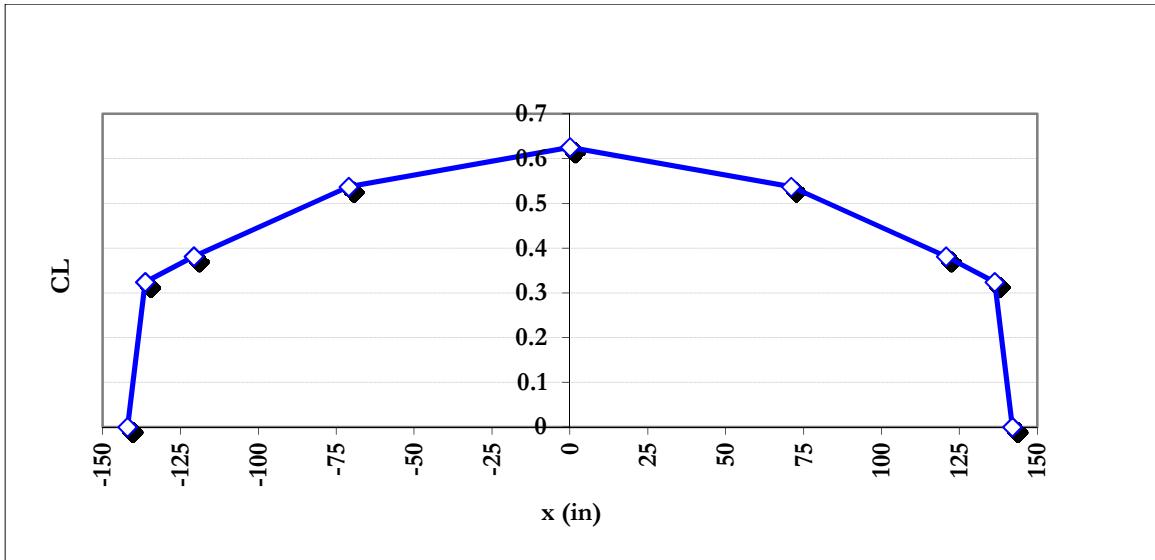


Figure 14: Lift Coefficient Distribution for Level Flight (Nordin, 2006)

As outlined in *Roskam Airplane Design Part VI* (Roskam, Airplane Design, Part I - VIII, 1990), and illustrated in Figure 15, the maximum lift coefficient for the wing, C_{Lmaxw} , is determined by obtaining the local C_{Lmax} at each wing station, and plotting these against the wing lift distribution curve. C_{Lmaxw} is found by increasing α for the trailing vortices solution, until the wing lift distribution curve reaches the local C_{lmax}

Table 4: Local $C_{L,MAX}$ for wing sections

chord [m]	1.31	1.11	0.91
C_{Lmax}	1.59	1.56	1.53
Re	3.81	3.24	2.65

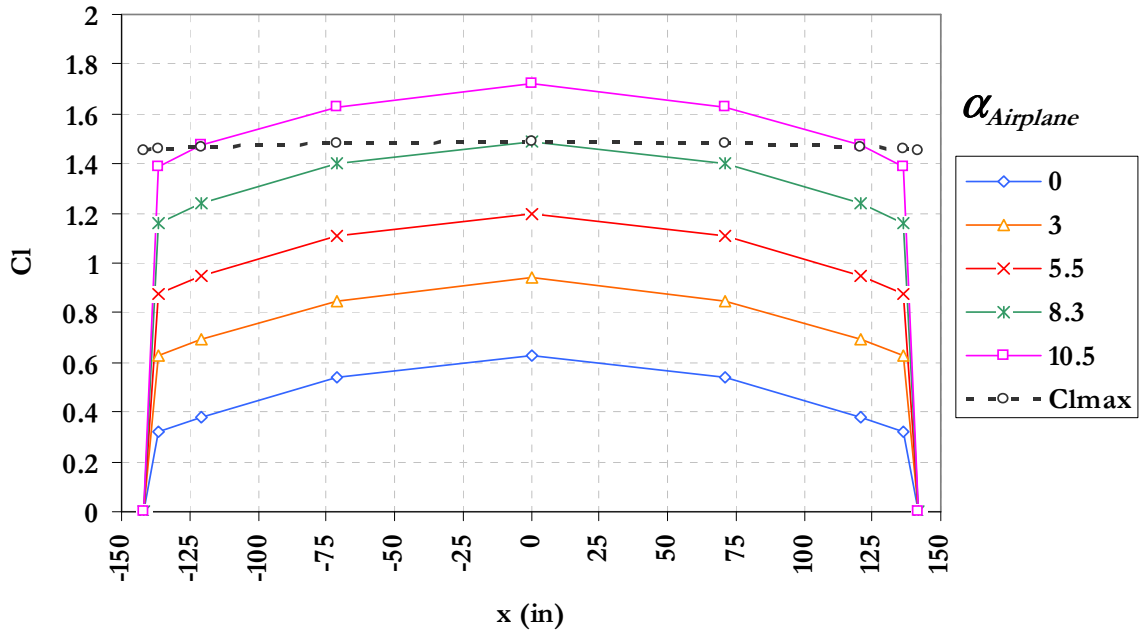


Figure 15: Local wing lift coefficient distribution for varying angle of attack (Nordin, 2006)

In this manner, the wing lift and drag parameters were found and tabulated as shown in

Table 5: Wing lift and drag parameters, where α_{0LW} is the angle of attack at zero lift

coefficient, $C_{L\alpha_w}$ is the wing lift curve slope, α_w^* is the linear limit of the lift vs. angle of

attack curve, α_{cLmax_w} is the angle of attack at maximum lift coefficient or stall angle, C_{Lmax_w} is

the maximum lift coefficient, C_{dio} is the induced drag coefficient at zero angle of attack.

Table 5: Wing lift and drag parameters

α_{0LW}	$C_{L\alpha_w}$	α_w^*	α_{cLmax_w}	C_{Lmax_w}	C_{dio}
-1.5	5.86	10	12	1.385	0.014

These parameters were used to build the wing lift vs. angle of attack curve.

As it is shown in Figure 16, $C_{L\alpha_w}$ and α_{cLmax_w} have been reduced due to the downwash.

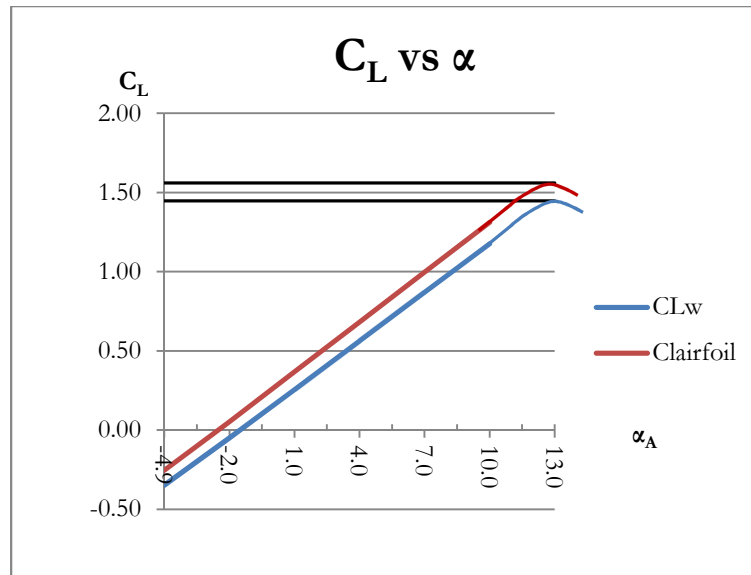


Figure 16: Wing lift vs. angle of attack

3.3. Airplane Lift and Drag

The wing is not the unique lifting part in an airplane; the tail and fuselage also generate some lift. The effect of these components is to slightly increase the airplane maximum lift and, as will be studied later, significantly alter the airplanes stability. The drag contribution of these and other components will also be study.

3.3.1. Airplane Lift

The calculation of the parameters needed to build the airplane lift and pitching moment curve is described in this section. The wing incident angle (i_w) and the stabilizer incident angle (i_h) will be used in this section. These angles are constant for the studied airplane. The assumption was made that control surface angles, such as the elevator deflection (δ_e), are zero.

3.3.1.1. Airplane zero-angle-of-attack lift coefficient, C_{Lo}:

The lift coefficient when the airplane's angle of attack is zero can be estimated as follow:

$$C_{L_o} = C_{L_{o_{wf}}} + C_{L_{\alpha_h}} \eta_h (S_h/S) (i_h - \epsilon_{o_h}) \quad 3.1$$

where:

- i_h is the stabilizer implant angle.
- S_h is the stabilizer area.
- ϵ_{o_h} is the downwash angle at the tail for airplane zero angle of attack.
- $C_{L_{o_{wf}}}$ is the wing-fuselage lift coefficient at zero lift, and is equal to:

$$C_{L_{o_{wf}}} = \{i_w - \alpha_{o_{Lw}}\} C_{L_{\alpha_{wf}}} \quad 3.2$$

where:

- $\alpha_{o_{Lw}}$ is found from Table 5.
- $C_{L_{\alpha_{wf}}}$ is estimated from equation 3.11
- $C_{L_{\alpha_h}}$ is the tail lift curve slope calculated as:

$$C_{L_{\alpha_h}} = 2\pi A_h / \left[2 + \left\{ (A_h^2 \beta^2 / k^2) \left(1 + \tan^2 \Lambda_{c/2} / \beta^2 \right) + 4 \right\}^{1/2} \right] \quad 3.3$$

where:

- A_h is the tail's aspect ratio as described in 0,

$$\beta = (1 - M^2)^{\frac{1}{2}} \quad 3.4$$

$$k = (c_{l\alpha})_{@M} / (2\pi/\beta) \quad 3.5$$

where $(c_{l\alpha})_{@M}$ is calculated with the following equation:

$$(c_{l\alpha})_{@M} = (c_{l\alpha})_{@M=0} / (1 - M^2)^{\frac{1}{2}} \quad 3.6$$

- $\Lambda_{c/2}$ is the semi-chord sweep angle of the horizontal stabilizer as illustrated in [Figure 43](#),

- η_h is the efficiency of the tail.

The wing and fuselage drag produce kinetic energy losses on the free stream. Due to these losses, and also because of the alteration of the dynamic pressure by the propeller on the propeller slipstream, the free stream dynamic pressure \bar{q} differs from the dynamic pressure at the tail. Therefore the efficiency of the tail is defined as $\eta_h = \bar{q}_h / \bar{q}$, and can be approximated as follows:

$$\eta_h = 1 + S_{hslip} / S_h * [(2200 P_{av}) / \{(\bar{q} U^2 \pi (D_p)^2)\}] \quad 3.7$$

where: S_{hslip} is the area of the tail submerged in the propeller slipstream, $U1$ is the free stream speed, D_p is the propeller diameter in ft, P_{av} is the available horse power.

The available horse power is equal to:

$$P_{av} = \{(\eta_{inl/inc} SHP_{av} - P_{extr}) \eta_p\} \eta_{gear} \quad 3.8$$

where: η_{gear} is the transmission efficiency, η_p is the efficiency of the propeller, P_{extr} is the power losses in electronics $\eta_{inl/inc}$ is the inlet lost coefficient, SHP_{av} is the available shaft horse power. The available shaft horse power is obtained from the manufacturer's engine performance charts and adjusted for altitude as follows:

$$SHP_{avh} = SHP_{avs} * P_h / 29.92 * \text{sqr}((273+15)/(273+t_h)) \quad 3.9$$

where SHP_{avs} is the shaft horse power available at standard test conditions, and P_h and t_h are the pressure and temperature at altitude respectively.

3.3.1.2. Airplane lift curve slope, $C_{L\alpha}$:

The variation of lift with airplane angle of attack may be calculated from:

$$C_{L\alpha} = C_{L\alpha_{wf}} + C_{L\alpha_h} * \eta_h (S_h/S) (1 - d\varepsilon/d\alpha) \quad 3.10$$

where: $C_{L\alpha_{wf}}$ is the wing-fuselage interference factor estimated by:

$$C_{L\alpha_{wf}} = K_{wf} C_{L\alpha_w} \quad 3.11$$

where: $C_{L\alpha_w}$ is found from Table 5, K_{wf} is the wing-fuselage interference factor given by:

$$K_{wf} = 1 + 0.025(d_f/b) - 0.25(d_f/b)^2 \quad 3.12$$

with d_f defined as the fuselage diameter $\sqrt{\frac{4}{\pi} * S_{fus}}$ (Roskam, Airplane

Design, Part I - VIII, 1990, p. 45) VI

$d\varepsilon/d\alpha$ = downwash gradient at the tail and equal to 0.35 for similar airplanes (Anderson, 1978).

All other quantities were defined in section 3.3.1.1. These parameters were tabulated as follows, and the airplane's lift vs. alpha curve was built.

Table 6: Airplane lift parameters

α_{0L}	C_{L0}	$C_{L\alpha}$	$\alpha^*_A = \alpha^*_w - i_w$	α_{CLmax}	C_{Lmax}
-4.908	0.5105	5.959	6.5	9.1	1.448

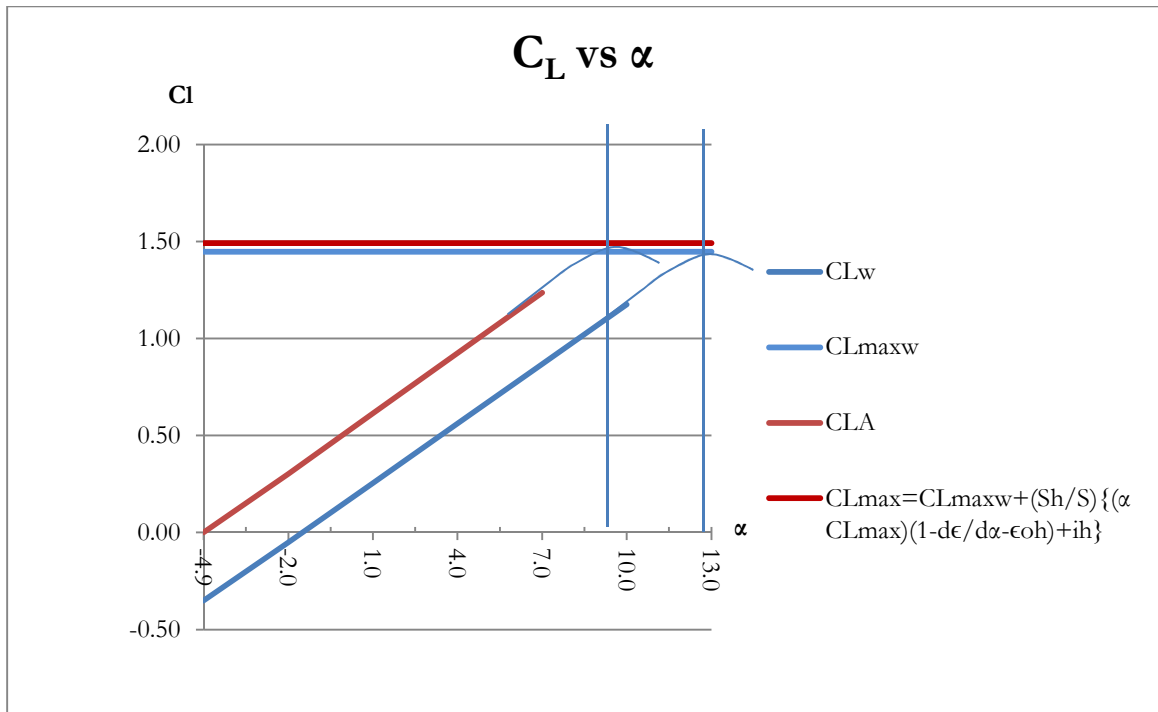


Figure 17: Airplane and wing lift vs. alpha curves

As can be observed in **Figure 17**, due to the contribution of the tail, the airplane maximum lift is slightly bigger than the wing maximum lift. The components studied in this section also contribute to the airplane drag. The study of this contribution comes next.

3.3.2. Airplane Drag

To determine the airplane's drag, a Class II drag polar methodology was followed, as described by Roskam (Roskam, Airplane Design, Part I - VIII, 1990). This methodology consists of estimating the drag contribution from the wing, fuselage, empennage, landing gear, canopy, and miscellaneous components, for a range of air speed where the airplane is expected to operate. For the studied airplane the range was from 5 to 225 m/hr. Equation

3.13 is the sum of all these drag contributions.

$$C_D = C_{D_{WING}} + C_{D_{FUSELAGE}} + C_{D_{EMPENNAGE}} + C_{D_{LANDING\ GEAR}} + C_{D_{CANOPY}} + C_{D_{MISC}} \quad 3.13$$

3.3.2.1. Wing Drag Coefficient Prediction, $C_{D_{WING}}$:

For subsonic flight, the wing drag coefficient is equal to:

$$C_{D_{WING}} = C_{D_{0W}} + C_{D_{LW}} \quad 3.14$$

where: $C_{D_{LW}}$ is the wing drag coefficient due to lift or induced drag ($C_{D_{iW}}$) found from the trailing vortices solution in section 3.2, and $C_{D_{0W}}$ is the zero-lift drag coefficient estimated from:

$$C_{D_{0W}} = R_{wf} R_{LS} c_{fw} \left\{ 1 + L'(t/c) + 100(t/c)^4 \right\} S_{wet_w} / S \quad 3.15$$

where:

- R_{wf} is the wing/fuselage interference factor found from (Roskam, Airplane Design, Part I - VIII, 1990) VI Figure 4.1.
- R_{LS} is the lifting surface correction factor found from (Roskam, Airplane Design, Part I - VIII, 1990) VI Figure 4.2.
- L' is the airfoil thickness location parameter as defined in from (Roskam, Airplane Design, Part I - VIII, 1990) VI Figure 4.4.

- t/c is the wing thickness ratio as defined in (Roskam, Airplane Design, Part I - VIII, 1990) VI Figure 4.5.
- S_{wet_w} is the wetted area of the wing as defined in (Roskam, Airplane Design, Part I - VIII, 1990) VI Figure 4.6 and Appendix B.
- c_{f_w} is the turbulent flat plate friction coefficient found from (Roskam, Airplane Design, Part I - VIII, 1990) VI. Because c_{f_w} is a function of Mach and Reynolds numbers (velocity), in order to calculate this coefficient for several speed values, an analytical function of c_{f_w} had to be built by interpolation. Figure 18 below is the plot of such a function using a Matlab script.

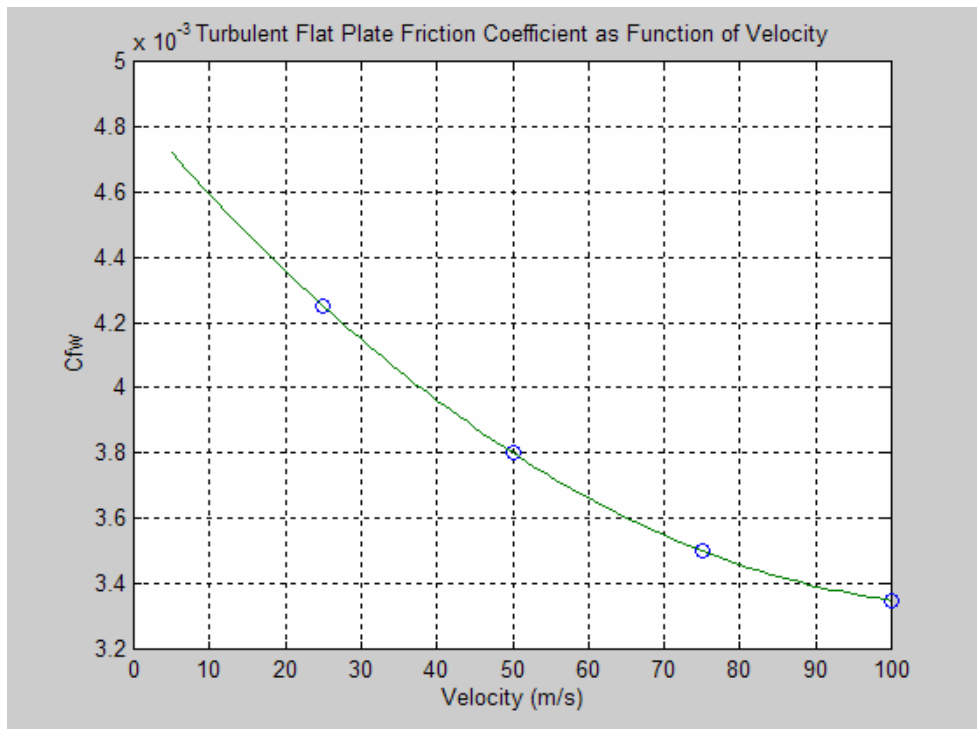


Figure 18: Turbulent Flat Plate Friction Coefficient as Function of Velocity (Nordin, 2006)

3.3.2.2. Fuselage Drag Coefficient Prediction, $C_{D_{FUSELAGE}}$:

As with the wing, the drag coefficient contribution of the fuselage can be divided in two components:

$$C_{D_{FUS}} = C_{D_{0_{FUS}}} + C_{D_{L_{FUS}}} \quad 3.16$$

where:

- $C_{D_{0_{FUS}}}$ is the zero-lift drag coefficient which can be estimated from:

$$C_{D_{0_{FUS}}} = R_{wf} C_{f_{FUS}} \left\{ 1 + 60 \left(l_f / d_f \right)^3 + 0.0025 \left(l_f / d_f \right) \right\} S_{wet_{FUS}} / S + C_{D_{b_{FUS}}} \quad 3.17$$

where:

- R_{wf} is the wing/fuselage interference factor, found in (Roskam, Airplane Design, Part I - VIII, 1990) VI Figure 4.1.
- l_f is the fuselage length as defined in (Roskam, Airplane Design, Part I - VIII, 1990) VI Figure 4.17.
- d_f is the maximum fuselage diameter, or equivalent diameter for non circular fuselages, as described in (Roskam, Airplane Design, Part I - VIII, 1990) VI Figure 4.17

- $S_{wet_{FUS}}$ is the wetted area of the fuselage, as described in (Roskam, Airplane Design, Part I - VIII, 1990) VI Figure 4.17 and (Roskam, Airplane Design, Part I - VIII, 1990) VI Appendix B.
- $C_{D_{b_{FUS}}}$ is the fuselage base drag coefficient as defined in (Roskam, Airplane Design, Part I - VIII, 1990) VI pg 46. Since the studied fuselage has no base, this coefficient is zero for the KR2.
- $C_{f_{FUS}}$ is the turbulent flat plate skin-friction coefficient of the fuselage, established from (Roskam, Airplane Design, Part I - VIII, 1990) VI Figure 4.3. As with the wing, $C_{f_{FUS}}$ is a function of velocity. In order to calculate this coefficient for several speed values, an analytical function had to be built by interpolation. Figure 19 below is the plot of such a function using a Matlab script.

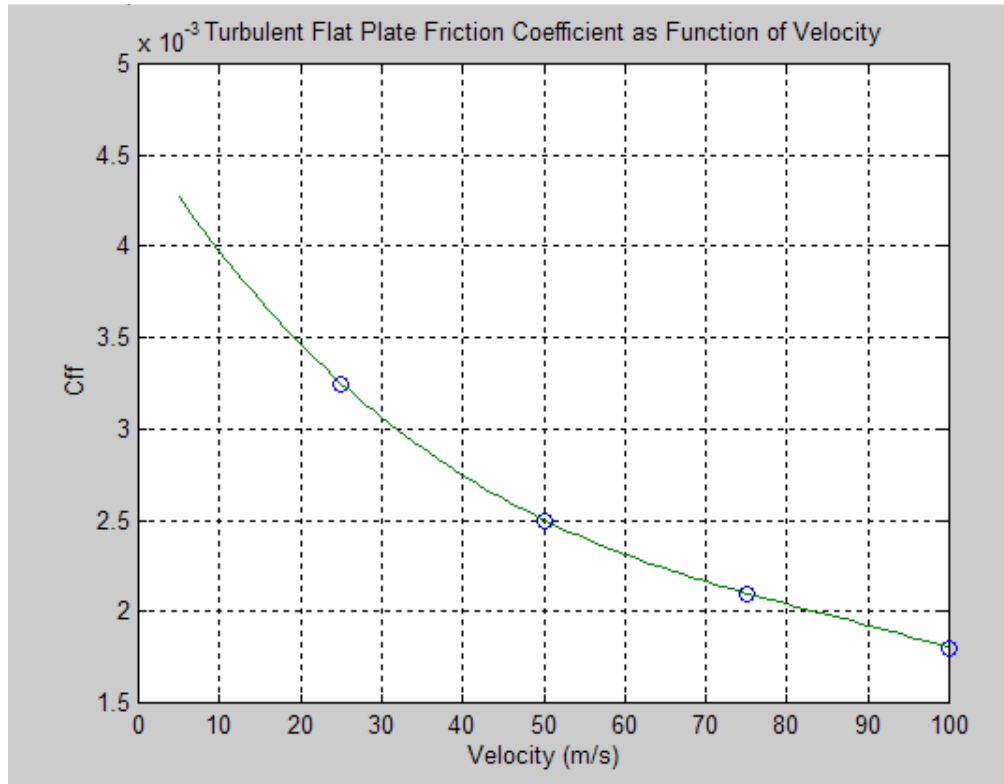


Figure 19: Fuselage Turbulent Flat Plate Friction Coefficient as Function of Velocity (Nordin, 2006)

- $C_{D_{L_{FUS}}}$ is the fuselage drag coefficient due to lift, which can be found with the equation:

$$C_{D_{L_{FUS}}} = \eta c_{d_c} |\alpha|^3 S_{plf_{FUS}} / S \quad 3.18$$

where:

- η is the drag's ratio of a finite cylinder to the drag of an infinite cylinder, established from (Roskam, Airplane Design, Part I - VIII, 1990) VI Figure 4.19.

- c_{d_c} is the circular cylinder's experimental steady state cross-flow drag, found from (Roskam, Airplane Design, Part I - VIII, 1990) VI Figure 4.20.
- $S_{plf_{FUS}}$ is the fuselage plan-projected area, as illustrated in (Roskam, Airplane Design, Part I - VIII, 1990) VI Figure 4.17.

3.3.2.3. Empennage Drag Coefficient Prediction, $C_{D_{EMPENNAGE}}$:

Following the same procedure as with the wing and fuselage, the empennage drag coefficients at zero lift ($C_{D_{0emp}}$), and the empennage drag coefficient due to lift ($C_{D_{Lemp}}$) are calculated separately:

$$C_{D_{emp}} = C_{D_{0emp}} + C_{D_{Lemp}} \quad 3.19$$

The empennage drag coefficient at zero lift is a consequence of the profile drag from the rudder and the stabilizer. These profile drags are calculated using equation 3.15 with the appropriate stabilizer and rudder parameters instead of the parameters of the wing.

The horizontal (or vertical) stabilizer zero-lift drag coefficient is found from:

$$C_{D_{0h}} = R_{LS} c_{f_h} \left\{ 1 + L'(t/c) + 100(t/c)^4 \right\} S_{wet_h} / S_h \quad 3.20$$

all terms have been describe in section 3.3.2.1.

The empennage drag coefficient due to lift is produced by the horizontal stabilizer and was calculated using the following equation:

$$C_{D_{Le mp}} = \left\{ (C_{L_h})^2 / \pi A_h e_h \right\} S_h / S \quad 3.21$$

where:

C_{L_h} is the stabilizer lift coefficient calculated from:

$$C_{L_h} = C_{L_{\alpha_h}} (\alpha_h - \alpha_{0_{L_h}}) \quad 3.22$$

with $\alpha_h = \alpha(1 - d\epsilon/d\alpha) + i_h$

3.3.2.4. Landing Gear Lift Coefficient, CDGear:

The drag coefficient due to the landing gear may be calculated from the following equation:

$$C_{D_{GEAR}} = \sum C_{D_{GEAR_{CL=0}}} S_{GEAR} / S \quad 3.23$$

where:

- $C_{D_{GEAR_{CL=0}}} = 0.565$ as described in (Roskam, Airplane Design, Part I - VIII, 1990)

VI Figure 4.54.

3.3.2.5. Airplane Drag Polar

All drag coefficient parameters calculated previously were tabulated for a speed range of 55 to 163 [mi/hr].

Table 7: Tabulation of Class II Drag Polar for Modified KR-2 (Nordin, 2006)

Velocity	Airplane angle of attack	Airplane lift coef	Wing zero lift drag coef	Wing lift coef	Wing induced drag coef	Wing drag coef	Fuselage zero lift drag coef	Fuselage drag coef due to lift	Fuselage drag coef	horiz. tail zero lift drag coef	Total drag coef	Cl / Cd	Drag	Power Required	Shaft brake horse power
V	alpha	Cl	Cdow	Clw	Cdlw	Cdw	Cdof	Cdlf	Cdf	Cdoh	Cd_total	Glide Ratio	Drag	Power Required	bhp
mi / hr	deg	n/a	n/a	n/a	n/a	n/a	n/a	n/a	n/a	n/a	n/a	n/a	N	HP	HP
55.9	16.8	1.865	0.012	1.958	0.189	0.202	0.007	0.007	0.013	0.011	0.240	7.8	614	21	24
58.2	15.4	1.724	0.012	1.810	0.162	0.174	0.007	0.005	0.012	0.011	0.211	8.2	584	20	24
60.4	14.2	1.574	0.012	1.659	0.135	0.151	0.006	0.004	0.011	0.011	0.187	8.6	558	20	24
62.6	13.1	1.424	0.012	1.508	0.108	0.133	0.006	0.003	0.010	0.010	0.167	8.9	536	20	24
64.9	12.1	1.274	0.012	1.357	0.081	0.117	0.006	0.002	0.009	0.010	0.150	9.2	518	20	24
67.1	11.2	1.295	0.012	1.360	0.091	0.104	0.006	0.002	0.008	0.010	0.136	9.5	503	20	24
69.3	10.4	1.213	0.012	1.273	0.080	0.092	0.006	0.002	0.008	0.010	0.125	9.7	491	20	24
71.6	9.7	1.138	0.012	1.195	0.071	0.083	0.006	0.001	0.007	0.010	0.115	9.9	481	21	24
73.8	9.0	1.070	0.012	1.124	0.063	0.075	0.006	0.001	0.007	0.010	0.106	10.1	474	21	25
76.1	8.4	1.008	0.012	1.059	0.056	0.068	0.006	0.001	0.007	0.010	0.099	10.2	468	21	25
78.3	7.8	0.951	0.012	0.999	0.050	0.061	0.006	0.001	0.007	0.010	0.092	10.3	464	22	26
80.5	7.3	0.899	0.012	0.944	0.044	0.056	0.006	0.001	0.006	0.010	0.087	10.4	461	22	26
82.8	6.9	0.851	0.012	0.894	0.040	0.052	0.006	0.000	0.006	0.010	0.082	10.4	460	23	27
85.0	6.4	0.807	0.012	0.847	0.036	0.047	0.006	0.000	0.006	0.010	0.078	10.4	460	23	28
87.2	6.0	0.766	0.012	0.805	0.032	0.044	0.006	0.000	0.006	0.010	0.074	10.3	462	24	28
89.5	5.7	0.728	0.012	0.765	0.029	0.041	0.006	0.000	0.006	0.010	0.071	10.3	464	25	29
91.7	5.3	0.693	0.012	0.728	0.026	0.038	0.006	0.000	0.006	0.010	0.068	10.2	467	26	30
94.0	5.0	0.661	0.012	0.694	0.024	0.036	0.006	0.000	0.006	0.010	0.065	10.1	472	27	31
96.2	4.7	0.630	0.011	0.662	0.022	0.033	0.005	0.000	0.006	0.010	0.063	10.0	477	27	32
98.4	4.4	0.602	0.011	0.632	0.020	0.031	0.005	0.000	0.006	0.010	0.061	9.9	483	28	34
100.7	4.2	0.576	0.011	0.604	0.018	0.030	0.005	0.000	0.005	0.010	0.059	9.8	490	30	35
102.9	3.9	0.551	0.011	0.578	0.017	0.028	0.005	0.000	0.005	0.010	0.057	9.6	497	31	36
105.1	3.7	0.528	0.011	0.554	0.015	0.027	0.005	0.000	0.005	0.010	0.056	9.5	505	32	37
107.4	3.5	0.506	0.011	0.531	0.014	0.025	0.005	0.000	0.005	0.010	0.054	9.3	514	33	39
109.6	3.3	0.485	0.011	0.510	0.013	0.024	0.005	0.000	0.005	0.010	0.053	9.1	523	34	40
111.9	3.1	0.466	0.011	0.489	0.012	0.023	0.005	0.000	0.005	0.010	0.052	9.0	533	36	42
114.1	2.9	0.448	0.011	0.470	0.011	0.022	0.005	0.000	0.005	0.010	0.051	8.8	543	37	44
116.3	2.7	0.431	0.011	0.453	0.010	0.021	0.005	0.000	0.005	0.010	0.050	8.6	554	39	45
118.6	2.6	0.415	0.011	0.436	0.010	0.021	0.005	0.000	0.005	0.010	0.049	8.4	565	40	47
120.8	2.4	0.400	0.011	0.420	0.009	0.020	0.005	0.000	0.005	0.010	0.048	8.3	577	42	49
123.0	2.3	0.385	0.011	0.405	0.008	0.019	0.005	0.000	0.005	0.010	0.048	8.1	589	43	51
125.3	2.2	0.372	0.011	0.390	0.008	0.019	0.005	0.000	0.005	0.010	0.047	7.9	602	45	53
127.5	2.0	0.359	0.011	0.377	0.007	0.018	0.005	0.000	0.005	0.010	0.046	7.8	615	47	55
129.7	1.9	0.346	0.011	0.364	0.007	0.018	0.005	0.000	0.005	0.010	0.046	7.6	629	49	58
132.0	1.8	0.335	0.011	0.352	0.006	0.017	0.005	0.000	0.005	0.010	0.045	7.4	643	51	60
134.2	1.7	0.324	0.011	0.340	0.006	0.017	0.005	0.000	0.005	0.010	0.045	7.3	657	53	62
136.5	1.6	0.313	0.011	0.329	0.006	0.016	0.005	0.000	0.005	0.010	0.044	7.1	671	55	65
138.7	1.5	0.303	0.011	0.319	0.006	0.016	0.005	0.000	0.005	0.010	0.044	7.0	686	57	67
140.9	1.4	0.294	0.011	0.310	0.006	0.015	0.005	0.000	0.005	0.010	0.043	6.8	702	59	70
143.2	1.3	0.285	0.011	0.302	0.006	0.015	0.005	0.000	0.005	0.010	0.043	6.7	717	62	72
145.4	1.2	0.276	0.011	0.290	0.004	0.015	0.005	0.000	0.005	0.010	0.042	6.5	733	64	75
147.6	1.1	0.268	0.011	0.281	0.004	0.015	0.005	0.000	0.005	0.010	0.042	6.4	750	66	78
149.9	1.1	0.260	0.011	0.273	0.004	0.014	0.005	0.000	0.005	0.009	0.042	6.2	766	69	81
152.1	1.0	0.252	0.010	0.265	0.004	0.014	0.004	0.000	0.004	0.009	0.041	6.1	783	71	84
154.4	0.9	0.245	0.010	0.257	0.004	0.014	0.004	0.000	0.004	0.009	0.041	6.0	801	74	87
156.6	0.9	0.238	0.010	0.250	0.004	0.014	0.004	0.000	0.004	0.009	0.041	5.8	818	77	90
158.8	0.8	0.231	0.010	0.243	0.003	0.013	0.004	0.000	0.004	0.009	0.040	5.7	836	80	94
161.1	0.7	0.225	0.010	0.236	0.003	0.013	0.004	0.000	0.004	0.009	0.040	5.6	854	82	97
163.3	0.7	0.219	0.010	0.230	0.003	0.013	0.004	0.000	0.004	0.009	0.040	5.5	872	85	100

As we can see in Table 7, cruise speed, the speed at 75% of available power, is 135 mph; while the maximum speed, the speed at 100% available power, is 152 mph.

The drag polar was built by cross-plotting C_L versus C_D parameters from Table 7. For validation this curve was compared with the drag polar of similar airplanes (Roskam, Airplane Design, Part I - VIII, 1990, p. 118) VI. It was found to be quite similar to the drag polar of the Cessna 177.

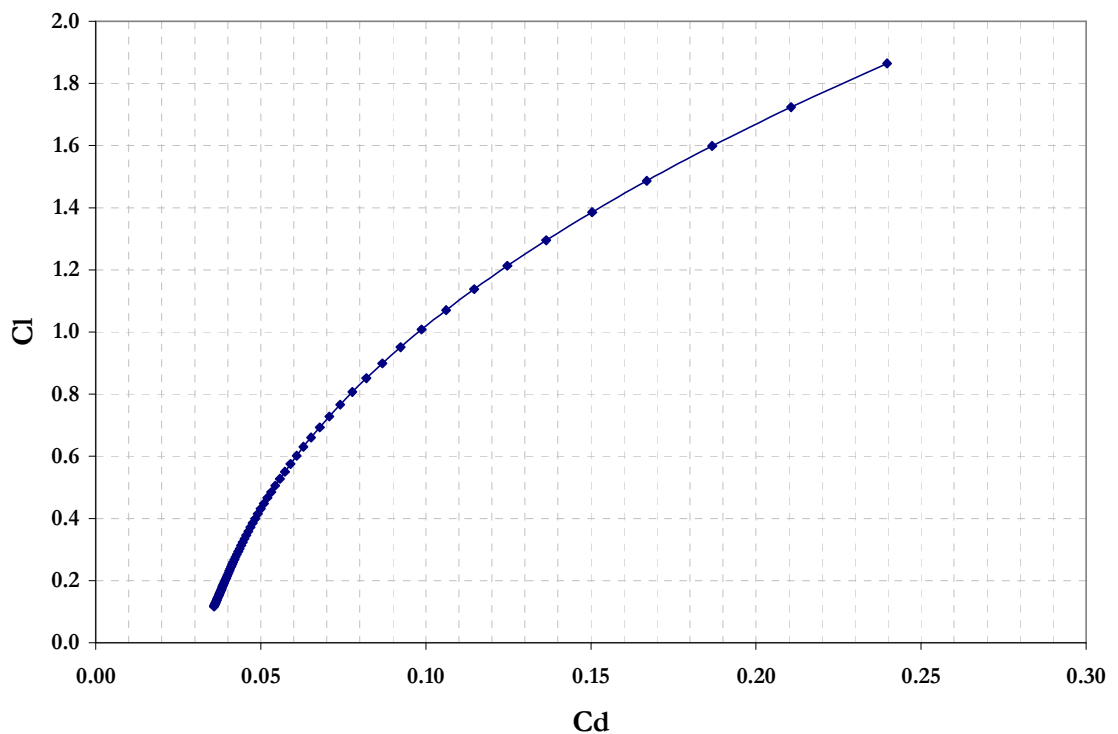


Figure 20: Drag Polar for Modified KR-2 at Gross Weight and at Density Altitude of 6000 Feet (Nordin, 2006)

Now that the airplane lift and drag has been estimated, all the required parameters for estimating the airplane performance are available.

3.4. Airplane Performance

Most performance characteristics of an airplane can be analyzed by determining the thrust or power requirements of an airplane to maintain unaccelerated level flight. At the same speed, the power available also determines descent and climb-rate characteristics of an airplane. The performance characteristics of the modified KR2 were studied by Michael Nordin (Nordin, 2006); his report should be studied, for a thorough review of the modified KR2 performance. Since the KR2 modifications were done to achieve a better performance at high altitudes, this section summarized the study of stall speed and take off distance from (Nordin, 2006).

3.4.1. Stall Speed

As illustrated in 1.1, the stall speed of an airplane is strongly influenced by the maximum lift coefficient and air density. Because the air density is smaller at high altitude, the stall speed will be higher.

Taking in to consideration the trust contribution, the stall speed may be calculated as follow.

$$V_s = \left[2 \frac{\{W - T \sin(\alpha_{C_{Lmax}} + \theta_T)\}}{\{\rho C_{Lmax} S\}} \right]^2 \quad 3.24$$

At maximum power, takeoff weight, and a 6000 ft density of 1.024, the stall speed is:

$$V_s = 26 \text{ m/s (58 mph)}$$

3.4.2. Take off

The lift off distance is calculated at 6000 feet, standard atmosphere. As described by (Anderson, 1978), the lift off distance s_{LO} is given by:

$$s_{LO} = \frac{1.44W^2}{g\rho_{\infty}SC_{L_{MAX}}T} \quad 3.25$$

At full static thrust (Wynne, 2004), takeoff weight, and a 6000 ft density of 1.024, the lift off distance is:

$$s_{LO} = 199 \text{ m (653 ft)}$$

This distance is nearly twice the take off distance for the original KR-2 at sea level (350 ft). This seems reasonable, considering the original KR2 is lighter and the air is thicker at sea level.

3.4.3. Climb

The climb rate for a given speed is defined as the excess power, or power available minus power required, divided by the weight of the aircraft:

$$R/C = \frac{\text{excess power}}{W} = \frac{P_A - P_R}{W} \quad 3.26$$

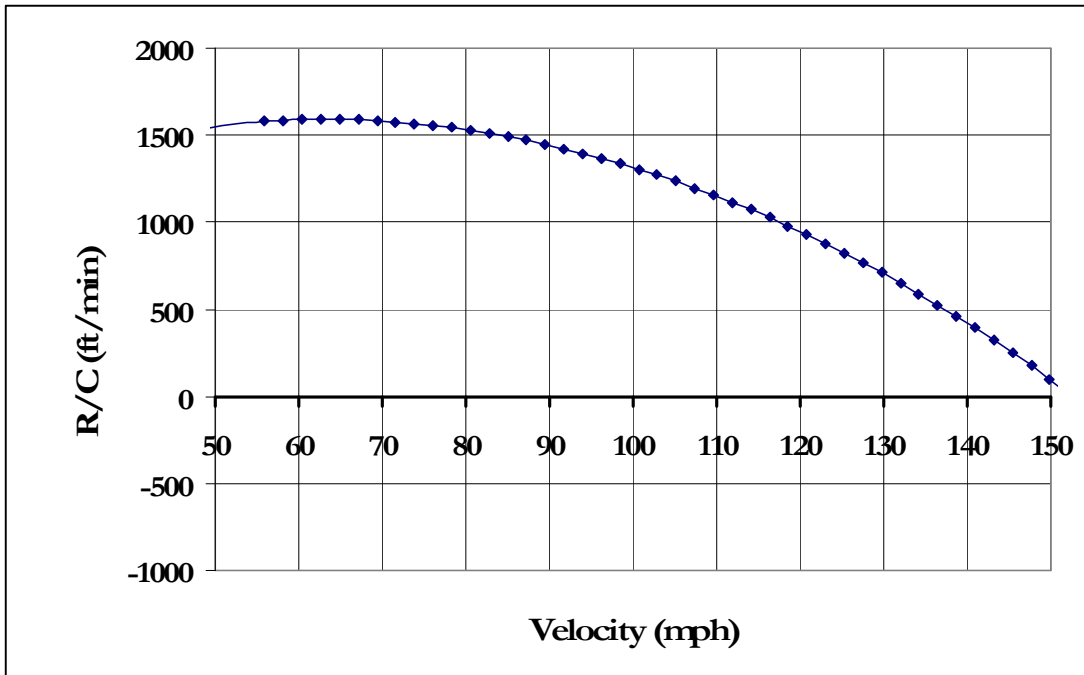


Figure 21: Rate of Climb vs. Velocity, 6000 Ft. Density Altitude (Nordin, 2006)

Since South Lake Tahoe airport has an 8,544 foot long runway, the estimated stall speed, take off, and climb performances suggest the modified KR2 should be capable of taking off from this runway. But, while these performance characteristics have been improved, the airplane cruise speed seems to be 15-20% lower than that for the original KR2. To improve cruise speed, according to (Nordin, 2006, p. 79), “An effort should be made to reduce the weight of the aircraft and to reduce drag where possible.”

Besides analyzing the resulting performance enhancements from the modifications applied to the KR2, it is very important to verify that these modifications haven’t affected the airworthiness of the airplane.

4. Airworthiness Analysis

As mentioned before, a preliminary design Class II method will be followed for the airworthiness study of the modified KR2. The objectives of the method are to assure the airplane is capable of satisfying its mission requirements while complying with the airworthiness regulations.

4.1. Regulations Requirements

The first step for analyzing the airworthiness of an airplane is to get familiar with the airplane's applicable regulations. These regulations depend on the projected use of the airplane. Based on **Table 8** the KR-2 airplane is categorized as a single engine propeller driven airplane. With this information, and

Table 9 it was found that the applicable regulations for the KR-2 are the FAR 23. Because the FAR23 regulations are vague regarding the dynamic longitudinal stability requirements, military regulations will be used when analyzing those requirements.

Table 8: Airplane Types (Roskam, Airplane Design, Part I - VIII, 1990)

1. Homebuilt Propeller Driven Airplanes	7. Transport Jets
2. Single Engine Propeller Driven Airplanes	8. Military Trainers
3. Twin Engine Propeller Driven Airplanes	9. Fighters
4. Agricultural Airplanes	10. Military Patrol, Bomb and Transport Airplanes
5. Business Jets	11. Flying Boats, Amphibious and Float Airplanes
6. Regional Turbopropeller Driven Airplanes	12. Supersonic Cruise Airplanes

Table 9: Relation between airplane type and applicable regulations (Roskam, 1990)

Airplane Type (See Table 1.2)	Passenger Limit	Weight Limit	Regulations
1	none	none	Experimental: FAR 21
2, 3, 4, 5, 11, 12	<9	12,500	Normal Category: FAR 23, Appendix A
3, 6, 7, 12	<19	<19,000	Commuter Category: FAR 23, Appendix A, see page 207
5, 6, 7, 11, 12	>19	none	FAR 25: Appendix A
8, 9, 10	none	none	Military: Appendix B

The applicable regulations for the KR-2, regarding static longitudinal controllability and stability are *FAR 23.143* and *FAR 23.171* respectively. Regulations *FAR23.181* and *MIL-F8785C* will be studied for dynamic longitudinal stability. These regulations require that the airplane must be safely stable, controllable and maneuverable during all flight phases. As illustrated in **Figure 22**, the flight phases for the modified KR2 are: take off, climb, level flight or cruise, descent, and landing.

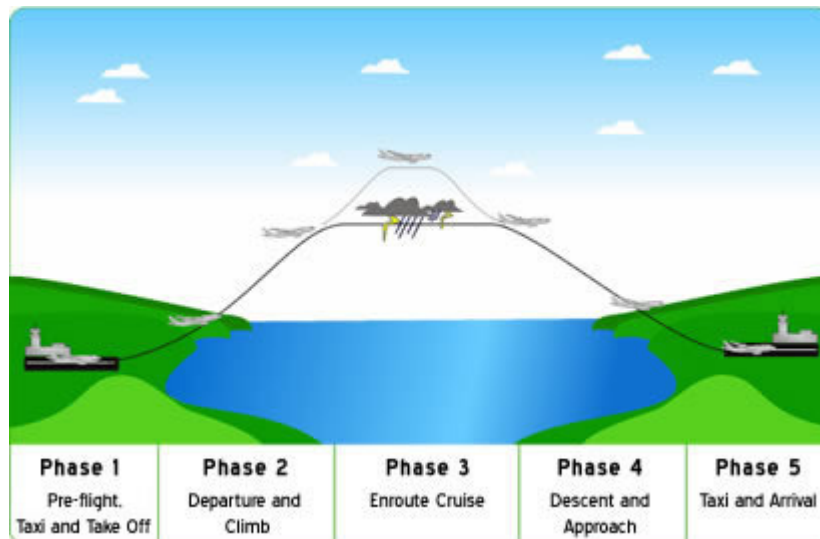


Figure 22: Flight phases

Studying the regulations, the requirement for all flight phases were found and tabulated as follows:

Table 10: Regulation Requirements

Flight Phases	Static Controllability		Static Stability	Dynamic Stability		
	F_s	δ_e	dF_s/dU_{trim}	ξ_p	ω_{nsp}	ξ_{sp}
(1) Takeoff	≤ 60	-28 to 23	< 0	≥ 0.04	3.2 to 15	0.35 to 1.3
(2) Climb	≤ 60	-28 to 23	< 0	≥ 0.04	3 to 13.5	0.3 to 2
(3) Level flight	≤ 60	-28 to 23	< 0	≥ 0.04	5 to 23.5	0.3 to 2
(4) Descent	≤ 60	-28 to 23	< 0	≥ 0.04	3.1 to 14.2	0.3 to 2
(5) Landing	≤ 60	-28 to 23	< 0	≥ 0.04	3.6 to 17	0.35 to 1.3

where F_s is the stick force, δ_e is the elevator angle, dF_s/dU_{trim} is the stick force-trim speed gradient, ξ_p is the phugoid damping ratio, ω_{nsp} is the short period undamped natural frequency, and ξ_{sp} is the short period damping ratio.

4.2. Configurations & Flight conditions

As required by the methodology, configurations and flight conditions were studied and tabulated for all flight phases as follows:

Table 11: Flight conditions

Flight Phases	Altitude [ft]	RE
(1) Takeoff	6000	1.69E+06
(2) Climb	6050-15000	2.03E+06
(3) Level flight	15000	3.24E+06
(4) Descent	15000-6050	2.20E+06
(6) Landing	6000	2.20E+06

Table 12: Flight Configurations

Flight Phases	Weight [lb]	Flap Position	Landing Gear	Engine Status
(1) Takeoff	833, 1073 , 990	up	down	On
(2) Climb	833, 1073 , 990	up	down	On
(3) Level flight	833, 1073 , 990	up	down	On
(4) Descent	833, 1073 , 990	up	down	On
(6) Landing	833, 1073 , 990	up	down	On,Off

Since the studied airplane has fixed landing gears and no flaps, the most critical airplane configuration happens at the most aft and most forward c.g. location.

4.3. Airplane Weight and Balance

To study the *cg* position for all flight phases a weight and balance of the airplane was necessary.

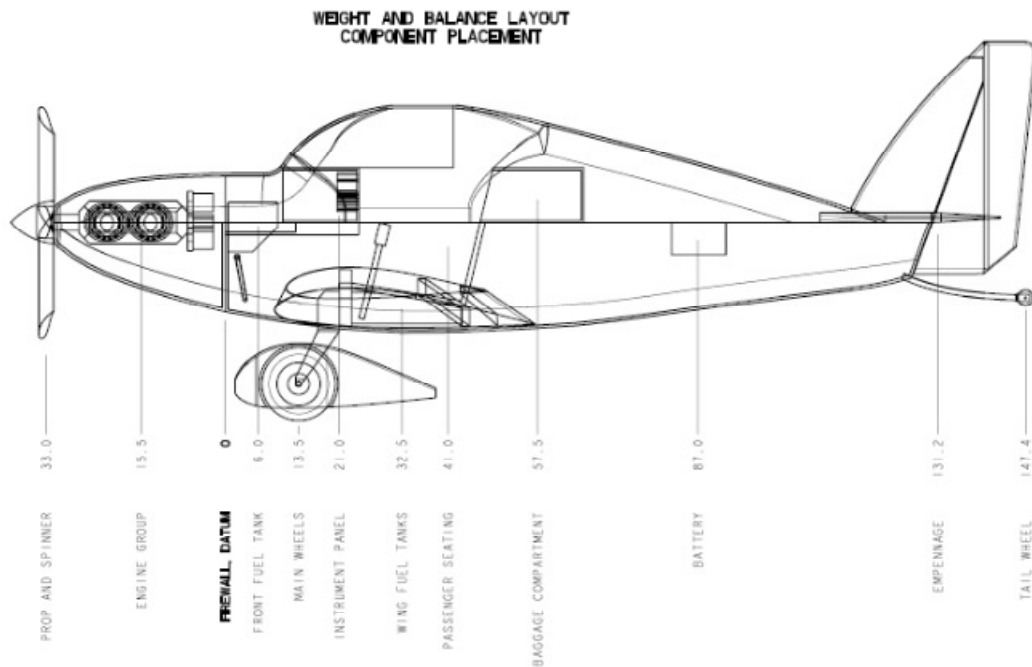


Figure 23: Locations of Major Components for Weight and Balance (Nordin, 2006)

This analysis was achieved by measuring the location and weight of all major components of the airplane as illustrated on [Figure 23](#).

An airplane cg diagram was necessary to study the evolution of the airplane's c.g. position upon different loading configurations.

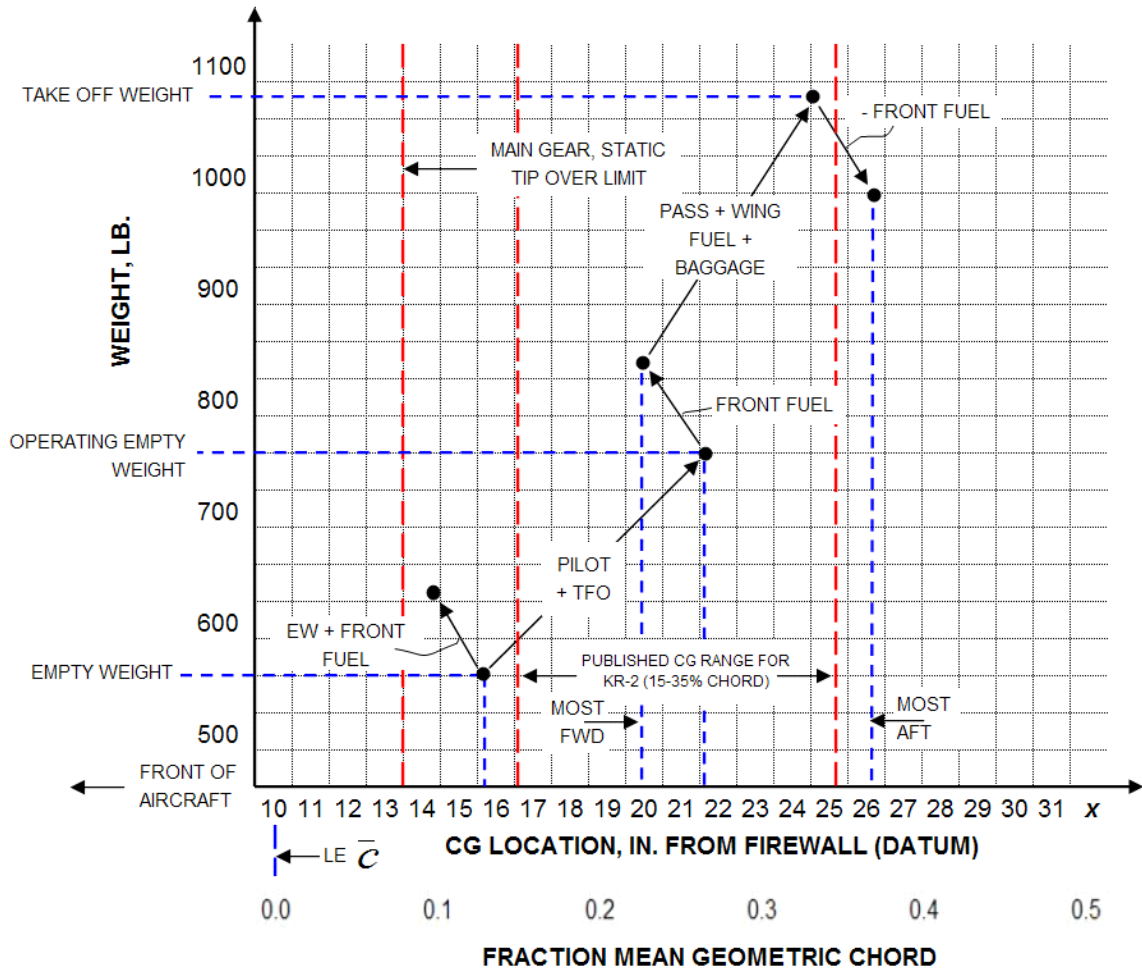


Figure 24: Airplane center of gravity (c.g.) diagram

As we can see in [Figure 24](#) and [Table 13](#), the airplane's cg position at takeoff weight (TOW) is located at 33% of the airplane's mean aerodynamic chord (mac). From this

analysis we can also see that while the most forward position (FRD), 23% of mac, happens at operating empty weight (OEW) plus front fuel load, the most aft position, 37% of mac, happens at TOW minus front fuel load. Therefore the airplane's *cg* range is from 23-37% of mac. The recommended *cg* range for the original KR2 is 15 to 35% of mac. Acknowledging the pitch sensitivity issue of this airplane, the *cg* positions needs to be chosen very carefully. Therefore the most forward *cg* position should be avoided. This could be done by rearranging some major components e.g., battery, or by making sure the airplane consumes the wing fuel before the front fuel.

Table 13: Weight and Balance Calculations and Summary

Empty Weight [kg, lb]	250.2	551.61
Operating Empty Weight (OEW) [kg, lb]	340.3	750.09
Maximum Take Off Weight (TOW) [kg, lb]	487	1073.49
Forward Extreme CG (FRW) [mm, in]	509	20.03
Aft Extreme CG (AFT) [mm, in]	666	26.21
X CG Range [mm, in]	157	6.18
Upper Extreme CG [mm, in]	739	29.09
Lower Extreme CG [mm, in]	712	28.02
Y CG Range [mm, in]	27	1.07
Main Wheel Arm [mm, in]	343	13.5
Mean Geometric Chord Leading Edge [mm, in]	254	10
Mean Geometric Chord Trailing Edge [mm, in]	1367	53.82

Several other important parameters such as: dynamic pressure, q , Mach number, M , were also studied and tabulated for the flight conditions and configurations defined previously.

Table 14: Other flight conditions and configurations

Flight Phases	M	$X_{cg}(FRD, TOW, AFT)$	q	ρ [kg/m ³]	P [in-hg]	T [C]	SHP
(1) Takeoff	0.073	0.23, 0.33, 0.37	314.900	1.024	23.98	3	85
(2) Climb	0.088	0.23, 0.33, 0.37	453.457	1.024	23.98	3	68
(3) Level flight	0.188	0.23, 0.33, 0.37	1387.800	0.771	16.9	-15	68
(4) Descent	0.095	0.23, 0.33, 0.37	532.182	1.024	23.98	3	0
(6) Landing	0.095	0.23, 0.33, 0.37	532.182	1.024	23.98	3	0

Table 15: Other flight conditions and configurations continuation

Flight Phases	V [m/s]	η_p	T	SHP_{avh}	P_{av}	η_h
(1) Takeoff	24.8	0.7	1319.556	69.590	47.739	1.193
(2) Climb	29.76	0.8	1005.376	55.672	43.647	1.102
(3) Level flight	60	0.85	529.833	40.581	33.804	1.013
(4) Descent	32.24	0.85	0.000	0.000	0.000	1.000
(6) Landing	32.24	0.85	0.000	0.000	0.000	1.000

where FRD , TO , AFT are the cg positions for the most forward, take off and most aft conditions, respectively. And SHP_{avh} , P_{av} , η_h , are the shaft horse power available, the available power and tail efficiency respectively. As we can see in equation 4.3, these terms have been adjusted for temperature and pressure at altitude, propeller efficiency, and transmission.

$$SHP_{avh} = SHP_{avs} * P_h / 29.92 * \text{sqr}((273+15)/(273+t_h)) \quad 4.1$$

$$P_{av} = \{(\eta_{inl/inc} SHP_{av} - P_{extr}) \eta_p\} \eta_{gear} \quad 4.2$$

$$\eta_h = 1 + S_{hslip} / S_h * [(2200 P_{av}) / \{(q U 1 \pi (D_p)^2\}] \quad 4.3$$

4.4. Airplane Trim diagrams

This section is devoted to construct the airplane trim diagram for the flight conditions and configurations defined previously. For this task the airplane's lift and pitching moment curves were required. Since the airplane's lift curve for cruise was built during the preliminary calculation, lift curves for the remaining flight phases were built following the same procedure.

The construction of the airplane's pitching moment curves was done following a preliminary design methodology as described by (Roskam, Airplane Design, Part I - VIII, 1990, p. 287 Part VI).

4.4.1. Construction of airfoil lift and pitching moment curves

Repeating the procedure from the preliminary calculations, the parameter needed to construct the airfoil lift and pitching moment curves, for all flight phases, were extracted from xfoil, and were tabulated as follows:

Table 16: Airfoil lift and pitching moment curve parameters

Flight Phases	α_{ol}	Cl_α	α^*	Cl^*	α_{clmax}	Cl_{max}	C_{mo}	dc_m/dc_l
(1) Takeoff	-2.5	0.104719755	10	1.4617	17.5	1.504	-0.0461	0.007
(2) Climb	-2.5	0.104760032	9.5	1.4567	17	1.527	-0.0461	0.007
(3) Level flight	-2.5	0.104907314	9.5	1.4874	17	1.561	-0.0469	0.007
(4) Descent	-2.5	0.104767058	9.5	1.4611	17.5	1.537	-0.0461	0.007
(6) Landing	-2.5	0.104767058	9.5	1.4611	17.5	1.537	-0.0461	0.007

4.4.2. Construction of wing lift and pitching moment curves

All the parameters for the construction of the wing lift curve at cruise were calculated in section 3.2. The same procedure was followed to calculate these parameters at all the required flight phases. The calculation of the wing pitching moment curve slope, and wing pitching moment coefficient at zero-lift was done as described by (Roskam, Airplane Design, Part I - VIII, 1990) VI.

4.4.2.1. Wing pitching moment coefficient at zero-lift, $C_{m_{0w}}$:

The wing pitching moment coefficient at zero-lift is evaluated from:

$$C_{m_{0w}} = \left\{ \frac{A \cos^2 \Lambda_{c/4}}{A + 2 \cos \Lambda_{c/4}} \right\} (C_{m_{0r}} + C_{m_{0t}}) / 2 + (\Delta C_{m_0} / \epsilon_t) \epsilon_t \quad 4.4$$

where $C_{m_{0r}}$ and $C_{m_{0t}}$ are the zero-lift pitching moment coefficient for the wing root and tip respectively. This parameter was determined with xfoil and can be found in section 3.1 and can be found in Table 16 for all flight phases. $\Delta C_{m_0} / \epsilon_t$ is found from (Roskam, Airplane Design, Part I - VIII, 1990) VI Figure 8.98.

4.4.2.2. Wing pitching moment curve slope, $(dc_m/dc_L)_w$:

The wing pitching moment curve slope is estimated as follows:

$$(dc_m/dc_L)_w = (\bar{x}_{ref} - \bar{x}_{ac_w}) \quad 4.5$$

where \bar{x}_{ref} and \bar{x}_{ac_w} are the location of the moment reference center, usually the cg, and the location of the wing ac as described by (Roskam, Airplane Design, Part I -

VIII, 1990)VI Figure 8.97b. For airplanes such as the KR2, with aspect ratios above 5 and sweep angles less than 35 degrees, x_{ac} can be approximated at 25% of the airplane mean geometric chord.

The wing lift and pitching moment parameters were calculated for all flight phases and tabulated as follows.

Table 17: Wing lift and pitching moment curve parameters

Flight Phases	Wing lift and pitching moment parameters						
	α_{olw}	$Cl_{\alpha w}$	α_w^*	α_{clmaxw}	Cl_{maxw}	C_{mow}	$(dc_m/dc_l)_w$
(1) Takeoff	-1.5	0.102	10	12	1.385	-0.0352	0.084
(2) Climb	-1.5	0.102	9.5	12.25	1.412	-0.0352	0.084
(3) Level flight	-1.5	0.102	9.5	12.6	1.448	-0.0358	0.084
(4) Descent	-1.5	0.102	9.5	12.4	1.428	-0.0352	0.084
(6) Landing	-1.5	0.102	9.5	12.4	1.428	-0.0352	0.084

These parameters are needed to calculate the airplane lift and pitching moment parameters.

4.4.3. Construction of Airplane lift and pitching moment curves

All the parameters for the construction of the airplane lift curve at cruise were calculated in section 1. The same procedure was followed to calculate these parameters at all of the required flight phases. The wing incident angle (i_w) and the stabilizer incident angle (i_h) will be used in this section. These angles are constant for the studied airplane. The assumption was made that control surface angles, such as the elevator deflection (δ_e), are zero. The calculation of the airplane pitching moment curve slope, and airplane pitching

moment coefficient at zero-lift was done as described by (Roskam, Airplane Design, Part I - VIII, 1990) VI.

4.4.3.1. Airplane pitching moment coefficient at zero-lift, C_{m_0} :

The airplane pitching moment coefficient at zero-lift is estimated from:

$$C_{m_0} = C_{m_{0wf}} + C_{m_{0h}} \quad 4.6$$

where: $C_{m_{0wf}}$ is the pitching moment coefficient at zero-lift of the wing-fuselage combination, estimated from:

$$C_{m_{0wf}} = \{(C_{m_{0w}}) + (C_{m_{0f}})\} \{(C_{m_0})_M / (C_{m_0})_{M=0}\};$$

where: $C_{m_{0w}}$ is found from equation 4.4

$$C_{m_{0w}} = \{(k_2 - k_1) / 36.55 \bar{c}\} [\text{Sum}_{i=1}^{13} \{(w_{fi}^2) (i_w + \alpha_{0L_w} + i_{cl_f}) \Delta x_i\}] \quad 4.7$$

where: $(k_2 - k_1)$ is found from (Roskam, Airplane Design, Part I - VIII, 1990) VI Figure 8.111

w_{fi}^2 , Δx_i , i_{cl_f} are: the average with of the fuselage, the length of a fuselage segment, and the incident angle of the fuselage camber respectively, as illustrated in (Roskam, Airplane Design, Part I - VIII, 1990) VI Page 321.

α_{0L_w} may be found from Table 5

$C_{m_{o_h}}$ is the zero-lift pitching moment coefficient due to the stabilizer, which may be estimated from:

$$C_{m_{o_h}} = -(\bar{x}_{ac_h} - \bar{x}_{ref})C_{L_{o_h}} \quad 4.8$$

where: where \bar{x}_{ref} is the location of the moment reference center, usually the cg, and \bar{x}_{ac_h} is the location of the tail ac measured from the leading edge of the wing mean geometric chord (mgc), as described by (Roskam, Airplane Design, Part I - VIII, 1990) VI Figure 8.114. Both parameters are measured in fractions of mgc.

4.4.3.2. Airplane pitching moment curve slope, (dc_m/dc_L) :

The airplane pitching moment curve slope is estimated as follows:

$$dC_m/dC_L = \bar{x}_{ref} \bar{x}_{ac_A} \quad 4.9$$

where: \bar{x}_{ac_A} is the airplane aerodynamic center in fractions of the mgc. It may be estimated with the following equation:

$$\bar{x}_{c_A} = [(\bar{x}_{ac_{wf}})C_{L_{\alpha_{wf}}} + \eta_h C_{L_{\alpha_h}} (1 - d\epsilon/d\alpha) (S_h/S) \bar{x}_{ac_h}] / C_{L_{\alpha}} \quad 4.10$$

$$\text{where: } \bar{x}_{ac_{wf}} = \bar{x}_{ac_w} + \Delta \bar{x}_{ac_{wf}} \quad 4.11$$

$\Delta\bar{x}_{ac_{wf}}$ is the shift in aerodynamic center due to the fuselage as described in section 4.4.3.3

η_h may be found from equation 3.7

$C_{L_{\alpha_{wf}}}$ is found from equation 3.11

$C_{L_{\alpha_h}}$ is estimated from equation 3.3

4.4.3.3. Aerodynamic center shift due to fuselage, $\Delta\bar{x}_{acf}$:

The contribution of the fuselage to the airplane stability was discussed in section 2 Literature Review. As explained by (Multhopp, 1942), this contribution can be found with:

$$\Delta\bar{x}_{acf} = -(dM/d\alpha) / (\bar{q} S \bar{c} C_{L_{\alpha_w}}) \quad 4.12$$

where: $C_{L_{\alpha_w}}$ is found from Table 5.

$dM/d\alpha$ is the variation of pitching moment with airplane angle of attack:

$$dM/d\alpha = (q/36.5) (C_{L_{\alpha_w}}/0.08) [\text{Sum}_{i=1}^{13} \{ (w_{fi}^2) (d\epsilon/d\alpha)_i \Delta x_i \}] \quad 4.13$$

where: Δx_i and i_{cl_f} were defined in section 4.4.3.1, $C_{L_{\alpha_w}}$ is found in Table 5: Wing lift and drag parameters, $(d\epsilon/d\alpha)_i$ is the variation of downwash with airplane angle of attack as found in (Roskam, Airplane Design, Part I - VIII, 1990) VI Figure 8.115 and explained in section 2.3.

With the equations described above, the airplane lift and pitching moment curve parameters were calculated for all flight phases. The tabulation of these parameters follows.

Table 18: Airplane lift and pitching moment parameters

Flight Phases	α_{0L}	C_{L0}	$C_{Lawf}=K_{wf}C_{Law}$	$C_{L\alpha}$	$\alpha^*_A=\alpha_w-i_w$	α_{CLmax}	C_{Lmax}
(1) Takeoff	-4.892	0.5105	5.85	5.979	6.5	8.5	1.385
(2) Climb	-4.900	0.5105	5.85	5.969	6	8.75	1.412
(3) Level flight	-4.908	0.5105	5.85	5.959	6	9.1	1.448
(4) Descent	-4.909	0.5105	5.85	5.958	6	8.9	1.428
(6) Landing	-4.909	0.5105	5.85	5.958	6	8.9	1.428

Table 19: Airplane lift and pitching moment parameters continuation 1

Flight Phases	C_{mowf}	$C_{mo}=C_{mowf}+C_{moh}$	$dM/d\alpha$
(1) Takeoff	0.0399	0.0399	13.585
(2) Climb	0.0399	0.0399	19.563
(3) Level flight	0.0393	0.0393	59.871
(4) Descent	0.0399	0.0399	22.959
(6) Landing	0.0399	0.0399	22.959

Table 20: Airplane lift and pitching moment parameters continuation 2

ΔX_{acf}	$X_{acwf}=X_{acw}+\Delta X_{acf}$	X_{acA}	$dC_m/dC_L=X_{ref}-X_{acA}$	CL^*
-0.0471	0.203	0.386	-0.0294	0.678
-0.0471	0.203	0.373	-0.0252	0.625
-0.0471	0.203	0.359	-0.0153	0.624
-0.0471	0.203	0.357	-0.0163	0.624
-0.0471	0.203	0.357	-0.0146	0.624

The parameters above were used to build the airplane lift curves for all flight phases

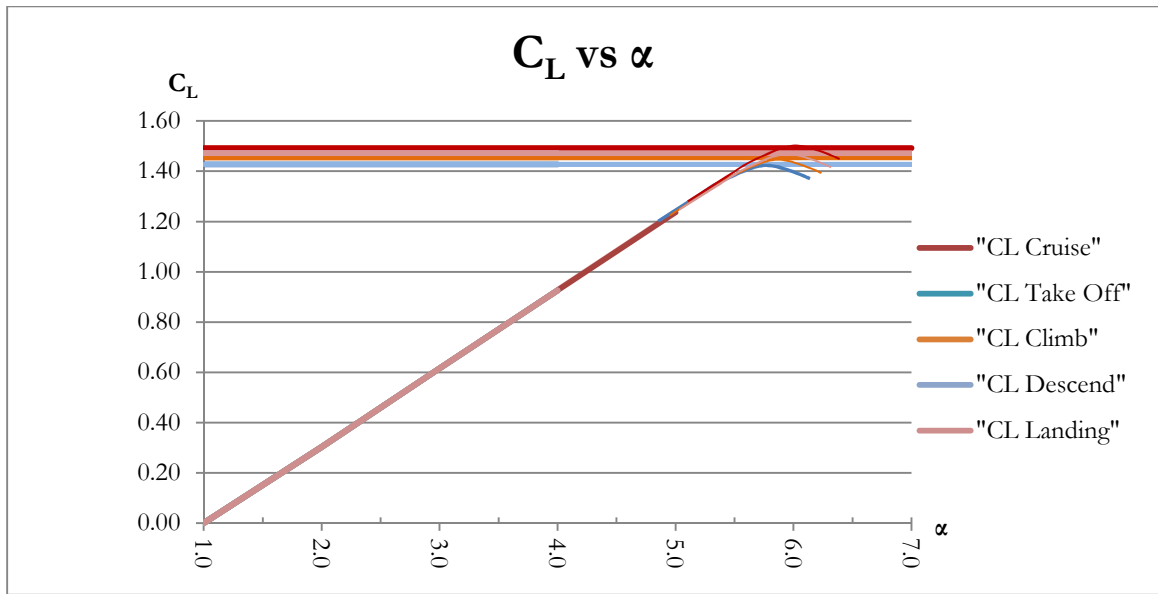


Figure 25: Airplane lift curves for all flight phases

As can be seen in Figure 25, while the lift curve slope stays relatively constant with changes in flight conditions and configurations, the maximum lift coefficient does change and is higher at cruise speed. This effect is attributed to the variation of the Reynolds number with speed and altitude.

4.4.4. Ground effect on airplane lift

As explained in section 0, and (Roskam, Airplane Design, Part I - VIII, 1990)VI Section 8.1.7, the presence of ground reduces downwash during landing and takeoff. Therefore, the effect of ground on airplanes lift can be studied by associating a change in angle of attack at constant lift. This change in angle of attack can be computed from:

$$\Delta\alpha_g = -F_{tv} \left\{ \frac{9.12}{A} + 7.16 \left(\frac{c_r}{b} \right) \right\} (C_{L_{wp}}) - \left\{ \frac{A}{2C_{L_{awp}}} \right\} \left(\frac{c_r}{b} \right) \left\{ \left(\frac{L}{L_0} \right) - 1 \right\} (C_{L_{wp}}) r_g \quad 4.14$$

where: F_{tv} factors the effect due to the image trailing vortex as found in (Roskam, Airplane Design, Part I - VIII, 1990)VI Figure 8.73; $C_{L_{wf}}$ is the lift coefficient of the wing and fuselage out of ground; $C_{L_{awf}}$ was found in section 3.3.1.2; (L/L_o-1) factors the effect due to the image bound vortex as found in (Roskam, Airplane Design, Part I - VIII, 1990)VI Figure 8.74; and r_g factor the effect of finite span as found in (Roskam, Airplane Design, Part I - VIII, 1990)VI Figure 8.75.

All these parameters were calculated and tabulated as follows.

Table 21: Ground effect on lift parameters

Flight Phases	$\alpha_o = \alpha_o + \Delta\alpha_o$	$C_{L\alpha} = (\Delta C_L / \Delta\alpha)_g$	$C_{L_o} = -C_{L\alpha} \alpha_o$	C_{Lmax}
(1) Takeoff	-4.929	7.193	0.619	1.426
(2) Climb	-4.915	5.952	0.511	1.455
(3) Level flight	-4.922	5.943	0.511	1.492
(4) Descent	-4.923	5.942	0.511	1.471
(6) Landing	-4.936	7.180	0.619	1.471

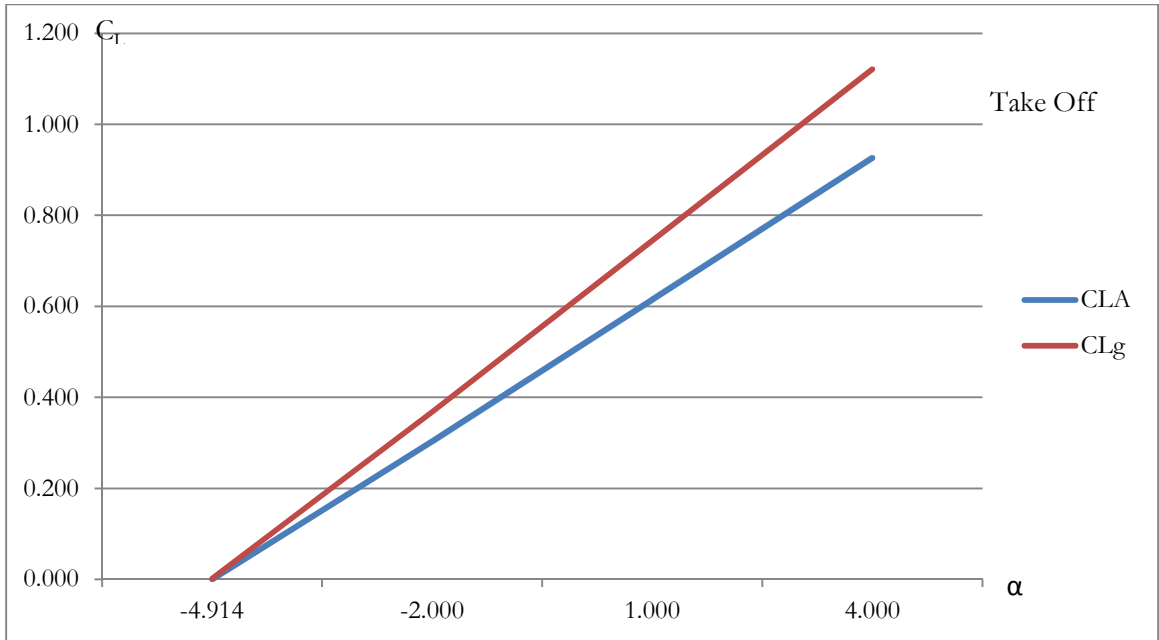


Figure 26: Ground effect on lift at take off

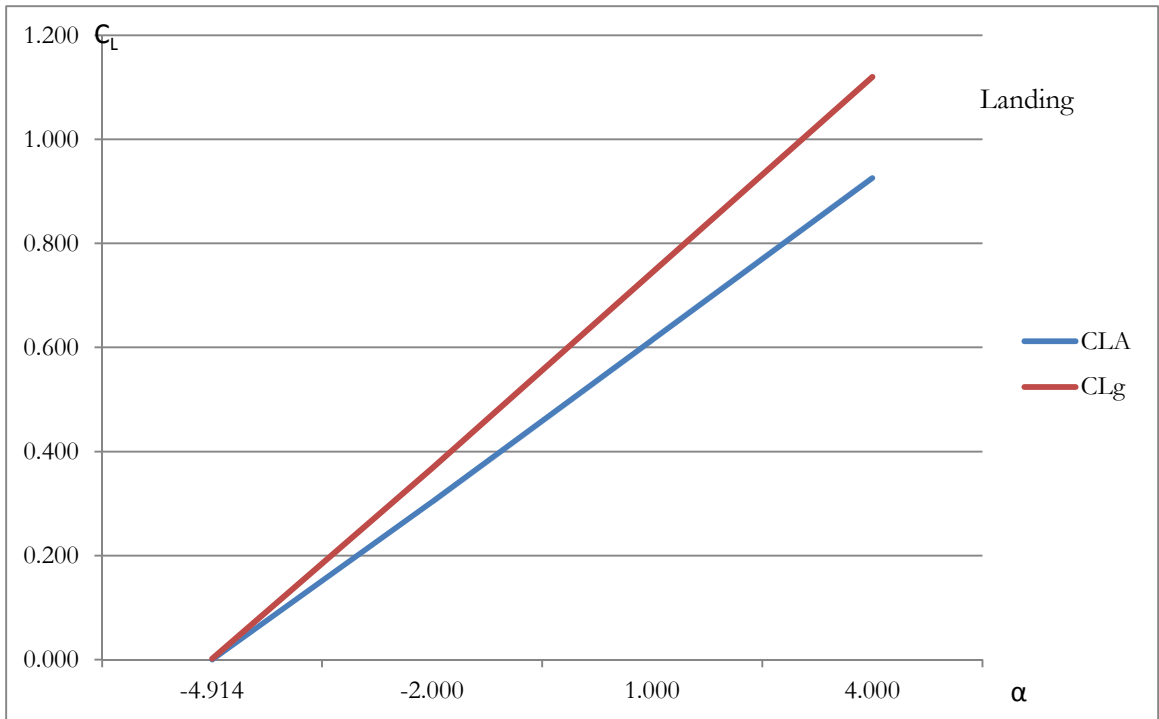


Figure 27: Ground effect on landing

As we can see in the lift curves above, the reduction of downwash due to the ground effect causes an increase on the airplane lift curve slope. The major effect due to the reduction of downwash happens at the tail. As will be shown next, this significantly alters the airplane pitching moment.

4.4.5. Ground effect on airplane pitching moment

The reduction of downwash due to ground effect increases the angle of attack at the tail. Considering that the major contribution to the airplane pitching moment comes from the tail, this is a significant effect. Assuming that the aerodynamic center of the airplane does not change due to ground effect, the pitching moment increment due to ground effect can be calculated from:

$$(\Delta C_m)_g = (\bar{x}_{ref} - \bar{x}_{acA})(\Delta C_{Lwf})_g + (\Delta C_{mh})_g \quad 4.15$$

where: $(\bar{x}_{ref} - \bar{x}_{acA})$ is the airplane pitching moment curve slope calculated in section 4.4.3.2; $(\Delta C_{Lwf})_g = (\Delta C_L)_g$ is illustrated in (Roskam, Airplane Design, Part I - VIII, 1990)VI, Figure 8.120.

$$(\Delta C_{mh})_g = -(\Delta C_{Lh})_g \eta_h (X_{ach} - X_{ref}) \quad 4.16$$

Where: X_{ach} and X_{ref} were defined in section 4.4.3.2; η_h is defined in section 1 and:

$$(\Delta C_{Lh})_g = -C_{L\alpha_h} (S_h/S) (\Delta \epsilon)_g \quad 4.17$$

where: $C_{L\alpha_h}$ was described in section 3.3.1.1; and $(\Delta\mathcal{E})_g$ is the decrease in tail downwash due to ground effect as defined in section 4.4.5.1.

4.4.5.1. Decrease in tail downwash due to ground effect, $(\Delta\mathcal{E})_g$:

The decrease in tail downwash due to ground effect may be computed from:

$$(\Delta\mathcal{E})_g = \epsilon \left[\frac{b_{eff}^2 + 4(H_h - H_w)^2}{b_{eff}^2 + 4(H_h + H_w)^2} \right] \quad 4.18$$

where: \mathcal{E} is the downwash at the tail as described in (Roskam, Airplane Design, Part I - VIII, 1990)VI page 333; H_h and H_w are the height above ground of the stabilizer and wing respectively, as illustrated in (Roskam, Airplane Design, Part I - VIII, 1990)VI Figure 8.122

$$b_{eff} = (C_{L_{wf}} + \Delta C_L) / \left\{ (C_{L_{wf}} / b'_w) + (\Delta C_L) / b'_f \right\} \quad 4.19$$

where: $C_{L_{wf}}$ was described in section 4.4.4; ΔC_L is the lift increment due to flaps; b'_w and b'_f are the close to ground effective wing span and flap span respectively, as described in (Roskam, Airplane Design, Part I - VIII, 1990)VI Figures 8.123 & 8.124.

After calculating all the parameters described above for all the flight conditions, they were tabulated as shown below.

Table 22: Ground effect on pitching moment

Flight Phases	$C_{mog}=C_{mo}+\Delta C_{mog}$	$(dC_m/dC_L)_g=(\Delta C_m/\Delta C_L)_g$
(1) Takeoff	0.0398	-0.0786
(2) Climb	0.0400	-0.0291
(3) Level flight	0.0394	-0.0153
(4) Descent	0.0400	-0.0130
(6) Landing	0.0399	-0.0573

These parameters were used to build the airplane pitching moment curves for takeoff and landing, see Figure 28 & 29. As is shown in these figures, ground effect makes the slope of the pitching moment curve more negative, resulting in a stabilizing effect in the airplane.

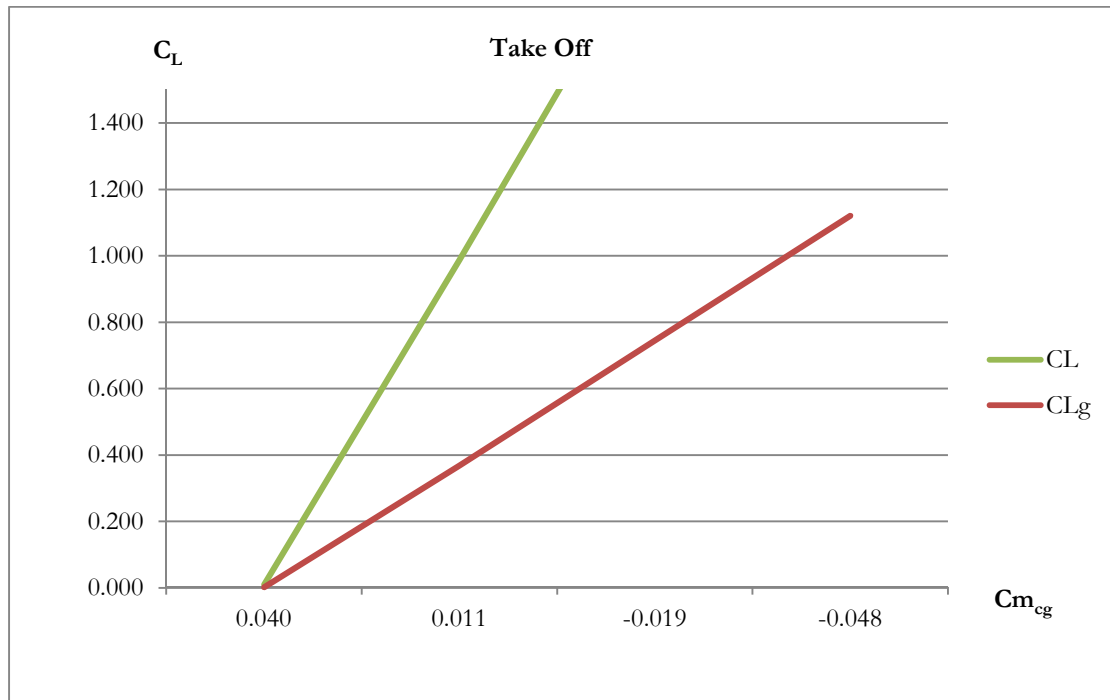


Figure 28: Ground effect on pitching moment for take off

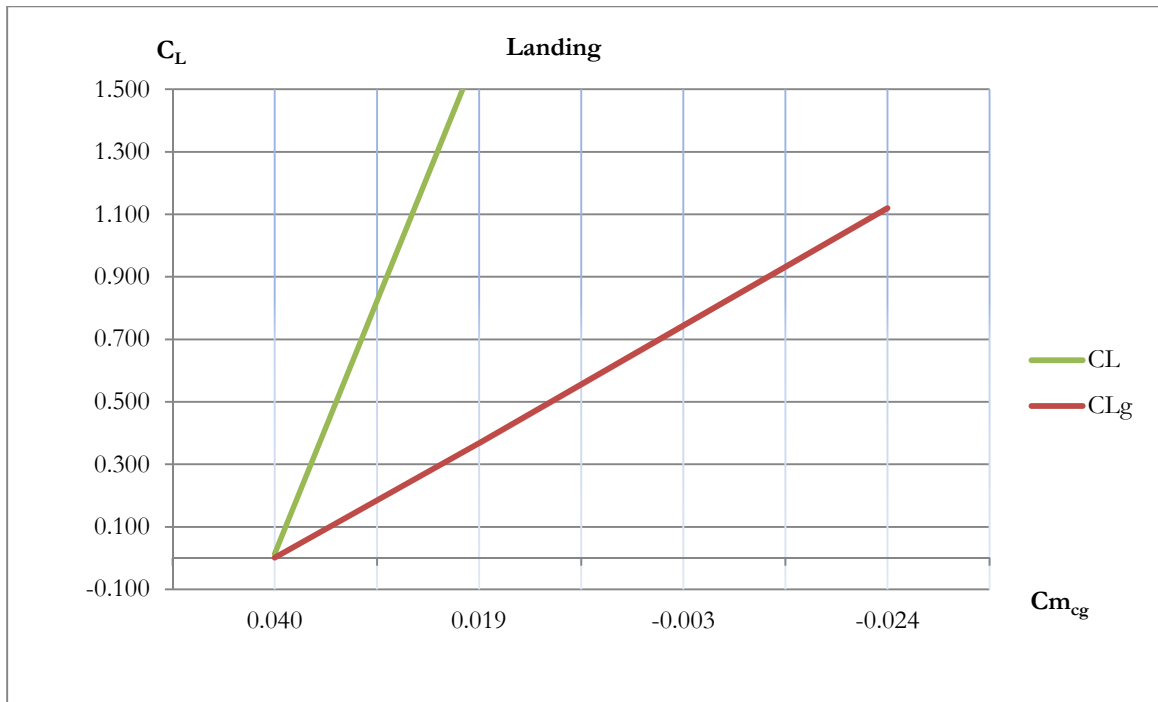


Figure 29: Ground effect on pitching moment for landing

4.4.6. Power effect on airplane lift

There are two main power effects on airplane lift. The effect of the thrust vertical component due to the tilt of the thrust line with respect to the free stream direction, and the effect due to the propeller slip stream acting on the wing. The last effect will be the only effect considered here.

The propeller increases the dynamic pressure on its slip stream. The result of this is that the lift of the wing portion that is submerged in the propeller slip stream is also increased. This increase in lift can be computed from:

$$\Delta C_{Lw} = \sum_{i=1}^n [(S_{p_i}/S)(C_{L_w})[(2200P_{av_i})/\{qU_1\pi(Dp_i)^2\}]]$$

4.20

where: S_{p_i} is the area of the wing portion that is submerged in the propeller slip stream as illustrated in (Roskam, Airplane Design, Part I - VIII, 1990) VI Figure 8.80; C_{L_w} is the lift coefficient at which the wing is operating, see section 4.4.2; P_{av_i} is the available power as described in section 3.3.1.1; U_I is the steady state speed of the airplane, and Dp_i is the propeller diameter.

The following table shows the airplane lift parameter, including power effect, for all flight phases of the airplane.

Table 23: Power effect on lift

Flight Phases	BHP	ΔC_{L_w}	$C_{L_{max(g+T)}}$	$C_{L\alpha}$
(1) Takeoff	100%	0.0248	1.452	7.298
(2) Climb	80%	0.0174	1.479	6.051
(3) Level flight	75%	0.0009	1.496	5.958
(4) Descent	0	0	1.472	5.942
(6) Landing	0	0	1.472	7.181

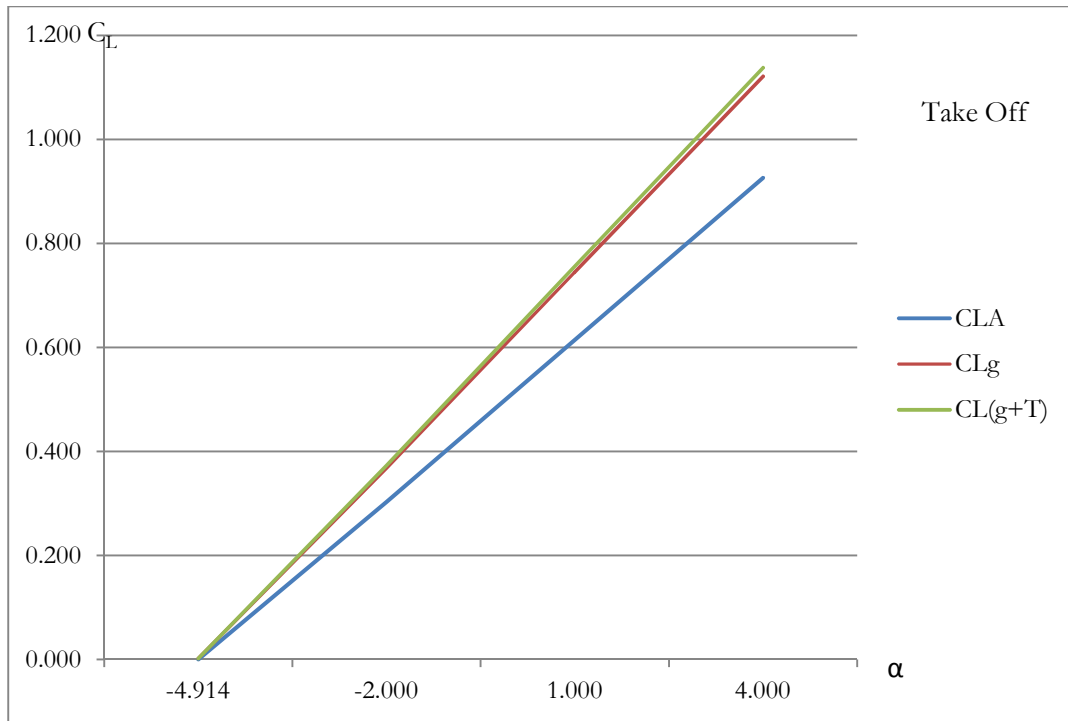


Figure 30: Power and Ground effect on lift for take off

Figure 30 above shows the variation of airplane lift curve slope with power and ground effect for takeoff. As depicted in this figure and Table 23, the power effect increases the airplane lift curve slope and maximum lift.

4.4.7. Power effect on airplane pitching moment

There are two main affects on airplane pitching moment due to power: a shift of pitching moment at zero lift coefficient due to the thrust line offset, the propeller slip stream; and a change in airplane pitching moment curve slope due also to thrust line offset, and due to the propeller normal force.

4.4.7.1. Power effect on pitching moment at zero lift coefficient, $\Delta C_{m\sigma}$

The power effect on pitching moment coefficient at zero lift coefficient can be computed from:

$$\Delta C_{m\sigma} = \Delta C_{mTL} + \Delta C_{mTS} \quad 4.21$$

where: ΔC_{mTL} is the pitching moment variation due to thrust line offset, which may be estimated from:

$$\Delta C_{mTL} = T_{av} d_T / \bar{q} S c \quad 4.22$$

where: T_{av} is the available installed thrust from the propeller; and d_T is the thrust line offset as illustrated in (Roskam, Airplane Design, Part I - VIII, 1990) VI Figure 8.126.

ΔC_{mTS} is the pitching moment variation due to propeller slipstream, which may be estimated as follows:

$$\Delta C_{mTS} = (\bar{x}_{acTS} - \bar{x}_{ref}) \Delta C_{Lw} \quad 4.23$$

where: \bar{x}_{acTS} and \bar{x}_{ref} are illustrated in (Roskam, Airplane Design, Part I - VIII, 1990) VI Figure 8.127; and ΔC_{Lw} is found from equation 4.20.

4.4.7.2. Power effect on longitudinal stability, $\Delta(dC_m/dC_L)_T$:

The power effect on longitudinal stability may be estimated from the following equation:

$$\Delta(dC_m/dC_L)_T = (dC_m/dC_L)_{TL} + (dC_m/dC_L)_N \quad 4.24$$

where: $(dC_m/dC_L)_{TL}$ is the power effect of thrust line offset on longitudinal stability, which may be estimated from:

$$(dC_m/dC_L)_{TL} = \sum_{i=1}^n [(dT_{ci}/dC_L) \{2(D_{pi})^2 dT_i / S\bar{c}\}] \quad 4.25$$

where: dT_{ci}/dC_L is the variation of thrust coefficient with the airplane coefficient of lift, which can be computed from:

$$dT_{ci}/dC_L = (3/2) K_{Ti} \eta_{pi} (C_L)^{1/2} \quad 4.26$$

where: η_{pi} is the efficiency of the propeller; and

$K_{Ti} = \{550(SHP_{avi})(\rho)^{1/2}\} / \{(2W/S)^{3/2}(D_{pi})^2\}$ as define in (Roskam, 1990)VI Page 340

D_{pi} is the diameter of the propeller, and dT_i is the propeller thrust line offset.

$(dC_m/dC_L)_N$ is the effect of propeller normal force on longitudinal stability, which may be computed as:

$$\left(\frac{dC_m}{dC_L}\right)_N = \sum_{i=1}^n \left[\left\{ \left(\frac{dC_N}{d\alpha}\right) p_i \left(1 + \frac{d\bar{e}_{pi}}{d\alpha}\right) (l_{pi}) (0.79)(D_{pi})^2 \right\} / S\bar{c}C_{L\alpha_w} \right] \quad 4.27$$

where: l_{p_i} is the moment arm of the propeller normal force to the reference point as illustrated in (Roskam, Airplane Design, Part I - VIII, 1990)VI Figure 8.129; $\frac{d\bar{\epsilon}_{p_i}}{d\alpha}$ is found from (Roskam, Airplane Design, Part I - VIII, 1990)VI Figure 8.155; $\left(\frac{dC_N}{d\alpha}\right)_{p_i}$ is the change in propeller normal force coefficient with angle of attack, which may be found from:

$$\left(\frac{dC_N}{d\alpha}\right)_{p_i} = \left\{ \left\{ (C_{N\alpha})_{p_i} \right\}_{K_{Ni}=80.7} \right\} [1 + 0.8 \{ (K_{Ni}/80.7) - 1 \}] \quad 4.27$$

where: $\left\{ (C_{N\alpha})_{p_i} \right\}_{K_{Ni}=80.7}$ is found from (Roskam, Airplane Design, Part I - VIII, 1990)VI Figure 8.130; and

$$K_{Ni} =$$

$$262 \{ (w_{pi}/R_{pi})^{0.3R_{pi}} \} + 262 \{ (w_{pi}/R_{pi})^{0.6R_{pi}} \} + 135 \{ (w_{pi}/R_{pi})^{0.9R_{pi}} \}$$

as described in (Roskam, Airplane Design, Part I - VIII, 1990)VI

Page 342.

The following table shows the airplane pitching moment parameter, including power effect, for all flight phases of the airplane.

Table 24: Power effect on pitching moment

Flight Phases	Δc_{mT}	Δc_{moTL}	Δc_{moTS}	$\Delta (dC_m/dC_L)_T$	$(dC_m/dC_L)_{TL}$	dT_{ci}/dC_L
(1) Takeoff	-0.063	-0.063	-1.323E-05	-0.08283	-0.0865	1.4596
(2) Climb	-0.060	-0.060	-1.243E-05	-0.05836	-0.0621	1.0469
(3) Level flight	-0.012	-0.012	-1.620E-06	-0.02144	-0.0251	0.4241
(4) Descent	0.000	0.000	0	0.00371	0.0000	0
(6) Landing	0.000	0.000	0	0.00371	0.0000	0

Table 25: Power effect on pitching moment continuation

Flight Phases	K_{Ti}	$(dC_m/dC_L)_N$	$(dC_N/d\alpha)_{pi}$	K_{Ni}	$(dC_m/dC_L)_{(g, T)}$
(1) Takeoff	1.0628	0.00371	0.156	110.637	-0.161
(2) Climb	0.8502	0.00371	0.156	110.637	-0.087
(3) Level flight	0.5378	0.00371	0.156	110.637	-0.037
(4) Descent	0	0.00371	0.156	110.637	-0.009
(6) Landing	0	0.00371	0.156	110.637	-0.054

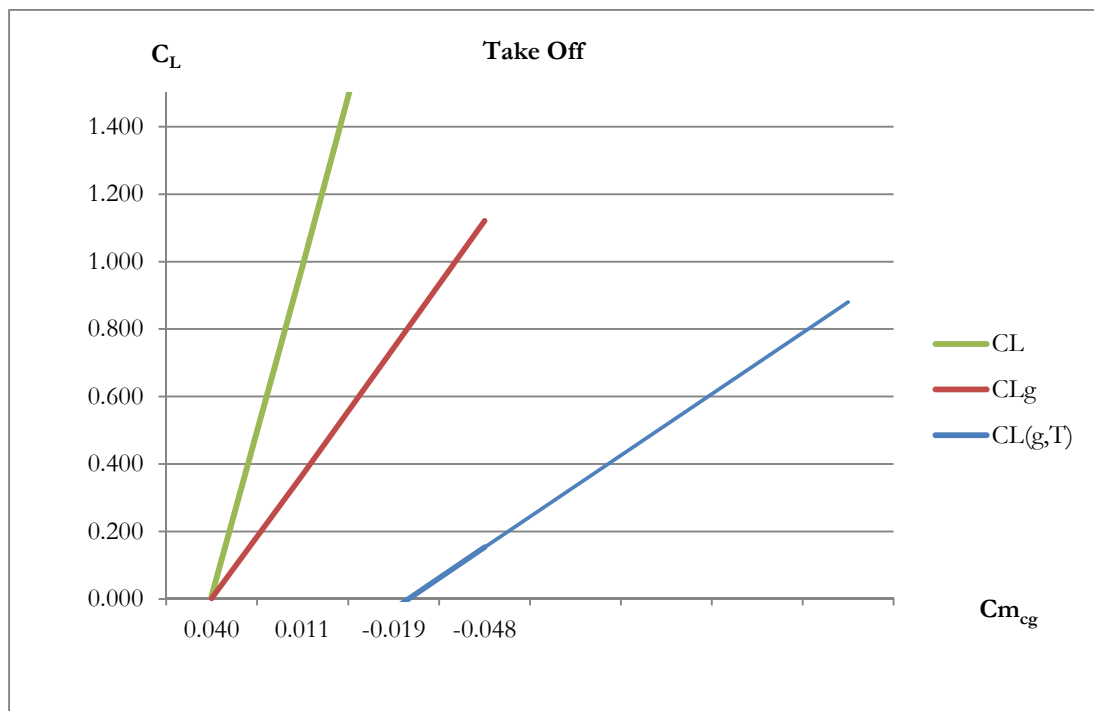


Figure 31: Power and Ground effect on pitching moment curve for take off

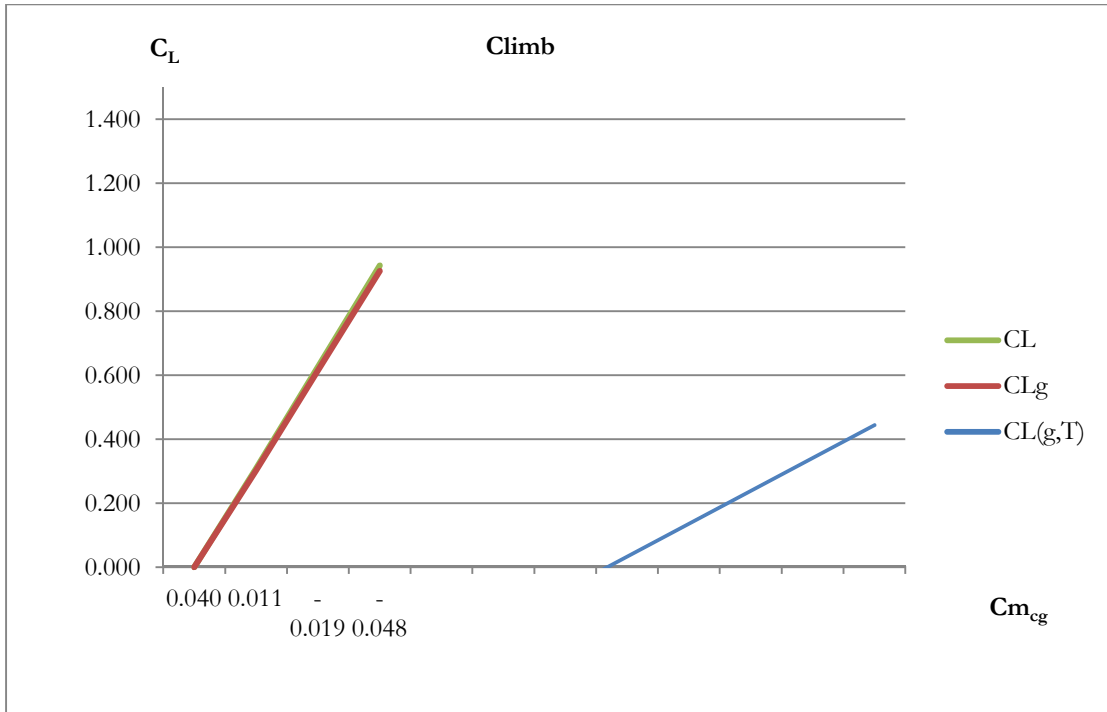


Figure 32: Power and Ground effect on pitching moment curve for climb

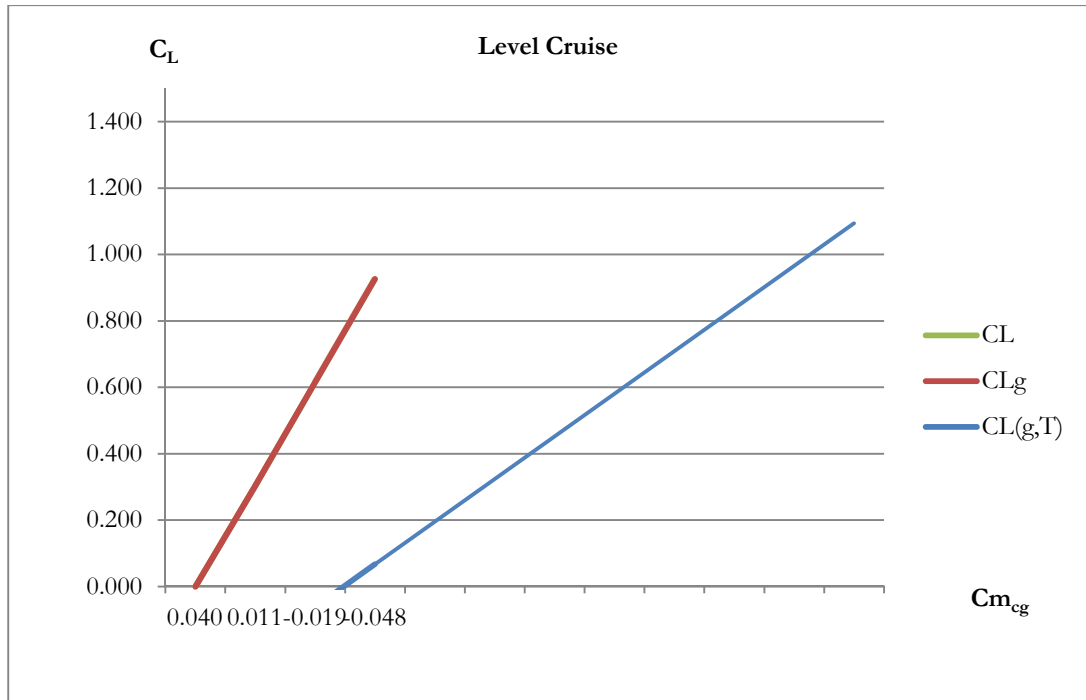


Figure 33: Power and Ground effect on pitching moment curve for level cruise

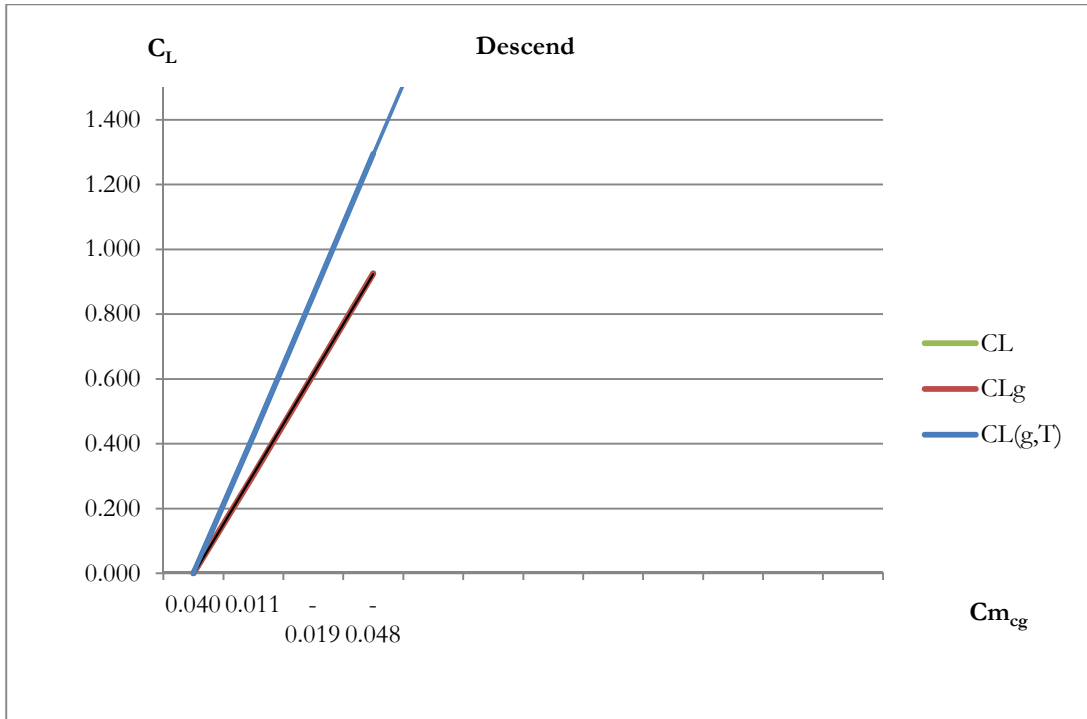


Figure 34: Power and Ground effect on pitching moment curve for descent

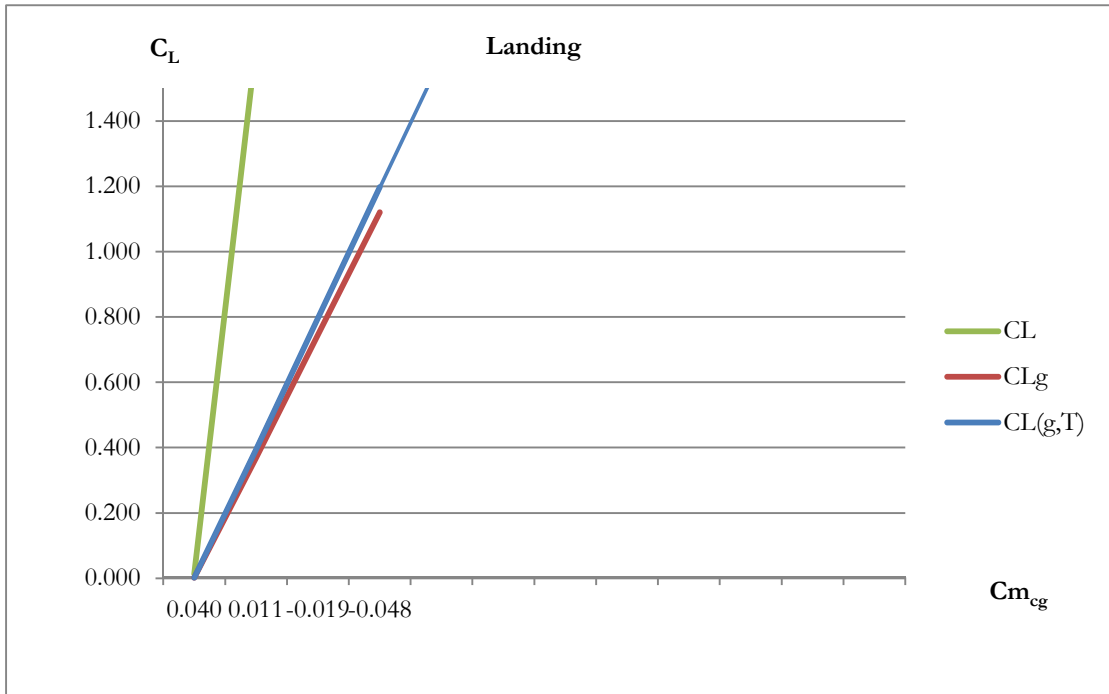


Figure 35: Power and Ground effect on pitching moment curve for landing

Figures 32 to 35 show power and ground effect on pitching moment for all flight phases of the airplane. It can be seen in these figures that when powered flying (takeoff, climb and cruise) occurs in the studied airplane, the power effect makes the variation of the pitching moment with lift more negative, resulting in a stabilizing effect in the airplane. On the other hand, when windmilling (descent and landing), a small destabilizing effect occurs, since the normal force of the propeller becomes predominant.

4.4.8. Prediction of trimmed lift and trimmed maximum lift coefficient

Up to this point, the prediction of airplane lift and pitching moment parameters has been done assuming all control surface deflections were zero. While equilibrium of forces has been considered, moment equilibrium has not been studied. This section is devoted to study the airplane at pitching moment equilibrium or trim, at all flight phases.

The following condition needs to be met for equilibrium:

$$C_m = 0 \quad 4.28$$

The equilibrium condition demands that the pitching moment coefficient of the airplane is zero. This condition is achieved by the deflection of control surfaces, which has an effect on the airplane lift and pitching moment.

The effect of control surface deflection on lift may be determined as follows:

$$\Delta C_{L_{ct}} = (C_{L_{\delta_e}}) \delta_e \quad 4.29$$

where: $C_{L_{\delta_e}}$ is the lift due to elevator derivative which may be estimated as:

$$C_{L\delta e} = \alpha_{\delta e} C_{L_{i_h}} \quad 4.30$$

where: $\alpha_{\delta e}$ is the elevator effectiveness as illustrated in (Perkins & Hage, 1949) Figure 5.33; and $C_{L_{i_h}}$ is the lift-due-to-stabilizer-incidence derivative, which may be estimated with:

$$C_{L_{i_h}} = \eta_h (S_h/S) C_{L_{\alpha_h}} \quad 4.31$$

Evaluating the equations 4.29-4.31, the effect of elevator deflection on lift was determined. This information is presented in Table 26 for all flight conditions and configurations.

Table 26: Effect of control surface deflection on lift

Flight Phases	$C_{L_{i_h}}$	$C_{L\delta e}$	$\Delta C_{L\delta e}$	$C_{L_{max}(g,T,\delta e)}$
(1) Takeoff	0.00841	0.00526	-0.079	1.373
(2) Climb	0.00836	0.00523	-0.047	1.432
(3) Level flight	0.00768	0.00480	0.007	1.503
(4) Descent	0.00756	0.00473	-0.047	1.424
(6) Landing	0.00756	0.00473	-0.047	1.424

The affect of control surface deflection on pitching moment may be determined as follow:

$$\Delta C_{m_{\delta e}} = (C_{m_{\delta e}}) \delta_e \quad 4.32$$

where: $C_{m_{\delta e}}$ is the pitching moment due to elevator derivative which may be estimated as:

$$C_{m\delta e} = \alpha_{\delta e} C_{m_{i_h}} \quad 4.33$$

where: $C_{m_{i_h}}$ is the-pitching-moment-due-to-stabilizer-incidence derivative,

which may be estimated with:

$$C_{m_{i_h}} = -\eta_h V_h C_{L\alpha_h} \quad 4.34$$

$$\text{where: } V_h = (x_{ach} - x_{cg})(S_h/S) \quad 4.35$$

Evaluating the equations 4.32-4.35, the effect of elevator deflection on pitching moment was determined. This information is presented in Table 27 for all flight conditions and configurations.

Table 27: Effect of control surface deflection on pitching moment

Flight Phases	$\Delta C_{m\delta e}$	$C_{m\delta e}$	$C_{m_{i_h}}$	V_h	δe trim	δe range
(1) Takeoff	0.172	-0.0115	-0.0184	0.309	-15	-24 to -9
(2) Climb	0.103	-0.0114	-0.0183	0.309	-9	-16.5 to 0.5
(3) Level flight	-0.016	-0.0105	-0.0168	0.309	1.5	-7.5 to 12.5
(4) Descent	0.103	-0.0103	-0.0165	0.309	-4	-11.5 to 4.5
to(6) Landing	0.103	-0.0103	-0.0165	0.309	-11	-19 to -4

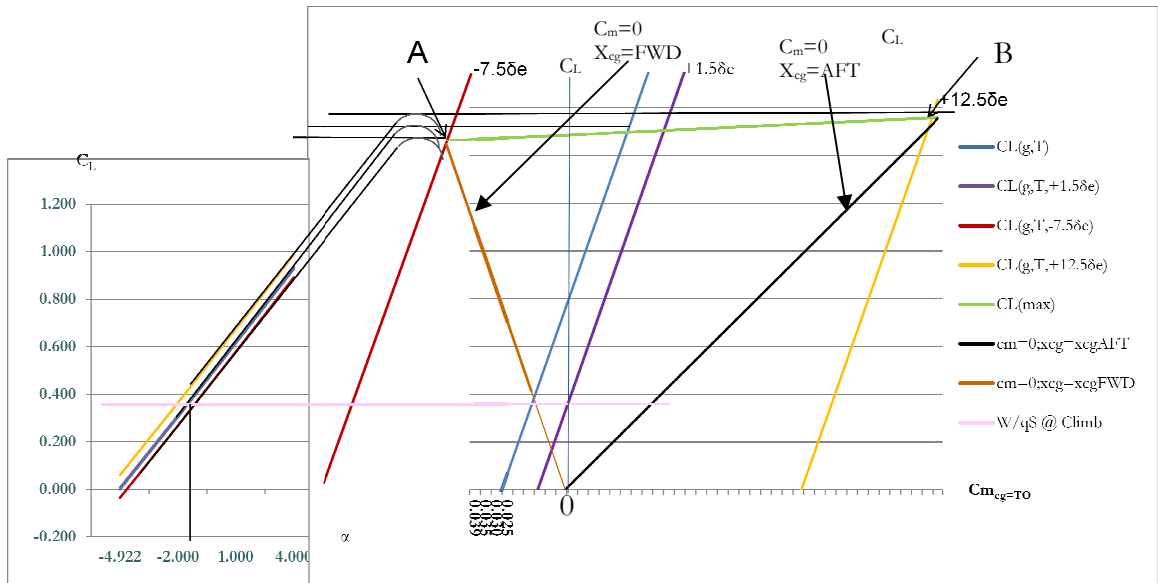


Figure 36: Trim diagram for cruise

Figure 36 is the trim diagram of the modified KR2 for cruise speed and takeoff weight. The $C_L/C_m-\alpha$ curves were built based on the airplane $C_L-\alpha/C_m-CL$ curves estimated in section 4.4.6/4.4.7, and the elevator deflection effect on lift and pitching moment. The triangle OAB in this diagram are formed by the wing stall locus, and the $C_m=0$ lines for most aft and most forward c.g. locations. Plotting $CL= W/qS$ across the $C_m=0$ lines for most aft and most forward c.g. locations, the elevator deflection required to trim the flight condition at the entire c.g. range is determined. Points A and B represent the maximum elevator deflection required to trim.

4.5. Longitudinal Controllability and Trim

An airplane has to be controllable in order to fly safely. The objectives of this analysis, as describe by (Roskam, 1990)VII, is to assure the airplane complies with the regulations. Regarding controllability, the regulations essentially require that:

- Sufficient control power is available to cope with all required configuration and flight condition changes.

This is determined by making sure the elevator control deflection (δ_e) is between the acceptable ranges specified by the regulations. The elevator deflection was calculated in section 4.4.8 and its values for all flight conditions and configurations are displayed in Table 27.

- The pilot is able to move the elevator without too much effort.

This is determined by making sure the Cockpit control forces are between the limits required by the regulations. The Cockpit control force may be determined with the following equation:

$$F_s = F_{sartificial} + Gq\eta_h S_e C_e [C_{ho} + C_{ha} \{ \alpha(1 - d\epsilon/d\alpha) + i_h - \epsilon_o \} + C_{h\delta e} \delta_e + C_{h\delta t} \delta_t] \quad 4.36$$

The stick-force and elevator deflection range were calculated for all flight conditions and configurations. These parameters were tabulated as follows.

Table 28: Longitudinal controllability parameters

Flight Phases	δ_e trim	δ_e range	δ_t	F_s	F_s -required	δ_e -required
(1) Takeoff	-15.0	-25 to -7.5	-1.32	34.847	=<60	-28 to 23
(2) Climb	-7.0	-15 to 1.5	-1.32	21.530	=<60	-28 to 23
(3) Level flight	1.5	-7.5 to 12.5	-1.32	0	=<60	-28 to 23
(4) Descent	-2	-10 to 6.5	-1.32	25.791	=<60	-28 to 23
(5) Landing	-10	-20 to -2.5	-1.32	25.791	=<60	-28 to 23

The maximum cock-pit stick-force specified by the regulations is sixty pounds. As we can see in Table 28, the maximum stick-force for our studied airplane is about 35 pounds

during takeoff. This verifies that the pilot will be able to control the airplane with their hands.

4.6. Static Longitudinal Stability

The static longitudinal stability of the airplane is verified by evaluating the cockpit stick-force to trim speed gradient with the following equation:

$$(dF_s/dU)_{trim} = -(2/U_{trim})\eta_h G S_e c_e (W/S) (C_{h\delta_e}/C_{m\delta_e}) (S.M._{free}) \quad 4.37$$

where $S.M._{free}$ is the stick-free static margin that can be estimated as follows:

$$S.M._{free} = x_{acA} - x_{cg} + (C_{m\delta_e}/C_{L\alpha})(C_{h\alpha}/C_{h\delta_e})(1 - d\epsilon/d\alpha) \quad 4.38$$

Table 29: Static longitudinal stability parameters

Flight Phases	$(dF_s/dU)_{trim}$	$S.M._{fix} = x_{acA} - x_{cg}$	$S.M._{free}$	dF_s/dU_{trim} - required
(1) Takeoff	-4.496	0.161	0.140	< 0
(2) Climb	-2.544	0.080	0.057	< 0
(3) Level flight	-2.264	0.037	0.016	< 0
(4) Descent	-3.087	0.028	0.006	< 0
(6) Landing	-1.617	0.064	0.004	< 0

As we can see in Table 29, while the stability parameters comply with the acceptable ranges specified by the regulations, the stick-fix static margin is below the recommended 10 percent for this type of airplane.

The static stability of an airplane doesn't guarantee the airplane is going to be dynamically stable. The next section explores the regulations that guarantee the dynamic stability of the airplane.

4.7. *Dynamic Longitudinal Stability*

When an airplane is statically very stable, the restoring moment tends to be too strong, and the correction may overshoot leading to an oscillatory motion that can get out of control. To avoid this problem, these oscillations have been studied and the frequency and damping requirements have been set by the regulations. Because the civil regulations regarding dynamic stability are vague, military regulations will be used to determine frequency and damping requirements.

The dynamic stability of an airplane is characterized by two relevant natural modes of perturbed motion: the phugoid (P) mode and the short-period (SP) modes. The following are the parameters of these modes as specified by the military regulations:

- Undamped natural frequency: $\omega_{n_{SP}}$
- Damping ratio: ξ_P and ξ_{SP}

4.7.1. Class II method for analysis of phugoid characteristics (Roskam, Airplane Design, Part I - VIII, 1990) VII

The evaluation of phugoid parameters is done with the following equations:

$$w_{np} = (1.414g/U1) \tag{4.39}$$

$$\xi_p = \sqrt{2(C_{D_u} - C_{T_{x_u}})/4C_{L_1}} \text{ (Roskam, 1995)} \tag{4.40}$$

where: U_1 is the free stream speed for the flight condition; g is the acceleration of gravity; C_{L_1} is the lift coefficient for the flight condition; C_{D_u} is the drag due to speed derivatives as defined in (Roskam, 1990)VI:

$$C_{D_u} = M_1(\partial C_D / \partial M) \quad 4.41$$

where: M_1 is the Mach number for the flight condition and $(\partial C_D / \partial M)$ is the variation of airplane drag with Mach number as illustrated in Figure 10.3

$C_{T_{x_u}}$ is the thrust due to speed derivatives as defined in (Roskam, 1995)II:

$$C_{T_{x_u}} = -3C_{T_{x_1}} + C_{T_{x_1}} U_1 / ND_p J \quad 4.42$$

where: $C_{T_{x_1}}$ is the airplane steady state thrust coefficient, which is equal to the drag coefficient; N is the propeller revolutions per second; D_p is the diameter of the propeller; and J is the advance ratio.

4.7.2. Class II method for analysis of short period characteristics (Roskam, 1990)VII

The evaluation of short period parameters is done with the following equations:

$$\omega_{n_{sp}} = \{ [(-\bar{q}_1 S(C_{L_\alpha} + C_{D_1})/m) (C_{m_q} \bar{q}_1 S \bar{c}^2 / 2I_{yy} U_1) / U_1] - (C_{m_q} \bar{q}_1 S \bar{c}^2 / 2I_{yy} U_1) \} \quad 4.43$$

$$\xi_{sp} = -\{ (C_{m_q} \bar{q}_1 S \bar{c}^2 / 2I_{yy} U_1) + [(-\bar{q}_1 S(C_{L_\alpha} + C_{D_1})/m) / U_1] + (C_{m_q} \bar{q}_1 S \bar{c} / I_{yy}) \} / 2 \omega_{n_{sp}} \quad 4.44$$

where: \bar{q}_1 is the steady state dynamic pressure; C_{mq} is the pitch dumping derivative as defined in (Roskam, 1990) VI Page 425

The required parameters were calculated and tabulated as follows.

Table 30: Dynamic longitudinal stability parameters

Flight Phases	$\xi_{p-required}$	ξ_p	$\omega_{nsp-required}$	ω_{nsp}	$\xi_{sp-required}$	ξ_{sp}
(1) Takeoff	≥ 0.04	0.089	3.2 to 15	3.22	0.35 to 1.3	0.54
(2) Climb	≥ 0.04	0.079	3 to 13.5	2.48	0.3 to 2	0.66
(3) Level flight	≥ 0.04	0.083	5 to 23.5	2.92	0.3 to 2	0.74
(4) Descent	≥ 0.04	0.081	3.1 to 14.2	1.94	0.3 to 2	0.83
(5) Landing	≥ 0.04	0.081	3.6 to 17	2.54	0.35 to 1.3	0.71

As shown in Table 30, while the phugoid damping and short period damping are between the acceptable ranges specified by the regulations, the short period undamped frequency is not. This may be why the KR2 has a known pitch sensitivity issue.

5. Conclusions

The airworthiness analysis of the modified KR2 has been performed, and the process has been explained throughout this paper.

Having poor performance at high altitude, the studied airplane was modified in order to improve its stall-speed and take off distance at elevation. As stated at the beginning, the goal of this project was to verify if the modifications resulted in the expected performance enhancement, while making sure the airworthiness of the airplane was not affected.

Class two preliminary design methods, as described by (Roskam, 1990), were mainly used for the analysis. While this publication described step by step procedures, it doesn't explain where things come from. For this matter, (Perkins & Hage, 1949) was often referred to.

Starting with the literature review, a pseudo experimental method for determining the stick-fix and stick-free stability of the airplane was studied. This research was very helpful to understand the science behind stability and controllability of an airplane.

Preliminary calculations of lift and drag were done during the first part of the project. These calculations started with the generation of the airfoil lift and drag curve using Xfoil. The wing and airplane lift curves were constructed after obtaining the wing lift coefficient distribution for several angles of attack using the trailing vortices theory.

As required by the methodology, the applicable regulations for our modified airplane regarding controllability and stability were studied and tabulated for all flight conditions and configurations. The regulations also required the study and tabulation of the center of gravity (CG), for which the Weight & Balance and the CG diagram of the airplane were completed.

All these parameters, coupled with the calculation of the elevator control derivatives were used to build trim diagrams. Finally, from these trim diagrams and the calculation of hinge moment derivatives, all the controllability and stability parameters were obtained and checked against the regulations for airworthiness compliance.

Checking all the required parameters against the regulations, it was found that the airplane complies with the controllability requirements, but its static stability is marginal for most flight conditions and configurations.

The dynamic stability analysis showed that the airplane doesn't comply with the specified acceptable values for the undamped short period frequency, during most flight conditions and configurations. This explains the pitch sensitivity that the airplane is well known for.

By performing a pitch sensitivity analysis it was found that the short period undamped frequency depends mainly on the distance between the center of gravity and the airplane aerodynamic center. Therefore the only solution for this airplane, which is already half built, is to move the cg forward by reconfiguring the load distribution of the airplane. For future constructions a longer arm for the tail moment is also recommended to improve stability.

6. Appendix

A. Airplane dimensions

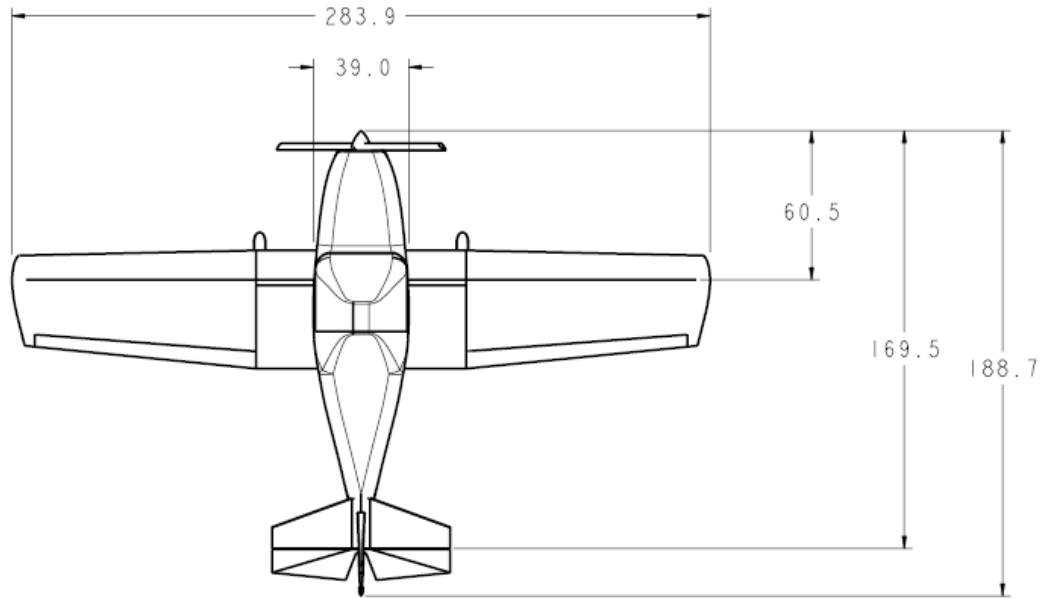


Figure 37: Airplane Top View (Nordin, 2006)

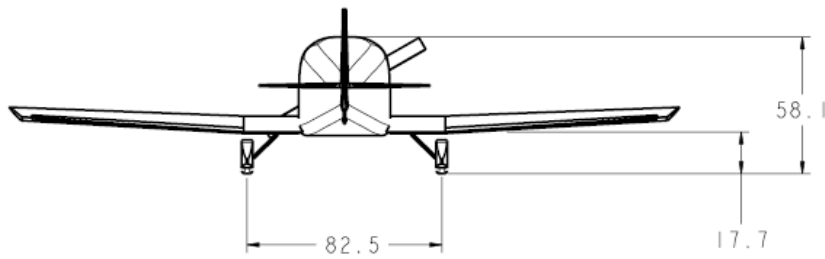


Figure 38: Airplane Back View (Nordin, 2006)

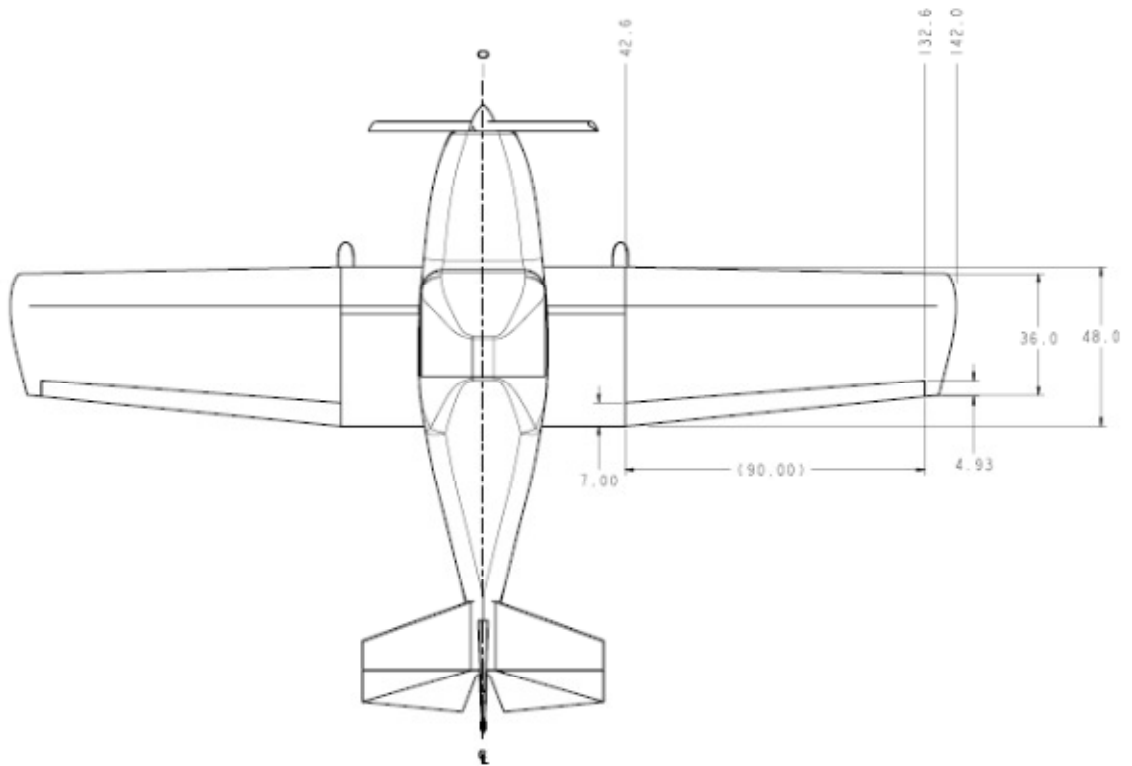


Figure 39: Airplane wing planform (Nordin, 2006)

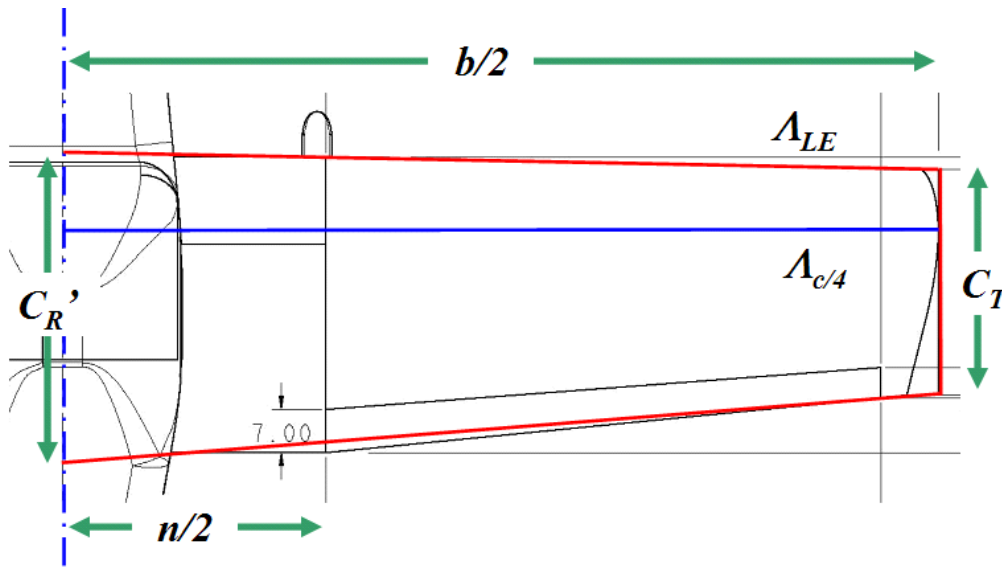
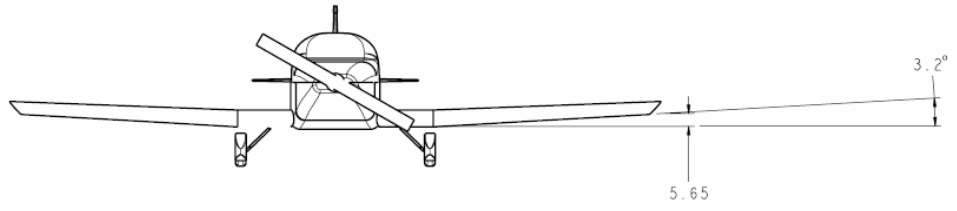


Figure 40: Equivalent wing planform (Nordin, 2006)

Table 31: Wing parameters (Nordin, 2006)

Wingspan	$b = 284 \text{ in} = 7.21 \text{ m}$
Geometric Chord at root	$C_R = 48 \text{ in} = 1.22 \text{ m}$
Geometric Chord at tip	$C_T = 36 \text{ in} = 0.91 \text{ m}$
Wing Area	$S = 12440 \text{ in}^2 = 8.03 \text{ m}^2$
Wetted Wing Area	$S_{wet_w} = 2(8.03 \text{ m}^2)\{1 + 0.25(.150)\}$ $S_{wet_w} = 16.66 \text{ m}^2$
Aspect Ratio	$A = b^2 / S = 6.47$
Equivalent Wing Planform	$S_{original} = C_T b + n(C_R - C_T) + (b - n)(C_R - C_T) / 2$ $S_{equivalent} = C_T b + (C_R' - C_T) b / 2$
Solving for C_R' :	$C_R' = 1.31 \text{ m}$
Taper Ratio	$\lambda = C_T / C_R' = 0.698$
$\frac{1}{4}$ Chord Sweep Angle	$\Lambda_{c/4} = 0$
Leading Edge Sweep Angle	$\Lambda_{LE} = 1.57^\circ$ from equivalent geometry
Wing Twist Angle	$\epsilon_T = -3.0^\circ$ (washout)

DIHEDRAL



WING INCIDENCE
3° WASHOUT

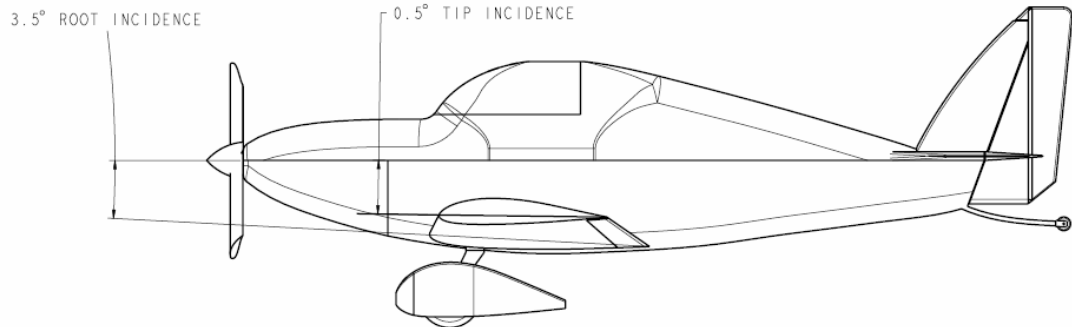
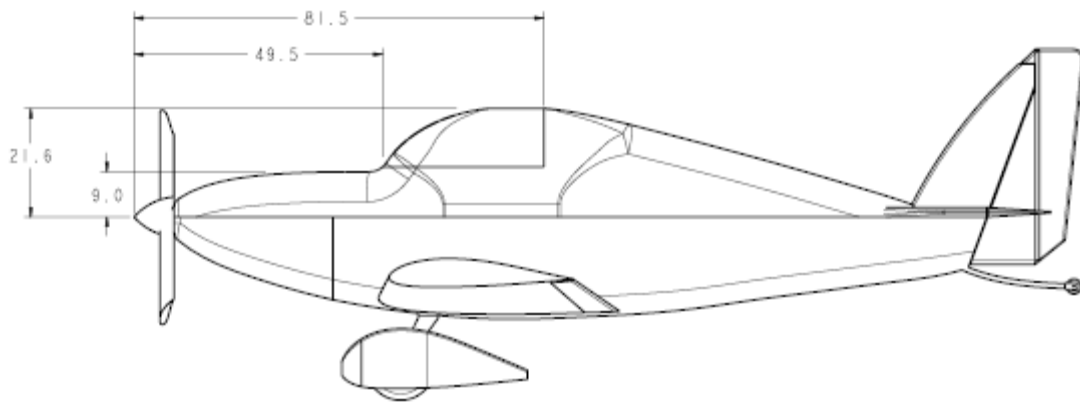


Figure 41: Wing dihedral and incident angle (Nordin, 2006)

CANOPY DIMENSIONS



WHEEL PANT DIMENSIONS

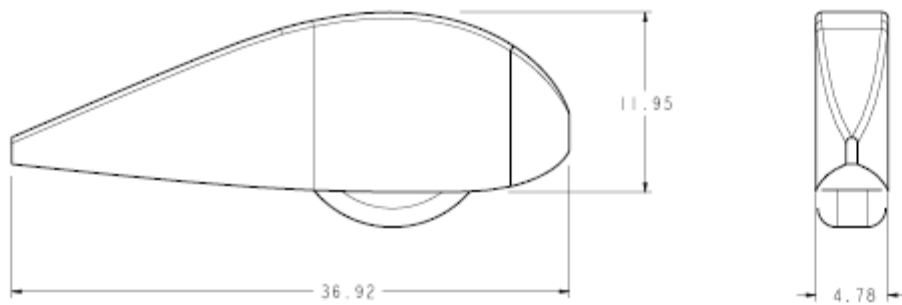


Figure 42: Canopy and wheel (Nordin, 2006)

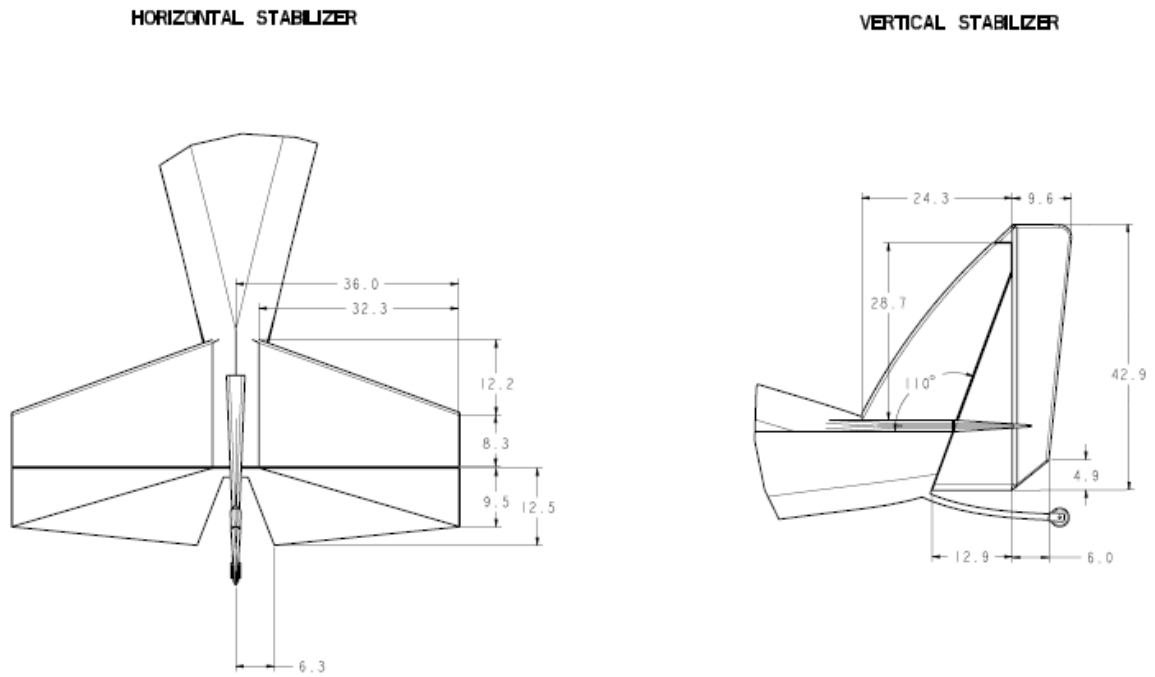


Figure 43: Empennage

Table 32: Empennage parameters (Nordin, 2006)

Horizontal Stabilizer Area	$S_h = 1760 \text{ in}^2 = 1.135 \text{ m}^2$
Horizontal Stabilizer Wetted Area	$S_{h_{WET}} = 2.1 \times S_h = 3696 \text{ in}^2 = 2.384 \text{ m}^2$
Horizontal Stabilizer Thickness Ratio	$(t/c)_h = 0.065$
Horizontal Stabilizer Incidence Angle	$i_h = 0^\circ$
Horizontal Stabilizer Mean Geometric Chord	$\bar{c}_h = 0.689 \text{ m}$
Vertical Stabilizer Area	$S_v = 880 \text{ in}^2 = 0.568 \text{ m}^2$

Vertical Stabilizer Wetted Area $S_{v_{WET}} = 2.1 \times S_v = 1848 \text{ in}^2 = 1.192 \text{ m}^2$

Vertical Stabilizer Thickness Ratio $(t/c)_v = 0.070$

Vertical Stabilizer Mean Geometric Chord $\bar{c}_v = 0.635 \text{ m}$

7. Acknowledgements

Mrs. Carmen Bravo	General support, paper review
Dr. Nikos Mourtos	Critical review
Dr. Periklis Papadopoulos	Critical review
Mr. Mike Nordin	Project partner, critical review
Mr. Gabriel Rombado	Critical review
Mr. Jan Nordin	Construction partner
Dr. Jeanne Linsdell	Technical writing
Prof. Vicki Parrish	Paper review

References

- Anderson, J. (1978). *Introduction to Flight*. New York: McGraw-Hill.
- Drela, M., & Youngren, H. (2001). *XFOIL 6.9 User Guide*. MIT Aero & Astro.
- Glove, S. (Ed.). (n.d.). Retrieved 09 25, 2011, from KR: <http://www.fly-kr.com/>
- Langford, M. (1997, May 23). *RAF48 airfoil*. Retrieved 11 16, 2011, from My KR Opinions, or "The Gospel According to Mark": <http://www.n56ml.com/kraf48.html>
- Lycoming. *Lycoming Flyer Operations*. Lycoming.
- Multhopp, H. (1942). *NACA-TM-1036*. Washington: NACA.
- Nordin, M. J. (2006). *VERIFICATION OF AIRWORTHINESS OF A MODIFIED KR-2 AIRCRAFT*. San Jose: San Jose State University.
- Perkins, C. D., & Hage, R. E. (1949). *Airplane Performance Stability & Control*. New York: John Wiley & Sons.
- Ribner, H. S. (1942). *NACA-report-820 Propellers In Yaw*. Washington: NACA.
- Roskam, J. (1990). *Airplane Design, Part I - VIII*. Lawrence: Roskam Aviation and Engineering Corporation.
- Roskam, J. (1995). *Airplane Flight Dynamics and Automatic Flight Controls*. Lawrence, KS: DARcorporation.
- Silverstain, A. (1942). *REPORT No. 651 Downwash And Wake Behind Plain And Flapped Airfoils*. Washington: Naca .
- Wynne, W. (2004). *Thrust Testing*. Retrieved 11 27, 2011, from The Corvair Authority: <http://www.flycorvair.com/thrustjune.html>